A study of temperature profiles in ceiling jets under horizontal unconfined ceilings with the CFD tools FLACS and FDS

Tone Øvrebø

A thesis submitted in partial fulfilment of the
requirements for the degree of Master of Science in
the subject of *Process Safety Technology*

Department of Physics and Technology
University of Bergen
Bergen, Norway
June 2017

Abstract

The key to controlling accidental fires, is early detection by the correct placement of devices such as smoke detectors and sprinkler systems. Smoke is accompanied by a temperature rise, brought about by the ceiling jet resulting from a fire. Accurate prediction of temperatures in the ceiling jet, by either empirical correlations or numerical methods, therefore gives ground for suggesting placement of devices. Numerical methods such as CFD (Computational Fluid Dynamics) codes are continuously improved and need validation. In this work, two CFD models, FLACS and FDS, are evaluated against experimental measurements and empirical correlations presented by Alpert [1]. By varying heat release rate (HRR), ceiling height and burner surface area, both weak and strong plume-driven flows are produced. Maximum temperatures for radial positions along the ceiling are found to be well predicted with both FDS and the correlation, but is over-predicted to a variable degree by FLACS. FDS also shows temperatures closer to experimental values near the fire, but for distances further away, temperatures drop too quickly towards room temperature, resulting in a too narrow ceiling jet. FLACS captures more of the temperature distribution below the ceiling and thereby predict ceiling jet thicknesses more accurately than FDS. The correlation predict thicknesses even closer to experimental values. Effects of changing HRR, ceiling height and burner size are found to be present to a variable degree, while the effect of grid size is found to be critical for accurate numerical results.

Acknowledgements

This thesis is the final product in connection with the master's programme Process Safety Technology at the University of Bergen, performed between August 2016 and June 2017 and supervised by Bjørn Arntzen. I would therefore like to start by giving my gratitude to him, for putting me in contact with Gexcon AS and Western Norway University of Applies Sciences (HVL) in Haugesund, as well as giving valuable feedback and motivation during the entire process.

I would like to thank Gexcon AS for offering me an exciting thesis topic and an office space at Fantoft. A very special thank you goes to Deiveegan Muthusamy for giving me a thorough introduction to FLACS Fire, and understanding when I decided to go a slightly different route with my thesis. Also from Gexcon AS, I have to offer my sincere gratitude to Bjørn Lilleberg, for taking the time to help troubleshooting when I was stuck, as well as looking at my final results and offering his thoughts and explanations.

Of course, I want to thank everyone I was in contact with at HVL, especially Nichlas Lyche for allowing me to be a part of his thesis, his supervisors, Bjarne Christian Hagen and David R.U. Johansen, for making it happen and giving thorough explanations whenever necessary, and HVL itself for providing location and equipment. I had a completely new positive outlook on the work with my thesis after being involved with this project, and for that I am eternally grateful.

I also want to thank the University of Bergen for financial support for the trip to Haugesund, and for a great office space. This brings me over to the wonderful people I share this office with. Thank you for some amazing lunch breaks, great cooperation and encouraging words throughout this process. A special thank you to Jon, for taking the time of going thoroughly through my thesis and giving feedback, to Wulme for proofreading, and to Anna Liisa for always saying the right things and boosting my confidence.

Last but not least, I want to thank my friends and family for their continuous cheering and admiration, and Petter for being my personal sounding board and biggest support.

Bergen, 1 June 2017

Tone Øvrebø

Department of Physics and Technology
University of Bergen
Bergen, Norway

Contents

Abstract i

Acknowledgements ii

Nomenclature viii

1 Introduction 1
- 1.1 Motivation 1
- 1.2 Previous work 2
- 1.3 Objective 3
- 1.4 Limitations 3
- 1.5 Outline of the thesis 4

2 Theory of Combustion, Fire Modelling and Ceiling Jets 5
- 2.1 Introduction to Combustion 5
  - 2.1.1 The fire tetrahedron 5
  - 2.1.2 Flame types 9
  - 2.1.3 Heat transfer 12
- 2.2 Fire modelling 14
  - 2.2.1 Governing equations 14
  - 2.2.2 Turbulence modelling 16
  - 2.2.3 Boundary conditions and sources 17
  - 2.2.4 Numerical solution 18
  - 2.2.5 FLACS 19
  - 2.2.6 Fire Dynamics Simulator (FDS) 19
- 2.3 Ceiling jets 20
  - 2.3.1 Ceiling jet thickness 21
  - 2.3.2 Temperatures in a weak plume-driven flow field 21
  - 2.3.3 Temperatures in a strong plume-driven flow field 22
  - 2.3.4 Heskestad flame height correlation 23

3 Method and Data 25
- 3.1 Experimental work 25
  - 3.1.1 Experimental setup 25
  - 3.1.2 Overview of performed experiments 30
- 3.2 Simulations 32
  - 3.2.1 Grid sensitivity analysis 32
  - 3.2.2 FLACS simulations 33
  - 3.2.3 FDS simulations 38
- 3.3 Post-processing of results 39

4 Results and Discussion **41**
4.1 Grid analysis 41
4.1.1 FLACS simulations 41
4.1.2 FDS simulations 45
4.2 Temperature fluctuations 46
4.3 Plume characterisation 49
4.4 Temperature comparisons 51
4.4.1 Effect of varying HRR 55
4.4.2 Effect of varying ceiling height 59
4.4.3 Effect of varying burner surface area 62
4.5 Ceiling jet thickness comparisons 63
4.5.1 Effect of varying HRR 63
4.5.2 Effect of varying ceiling height 66
4.5.3 Effect of varying burner surface area 67
4.6 Choosing the right prediction tool 67
4.7 Uncertainties 68

5 Conclusion **72**
5.1 Suggestions for further work 73

Bibliography **75**

Appendix A Scenario (cs-)file for FLACS input **77**

Appendix B Scenario (.fds) file for FDS input **83**

Appendix C MATLAB code for post-processing temperature results **85**

Appendix D MATLAB code for plotting temperature results **88**

Appendix E Temperature plots **91**

Appendix F Ceiling jet thickness plots **124**

Nomenclature

Latin symbols

A	Area	m^2
b	Fire plume radius	m
$c_{p,i}$	Specific heat capacity of species i	$\mathrm{J \cdot K^{-1} kg^{-1}}$
D	(Effective) diameter of fire source	m
D	Characteristic length (macroscale)	m
D^*	Characteristic diameter of a fire	m
D_α	Diffusion coefficient for species α	$\mathrm{m^2 \cdot s^{-1}}$
$\mathbf{f}$	Body force vector (per unit mass)	$\mathrm{m \cdot s^{-2}}$
F	Geometric view factor	–
g	Gravitational acceleration, ≈ 9.81	$\mathrm{m \cdot s^{-2}}$
H	Ceiling height	m
h	Heat transfer coefficient	$\mathrm{W \cdot m^{-2} K^{-1}}$
h	Height above fire source	m
h_0	Elevation of virtual origin of fire source	m
h_i	Specific enthalpy of species i	$\mathrm{J \cdot kg^{-1}}$
k	Thermal conductivity	$\mathrm{W \cdot m^{-1} K^{-1}}$
k	Turbulent kinetic energy	$\mathrm{J \cdot kg^{-1}}$
L	Flame height	m
$\dot{m}'''_\alpha$	Mass source/sink of species α	$\mathrm{kg \cdot s^{-1} m^{-3}}$
M	Molecular weight	$\mathrm{kg \cdot mol^{-1}}$
m	Mass	kg
n	Number of moles	–
p	Pressure	Pa
$\dot{Q}$	Heat release rate	W

q	Heat transfer rate	W
R	Ideal gas constant ≈ 8.314	$\mathrm{J \cdot K^{-1} mol^{-1}}$
r	Radial position of ceiling jet	m
Re	Reynolds number	–
s_L	Laminar burning velocity	$\mathrm{m \cdot s^{-1}}$
T	Temperature	°C/K
t	Time	s
$\mathbf{u}$	Local velocity vector	$\mathrm{m \cdot s^{-1}}$
u, v, w	Velocity in x-, y- and z-direction	$\mathrm{m \cdot s^{-1}}$
W	Emissive power (emittance) of a body	$\mathrm{W \cdot m^{-2}}$
w_j	Mass fraction of element j	–
x, y, z	Position/distance in Cartesian directions x,y,z	m
z	Distance below ceiling	m
Z_i	Elemental mass fraction of element i	–

Greek symbols

Δ	Difference operator	
δx	Grid size	m
$\delta_{T_{max}}$	Thermal boundary layer thickness	m
ε	Emissivity	–
ε	Rate of turbulent kinetic energy dissipation	$\mathrm{J \cdot kg^{-1} s^{-1}}$
μ	Dynamic viscosity	$\mathrm{Pa \cdot s}$
μ_{ij}	Mass proportion of element i in species j	–
ν	Kinematic viscosity	$\mathrm{m^2 \cdot s^{-1}}$
ν_T	Turbulent exchange coefficient	$\mathrm{m^2 \cdot s^{-1}}$
ρ	Density	$\mathrm{kg \cdot m^{-3}}$
σ	Standard deviation	
σ	Stefan-Boltzmann constant $\approx 5.672 \cdot 10^{-8}$	$\mathrm{W \cdot m^{-2} K^{-4}}$
τ	Shear and normal stress	Pa
Φ	Fuel-air equivalence ratio	–
ξ	Mixture fraction	–

Subscripts

∞	Ambient
C	Combustion
c	Convective
F	Flame
f	Fuel
L	Laminar
ox	Oxidizer
p	Plume
R	Reaction
st	Stoichiometric
T	Turbulent
u	Unburned

Superscripts

$''$	Flux; rate of flow of a property per unit area
$+$	Non-dimensional quantity
$-$	Time average
$\cdot$	Time derivative
$'$	Fluctuation

Other symbols

ℓ_0,ℓ_λ,ℓ_k	Integral, Taylor, Kolmogorov length scale	m
ℓ_T	Thermal ceiling jet thickness	m
ℓ_V	Momentum ceiling jet thickness	m
$\equiv$	Definition	
∇	Gradient	
$\nabla\cdot$	Divergence	
∂	Partial derivative	
$\sum$	Summation	

Abbreviations

CASD	Computer Aided Scenario Design
CFD	Computational Fluid Dynamics
CPU	Central Processing Unit
DNS	Direct Numerical Simulation
DTM	Discrete Transfer Method
EDC	Eddy Dissipation Concept
FDS	Fire Dynamics Simulator
FLACS	FLame ACceleration Simulator
HRR	Heat Release Rate
HVL	Høgskulen på Vestlandet (Western Norway University of Applied Sciences)
LES	Large Eddy Simulation
LFL	Lower Flammability Level
MIE	Minimum Ignition Energy
PDE	Partial Differential Equation
RANS	Reynolds-Averaged Navier-Stokes
rms	Root-mean-square
TC	Thermocouple
UFL	Upper Flammability Level

Definitions

Ceiling jet:	Flow of hot combustion products in a shallow layer below ceiling surface.
Fire plume:	Buoyant flow of hot gases above a fire source.
Alpert's temperature criterion:	$\Delta T / \Delta T_{max} = 1/e$
TC1, TC2(...) :	Thermocouple tree number one, two(...)
TC1-1, TC1-2, TC1-3(...) :	Top, second, third(...) thermocouple of tree number one.

Chapter 1

Introduction

1.1 Motivation

Every year, many private households and industrial buildings experience accidental fires. According to Statistics Norway (SSB) [2], two thirds of all fires in Norway involve private households, and the total number of such fires was 3001 in year 2016, corresponding to approximately six fires per 10,000 inhabitants. Luckily, the trends show a reduction in fires over the last ten years, which might be a result of the great expenditures on both fire and accident protection and preparedness. Statistics show that the expenditures have grown steadily from NOK 1066 per capita in year 2008, to NOK 1496 in year 2016, which corresponds to a growth of 40 % .

An important key to fire prevention and controlling, is early detection and suppression, which has been made possible by ever more effective smoke detectors and sprinkler systems. The activation of automatic sprinklers and smoke detectors relies on a temperature rise and/or a rise in smoke concentration below the ceiling, where such devices are placed. This temperature and smoke concentration rise is brought about by the ceiling jet resulting from a fire. Knowledge about the characteristics of ceiling jets is therefore important in a fire safety aspect, and the design of fire control systems such as placement of sprinklers (especially distance below ceiling) is highly dependent on a complete picture of temperature and velocity profiles in ceiling jets.

In some cases it is difficult, or even impossible, to perform experiments to study fire parameters. Therefore, as a tool for prediction of maximum temperature and thickness of the ceiling jet, several empirical correlations are available. Also, fire modelling using CFD (Computational Fluid Dynamics) is an alternative. These are tools that at low cost can predict several fire parameters, such as temperature, velocities, concentrations, turbulence level etc., and can be used in calculations of sprinkler activation time, evacuation time, heat dose to occupants and so forth.

It is important that the models are trustworthy, giving accurate predictions of fire parameters. To check if the mathematical modelling with governing fluid equations accurately predict the physical conditions they represent, and to unveil limitations of the models, they need to be validated. Typically, this is carried out by comparing numerical results with experimental data, potentially applying changes to the model and re-testing it.

1.2 Previous work

The concept of ceiling jets was originally studied by Alpert in the 1970s, who based on large-scale experiments developed empirical correlations for both temperature and velocity profiles, continuously refined to the ones used in the current work [1]. Taking part of this refinement are among others Motevalli and Marks [3], conducting a series of experiments resulting in some changes to the correlations, which Alpert has taken into account in his newer reports. To include strong plume-driven ceiling jets, correlations were made by Heskestad and Hamada [4], making use of the plume radius and virtual origin as earlier defined by Heskestad.

Other refinements to the Alpert empirical correlations, as well as independent correlations, have been proposed by several other authors. For instance, Cooper [5] developed an algorithm to predict instantaneous rate of convective heat transfer to the ceiling, for use in two-layer zone-type fire models. Based on this, he also presented a new correlation for velocity and temperature distributions in the ceiling jet.

However, the prevailing empirical correlations for large-scale steady unconfined ceiling jets, are the refined Alpert equations. This is especially the case for situations where there is no presence of a stagnant upper layer of smoke, which would reduce momentum of the ceiling jet due to shear forces. In the current work, a ceiling over an open room is researched, and smoke is drawn upwards through an exhaust fan. There will thereby never form an upper layer, and it is reasonable to only test the correlations presented by Alpert [1].

Numerical studies of unconfined ceiling jets have previously been performed in many cases with both RANS and LES modelling in different computer programs. Below is only a small selection listed, of the many scientific studies conducted on the field.

Nam and Bill [6] used the computer code PHOENICS with the standard k-ε model to simulate thermal plumes. They reported that the model was well known for over-predicting the velocities and temperatures along the plume centerline, consequently under-predicting the plume width. They modified the model to improve accuracy, by adding a term of turbulence kinetic energy generated by buoyancy and changing constants related to turbulent viscosity and Prandtl number (ratio of momentum diffusivity to thermal diffusivity). The modified model was tested on ceiling jet simulations, and validated against data from experiments performed by Heskestad and Hamada [4], showing a great improvement.

Hara and Kato [7] used the standard k-ε model in 3D CFD package STAR-CD to compare ceiling jet properties with the experiments performed my Heskestad and Hamada [4]. They were particularly interested in the dependence of grid size, incompressible or compressible flow assumption (the Boussinesq assumption), and the initial values of k and ε at the inflow. They determined that the numerical predictions consistently overestimated the measurements, but usually no less than 10 % with a sufficiently fine grid. They also concluded that a simplified compressibility assumption gave better results than incompressible results, and that assuming the fluctuating velocity for k to be 20 % of the inflow velocity in z-direction, specifying k and ε accordingly, gave sufficiently adequate results.

The validation guide of the FDS software [8] lists several ceiling jet experiments, where temperature measurements have been made to evaluate the model's ability to predict temperature at a given point in a compartment. An independent study with FDS is conducted by O'Grady and Novozhilov [9], comparing the temperature and velocity profile of a large-scale strong plume-driven ceiling jet with experimental data. The main focus of the study was to simulate the interaction between fire ceiling jet and water sprinkler spray, to see if the cooling effect of sprinklers to prevent flashover was captured in the simulations. They expected the LES method to perform better than earlier RANS modelling, due to its suitability for droplet interaction with turbulence, as these are mostly affected only by large eddies. They found this to be the case, and also determined that the relative prediction error was in the order of 12 % for temperature, which is held to be a good agreement, considering many parameters of a flame are estimated with high uncertainty.

Novozhilov [10] further compared two sets of experiments performed by Motevalli and Marks [3] with LES and RANS predictions, as well as with correlations from dimensional analysis. He found that the two methods (LES and RANS) gave similar results at the two radial positions presented in the paper, but with an under-prediction close to the ceiling at r/H=0.26. Since fire detection/suppression devices are usually located a few centimetres below the ceiling, where both methods performed reasonably accurate, he concluded that this under-prediction was not a problem.

Chatterjee et al. [11] recently published a study where they simulated ceiling jets of strong fire plumes using the compressible LES code FireFOAM, and compared with experimental results. In the same work they also compared their numerical results with the experimental work of Heskestad and Hamada [4]. They found that for cases where the flame was impinging on the ceiling, the temperature predictions were higher than the experimental values and thereby that the thermal boundary layer was thicker. When the fires were not impinging on the ceiling, the predictions were close to the experimental data. They concluded that several features of the model need investigating to attain more accurate results for the impinging fires, such as the heat transfer, combustion model and turbulence model.

1.3 Objective

The objective of the current work is to validate ceiling jet temperature prediction in two CFD tools, FLACS and FDS, against experimental data conducted by a fellow master's student, Nichlas Lyche, during the work with his thesis. By varying heat release rate, height between burner surface and ceiling, as well as burner surface area, ceiling jets controlled by different mechanisms will be produced. This way, a detailed picture of the temperature profiles in weak and strong plume-driven ceiling jets can be obtained. The empirical correlations for ceiling jet temperature and thickness presented by Alpert [1] are also tested. In this manner, the two models RANS (in FLACS) and LES (in FDS) can be compared against both experimental and empirical results, as well as to each other, to check for differences and make a suggestion to which method performs better. The effect of varying grid size is tested in both simulation tools.

1.4 Limitations

This work limits to evaluating the performance of FLACS and FDS with the models available today. No modification and re-testing of the models is carried out.

Only temperature is measured in the experiments, and is thereby the main variable of focus in the simulations too, even though some light is also shed on heat transfer, velocity and turbulence level to explain the temperature results.

Although several highly acknowledged empirical correlations are available in literature, only the ones presented by Alpert [1] are used in the current work, due to their simplicity and area of validity.

1.5 Outline of the thesis

In Chapter 2, some of the essential background theory needed to shed light on the theme is presented. The chapter is divided into three parts. First, there is an introduction to combustion (Section 2.1), where some of the mechanisms behind different fires are presented, such as turbulence and heat transfer. Next is a section about fire modelling (Section 2.2), presenting CFD and the governing equations used for fire and turbulence modelling, as well as introducing the two simulation tools used in the current work; FLACS and FDS. Last of the three theory sections is the one about ceiling jets (Section 2.3), including the definition of a ceiling jet and its thickness, as well as temperature and flame height correlations.

Chapter 3 describes the methods and data used in the thesis work, such as experimental and numerical setup, and how the results were post-processed.

The results are presented and discussed in Chapter 4, which separates the results from grid analysis, temperature results and ceiling jet thickness results. The chapter is ended with a description of uncertainties in experimental and numerical setup, HRR, boundary conditions, models etc.

A conclusion is presented in Chapter 5, including some suggestions for further work.

Chapter 2

Theory of Combustion, Fire Modelling and Ceiling Jets

2.1 Introduction to Combustion

2.1.1 The fire tetrahedron

According to the online Oxford dictionary [12], a fire is defined as "a process in which substances combine chemically with oxygen from the air and typically give out bright light, heat, and smoke". This process is known as burning or combustion. For a long time, the fire triangle was used to explain the concept of fire; to start a combustion process one would need the three elements heat, oxidizer and fuel. More recently, a fourth element has been added, without which combustion cannot be maintained, namely chemical chain reactions. The four elements make up what we now know as the fire tetrahedron, see Figure 2.1, otherwise illustrated by a pyramid or a square. If a fire exists, removing one of the elements will extinguish the fire.

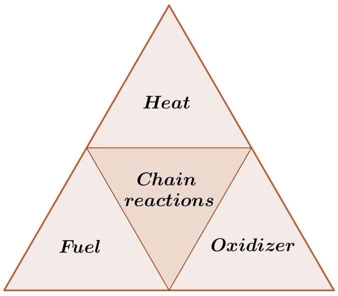

Figure 2.1: The fire tetrahedron, showing the four different elements needed to sustain a fire.

Each of the elements in the fire tetrahedron require some additional explanation, see the next few sections.

Fuel and oxidizer

Fuel exists in the three states; solids (such as wood and charcoal), liquids (such as diesel and gasoline) and gases (such as natural gas). However, the combustion of these fuels happens mainly in the gas phase. In a combustion process, the *oxidizing* agent is usually oxygen in air. Air consists of different gases, such as nitrogen (≈ 78 %), oxygen (≈ 21 %), argon (≈ 1 %) and many other trace components.

To accurately describe the concept of fire, one should primarily address the *mixture* between the fuel and oxidizer. The ratio between fuel and oxidizer in a mixture is called the fuel-air equivalence ratio, denoted by Φ , and is defined in Equation (2.1) as follows:

$$\Phi = \frac{\mathrm{fuel-to-oxidizer\ ratio}}{(\mathrm{fuel-to-oxidizer\ ratio})_{st}} = \frac{m_f/m_{ox}}{(m_f/m_{ox})_{st}} = \frac{n_f/n_{ox}}{(n_f/n_{ox})_{st}} \ , \tag{2.1}$$

where m is mass and n is number of moles. Subscripts f, ox and st represent fuel, oxidizer and stoichiometric respectively.

When $\Phi = 1$ the mixture is *stoichiometric*, meaning that all the fuel and oxidizer is consumed in the chemical reaction. For hydrocarbon fuels, this leaves only carbon dioxide and water as products, and the combustion is thereby *complete*. Such a combustion is illustrated by the reaction equation (2.2), involving a general hydrocarbon fuel, $\mathrm{C_nH_m}$, in air. For simplicity, one often assumes that air is a mixture of 21 % oxygen and 79 % nitrogen, leaving the oxygen-nitrogen ratio to be 1:3.76.

$$\mathrm{C_nH_m} + \left(\mathrm{n} + \frac{\mathrm{m}}{4}\right)(\mathrm{O_2} + 3.76\mathrm{N_2}) \rightarrow \mathrm{nCO_2} + \frac{\mathrm{m}}{2}\mathrm{H_2O} + 3.76\left(\mathrm{n} + \frac{\mathrm{m}}{4}\right)\mathrm{N_2} \ . \tag{2.2}$$

When $\Phi < 1$, the mixture is fuel *lean* and all the oxygen will not be entirely consumed in the reaction, leaving some excess oxygen on the product side of the reaction equation (2.3). For readability, the general hydrocarbon now reacts with pure oxygen only.

$$\mathrm{C_nH_m} + \frac{1}{\Phi}\left(\mathrm{n} + \frac{\mathrm{m}}{4}\right)\mathrm{O_2} \rightarrow \mathrm{nCO_2} + \frac{\mathrm{m}}{2}\mathrm{H_2O} + \frac{1-\Phi}{\Phi}\left(\mathrm{n} + \frac{\mathrm{m}}{4}\right)\mathrm{O_2} \ . \tag{2.3}$$

Reactions (2.2) and (2.3) described complete combustion. However, when $\Phi > 1$ the mixture is fuel *rich*, and there is not enough oxygen for the fuel to be completely oxidized. The combustion is *incomplete*. In these cases, the reaction products are not as readily given, and may include carbon monoxide, hydrogen, unburned hydrocarbons and/or elemental carbon (soot), as shown in reaction equation (2.4).

$$\mathrm{C_nH_m} + \frac{1}{\Phi}\left(\mathrm{n} + \frac{\mathrm{m}}{4}\right)\mathrm{O_2} \rightarrow \lambda\mathrm{C(s)} + \mathrm{aCO} + \mathrm{bCO_2} + \mathrm{cH_2} + \mathrm{dH_2O} + \mathrm{eO_2} + \mathrm{fOH} + \mathrm{gC_nH_m} \ . \tag{2.4}$$

For some mixtures of fuel and oxygen, the equivalence ratio is too high or too low for the combustion to take place at all, i.e. it is outside the flammable region, or in other words, outside upper (UFL) or lower (LFL) *flammability limits.*

Upon combustion, the fuel and oxidizer may be premixed or non-premixed, where the latter is also known as a diffusion flame. For a premixed flame, the fuel and oxidizer are mixed on a molecular level before ignition; as for instance in a spark-ignition engine. In the non-premixed case, the mixing and burning occur simultaneously, and the chemical reactions thereby only take place in the interface between the fuel and the oxygen; as in a candle or a wood fire. The difference between the two is further illustrated in Figure 2.2, collected and adapted from Eckhoff [13, p. 12].

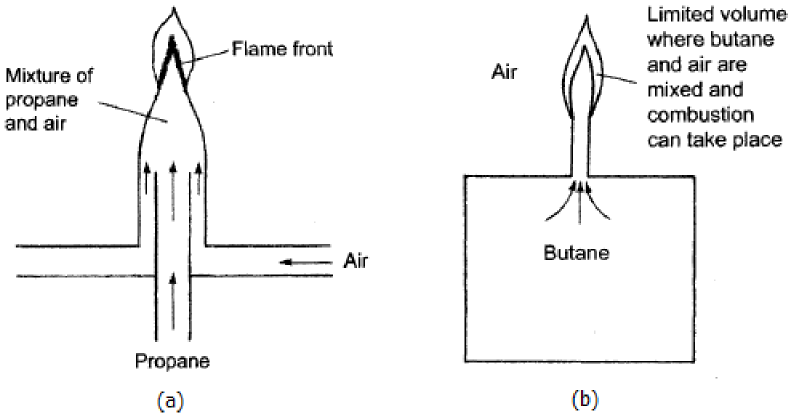

Figure 2.2: An illustration of the differences between (a) premixed flames and (b) non-premixed flames, collected and adapted from Eckhoff [13, p. 12].

For a non-premixed case, the degree of mixing during combustion can be described using the mixture fraction, ξ. The mixture fraction is defined by an *elemental* mass fraction, Z_i, see Equation (2.5) [14]:

$$Z_i = \sum_{j=1}^{S} \mu_{ij} w_j \quad ; \quad i = 1, ..., M \ , \tag{2.5}$$

where μ_{ij} represents the mass proportion of element i in species j, and w_j is the total mass fraction of species j, $w_j = m_j / m_{total}$. The mixture fraction is made up by the elemental mass fractions in the two streams of fuel and oxidizer, see Equation (2.6):

$$\xi = \frac{Z_i - Z_{i,ox}}{Z_{i,f} - Z_{i,ox}} \ . \tag{2.6}$$

Heat

The next element of the fire tetrahedron is heat, usually first provided to the system from some sort of ignition source. For a specific mixture of fuel and oxidizer, this ignition source must provide enough energy for ignition to take place, that is, enough heat for the first chemical reaction to start. This is known as the system's *minimum ignition energy* (MIE). In addition to fuel-oxidizer mixture, this energy is highly dependent on several factors, such as pressure, ambient temperature, ignition method and duration. According to Eckhoff [13], some common ignition sources in the process industries are:

- open flames and glowing or smoldering materials
- hot solid surfaces or jets of hot combustion gases
- burning metal particles and "thermite" flashes from impacts, grinding etc.
- electrical and electrostatic sparks, arcs, and other discharge forms
- adiabatic compression or light radiation

After ignition has occurred, the energy produced by the chemical reaction will itself be the source of heat to the combustion process. Different fuels have different heating potentials, often defined as the enthalpy of reaction, Δh_R, as seen in Equation (2.7). Combustion reactions are exothermic, and thereby characterized by negative enthalpies of reaction.

$$\Delta h_R = h_{products} - h_{reactants} \ . \tag{2.7}$$

Here, lower case h means specific enthalpy, i.e. per mass of the species. The specific enthalpy for a species i at a given temperature (T) is expressed using the relationship:

$$h_i(T) = h^0_{f,i}(T = T_{ref}) + \Delta h_{s,i}(T) \ , \tag{2.8}$$

where $h^0_{f,i}$ is the enthalpy of formation of species i at standard reference state (p=1 atm and T_{ref}=298 K), which is a known tabular value for several compounds. $\Delta h_{s,i}(T)$ represents the sensible enthalpy change in going from temperature T_{ref} to T [15]. This value is thereby a function of temperature, and is expressed by the compounds' *specific heat capacity*, $c_{p,i}$, defined as the amount of energy required to raise the temperature of one unit mass of the compound by one degree. The final expression for the temperature dependent specific enthalpy for species i is thereby:

$$h_i(T) = h^0_{f,i}(298 \text{ K}) + \int\limits_{298 \text{ K}}^{T} c_{p,i} \ dT \ . \tag{2.9}$$

Once the fire has been established, its temperature is often described by the *adiabatic flame temperature*, which has been listed as tabular values for most fuels, and is typically several thousand kelvins [15]. Some other temperatures of interest, by which fuels are often classified with regards to fire hazard, are the fire point, the flash point and the autoignition temperature. Their definitions, according to the Encyclopedic Dictionary of Polymers [16], are as follows:

Flash point: *The lowest temperature at which a combustible liquid will give off a flammable vapour that will momentarily burn when exposed to a small flame.*

Fire point: *The temperature at which a material, when once ignited, continues to burn for a specified period of time. It is the lowest temperature at which a liquid evolves vapours fast enough to support continuous combustion.*

Autoignition: *The temperature at which a combustible material will ignite and burn spontaneously under specified conditions.*

The first two require some sort of forced ignition (an ignition source), while the latter does not. From this it is clear that for a compound, the flash point is the lowest of the three temperatures, the fire point is somewhat higher, and the autoignition temperature is the highest.

Chain Reactions

The last element of the fire tetrahedron is made up by the chain reactions. A chain reaction is defined by the Encyclopedic Dictionary of Polymers [16] as "[...] a reaction type characterized by the formation of products of a later step (chain carriers), which are reactants for an earlier step." The basis for combustion processes are radical chain reactions, that is, the overall reactions given in Section 2.1.1 are divided into smaller reactions, in which free radicals (atoms, molecules or ions with unpaired electrons) are involved. In such reactions there are four steps: initiating, branching, propagating and terminating. Warnatz et al. [14] illustrates them by looking at the most important reactions in combustion of hydrogen in oxygen:

$$\begin{aligned}
H_2 + O_2 &= 2OH\bullet && \text{chain initiation} \\
OH\bullet + H_2 &= H_2O + H\bullet && \text{chain propagation} \\
H\bullet + O_2 &= OH\bullet + O\bullet && \text{chain branching} \\
O\bullet + H_2 &= OH\bullet + H\bullet && \text{chain branching} \\
H\bullet &= 1/2H_2 && \text{chain termination (heterogeneous)} \\
H\bullet + O_2 + M &= HO_2 + M && \text{chain termination (homogeneous)}
\end{aligned}$$

where M is an arbitrary molecule colliding and giving energy in the reaction. In the first, initiating reaction, radicals are formed from stable species. In the next, propagating reaction, radicals change in type but not in number, while in the branching reactions the total number of radicals increases. This chain branching is the type of reactions which is most important in ignition processes, and if not controlled, can lead to an explosion. The last two reactions are terminating; they form stable species from radicals. To uphold a fire, free radicals must keep on being formed, thus the chain reactions will have to continue without all of them being terminated.

2.1.2 Flame types

The concept of premixed and non-premixed flames was briefly introduced in Section 2.1.1, but these two are usually further divided in two subcategories based on the motion of the fuel, namely laminar and turbulent fires. That is, there are four different flame types, as shown in Table 2.1 with corresponding examples [14]. These four could be explained and discussed in great detail, but in the extent of this work, it is sufficient to only describe some differences between laminar and turbulent flames.

The flames studied in the current work fall under the category turbulent diffusion (non-premixed) flames, as seen in Table 2.1.

Table 2.1: The different flame types according to mixing and flow pattern, with corresponding examples.

Mixing type	Fluid motion	Examples
Premixed	Laminar	Bunsen flame Flat flame
	Turbulent	Gas explosion Gasoline engine with spark ignition
Nonpremixed	Laminar	Candle Wood fire
	Turbulent	Jet flame Diesel engine

Laminar flames

Laminar flows, as opposed to turbulent ones, involves no lateral mixing or eddies, meaning that the adjacent layers of fluid only move parallel along each other [17]. *Reynolds number*, Re, is a dimensionless quantity which was originally used to describe the critical conditions at which laminar flow changes to turbulent. It is dependent on flow velocity, geometry, density and viscosity, and is defined by Equation (2.10);

$$Re = \frac{D\overline{v}\rho}{\mu} = \frac{D\overline{v}}{\nu} \ , \tag{2.10}$$

where D is characteristic length (for instance diameter of a pipe), $\overline{v}$ is average flow velocity, ρ is density, μ is dynamic viscosity and ν is kinematic viscosity.

In a pipe, flow is always laminar for $Re < 2100$, always turbulent for $Re > 4000$, and for Reynolds numbers in between, there is a transition stage [17]. Thereby, laminar flames typically occur at lower fuel velocity.

Laminar burning velocity, s_L, also known as flame speed, is defined as the relative velocity with which the reactants enter the flame, normal to the flame sheet [15]. It is dependent on mixture composition, pressure and temperature, and makes up only part of the velocity of a flame spread relative to its ignition point; the flame propagation. This spatial flame velocity, v_F, is the sum of the laminar burning velocity and the velocity of the unburned gases, v_u, and can be determined using among others the Schlieren technique. It can also be measured, for example using a hot-wire anemometer [14]. The laminar burning velocity can thereby be determined using the relation, $s_L = v_F - v_u$.

Turbulent flames

According to Turns [15] a turbulent flow occurs when "instabilities in a flow are not sufficiently damped by viscous action and the fluid velocity at each point in the flow exhibits random fluctuations." These velocity fluctuations can cause further fluctuations in scalars such as density, temperature and composition of a mixture [14]. A good way to illustrate such flow, is by the use of mean and fluctuating values, applied to for instance velocity. Mean velocity is denoted $\overline{v}$, while velocity fluctuation at time t is denoted $v'(t)$. At all times, the instantaneous velocity, $v(t)$, is defined as the sum of the mean and fluctuating component:

$$v(t) = \overline{v} + v'(t) \ , \tag{2.11}$$

which can be described graphically as in Figure 2.3, based on a figure from Turns [15, p. 425]. Intensity of the turbulent fluctuations is often described by root-mean-square quantities, such as:

$$v'_{rms} \equiv \sqrt{\overline{v'^{\,2}}} \ . \tag{2.12}$$

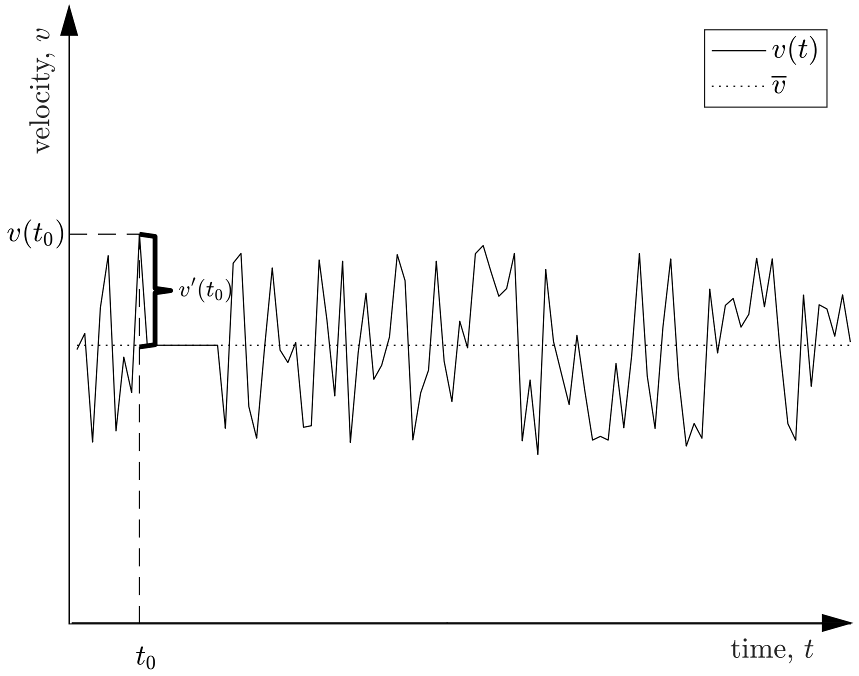

Figure 2.3: One-dimensional velocity at a fixed point in a turbulent flow as a function of time, $v(t)$. Mean velocity, $\overline{v}$, as well as the total velocity and fluctuation at time t_0, are marked on the figure. Based on a figure from Turns [15, p. 425]

The fluctuations in flow parameters result in lateral mixing between the layers of fluid, resulting in vortices, or *eddies*, of varying sizes. This is what characterizes a fully turbulent flow, namely a wide range of *length scales* (eddy sizes) [15]. Reynolds number was already defined in Section 2.1.2, but for turbulent flows it is a measure of the range of length scales, i.e. a larger Reynolds number represents a wider range of length scales present [15]. There are four different length scales, all of which are defined in Table 2.2 in decreasing order of size [15].

Table 2.2: The four different length scales used in modelling of turbulent flows in decreasing order of magnitude, with corresponding description.

Symbol	**Name**	**Description**
D	Characteristic width of flow or macroscale	Upper bound for the largest possible eddies. Defined by the geometry of the system.
ℓ_0	Integral scale or turbulence macroscale	Represents the mean size of the largest eddies in a turbulent flow. Slightly less than D.
ℓ_λ	Taylor microscale	Intermediate length scale related to the mean rate of strain.
ℓ_k	Kolmogorov microscale	Smallest length scale associated with turbulent flow. Representative of the dimension at which the dissipation of turbulent kinetic energy into internal energy occurs.

To describe the degree of turbulence in a flow, turbulence Reynolds numbers based on the last three length scales of Table 2.2 has been proposed, expressed by the root-mean-square velocity.

For the integral length scale, the turbulence Reynolds number is defined as follows [15]:

$$Re_{\ell_0} \equiv v'_{rms}\ell_0/\nu \ . \tag{2.13}$$

The other turbulence Reynolds numbers are defined similarly. The length scales are related as follows [14]:

$$\ell_0/\ell_k = Re_{\ell_0}^{3/4} \tag{2.14}$$

and

$$\ell_0/\ell_\lambda = Re_{\ell_0}^{1/2} \ . \tag{2.15}$$

2.1.3 Heat transfer

The information in this section is collected from *Unit Operations of Chemical Engineering* [17] unless stated otherwise.

Heat transfer between two objects can be summarized by the following statement: "When two objects at different temperatures are brought into contact, heat flows from the object at the higher temperature to that at the lower temperature". There are three different mechanisms of heat transfer, namely *conduction*, *convection* and *radiation.*

Conduction

This is first and foremost a solid phase phenomena, occurring if a temperature gradient exists within an object. To calculate the spatial variation of temperature, Fourier's law is used. For a one-dimensional homogeneous and isotropic object, it is defined in Equation (2.16):

$$q'' = -k\frac{dT}{dx} \ , \tag{2.16}$$

where q'' is rate of heat transfer per unit area, in the direction normal to the surface. The proportionality constant k is thermal conductivity, which is a physical property of the material. Finally, x is distance normal to the surface.

Convection

Convection refers to the heat transfer originating from fluid movement. This mechanism is very important when it comes to fires, as it transports the energy from the hot gases produced by the fire, to the surroundings. There is a distinction between *natural* and *forced convection*, dependent on whether the currents in a fluid is a result from buoyancy due to density differences caused by temperature gradients in the fluid, or whether they are results of some mechanical device, respectively. In a fire, the fluid motion is usually due to the fire itself, i.e. by natural convection, but it can also be induced by an external force, such as wind. The convective flux can be described by Newton's law of cooling as in Equation (2.17):

$$q'' = hdT \ , \tag{2.17}$$

where h is the heat transfer coefficient, and dT is the temperature difference between the surface temperature and the bulk temperature of the fluid, far from the surface.

Radiation

Thermal radiation allows separated objects of different temperature to transfer heat to each other by electromagnetic waves, like the Sun transfers heat to Earth even though it is very far away. It is thereby clear that radiation is an important parameter when studying fire safety, as objects far away from the actual fire are influenced and may even auto-ignite and cause fire spread.

All substances with a temperature above the absolute zero, emit radiation. Some of the radiation that falls on an object will be *reflected*, some *transmitted* and the rest *absorbed*, where the latter is what causes the object to be heated. Radiation heat transfer from an object can be described by the Stefan-Boltzmann law:

$$W = \varepsilon \sigma T^4 \ , \tag{2.18}$$

where W is emissive power or emittance, ε is emissivity, and σ is the Stefan-Boltzmann constant ($5.672 \cdot 10^{-8}\ \mathrm{W} \cdot \mathrm{m}^{-2}\mathrm{K}^{-4}$). The unit of this emissive power is $\mathrm{W} \cdot \mathrm{m}^{-2}$, which thereby corresponds to q''. But in the final expression for radiation between two surfaces, it is important to account for the orientation between them, which can be accomplished by introducing the dimensionless geometric factor, F, often referred to as the *view factor*, incorporating geometric factors such as angle and area. The net heat transfer by radiation between surface 1 and 2, when $T_1 > T_2$, is thereby expressed as:

$$q''_{12} = \sigma F(\varepsilon_1 T_1^4 - \varepsilon_2 T_2^4) \ . \tag{2.19}$$

Radiation between surfaces has now been briefly introduced, but where are these "surfaces" in a fire? Most hydrocarbon diffusion flames are luminous due to glowing soot particles, and the yellow colour people have come to know as the "flame colour" is because of the higher emissivity of these soot particles compared to that of the gas mixture. These particles, made up mainly of elemental carbon, thereby increase the radiation heat transfer of a flame, something we take advantage of in a furnace to make use of the heat. The presence of soot can, however, damage equipment and present a hazard for people's health and the environment.

Heat Release Rate (HRR) in a fire

When quantifying fire hazard, one of the most important tasks is quantifying the size of the fire. This can be determined by measuring the heat release rate (HRR), namely the rate at which heat is generated by the fire. The HRR ($\dot{Q}$) of a fire is measured in Watt ($\mathrm{J} \cdot \mathrm{s}^{-1}$), or rather kW or MW due to magnitude, and is given by the expression in Equation (2.20):

$$\dot{Q} = \Delta h_C \dot{m}_f \ , \tag{2.20}$$

where Δh_C is heat of combustion ($= -\Delta h_R$, see Section 2.1.1) and $\dot{m}_f$ is the mass flow of fuel.

2.2 Fire modelling

To prevent major accidents with loss of life and/or material value, a lot of effort has been put into understanding fire behaviour, by a huge amount of experimental testing. However, full scale testing can sometimes be very difficult and expensive to conduct. With the ongoing development of ever stronger computers, a new way of researching fires has emerged, namely by numerical modelling through different fire simulation software. Fire models can relate chemical and physical processes to each other through mathematical expressions, and thereby estimate the different parameters of a fire [18]. Knowing such parameters is an important factor in deciding which safety devices to install to prevent or control unwanted fires.

There are essentially two types of fire models, namely *zone models* and *field models*. Historically, zone models have been most widely used, due to their simplicity and low computational cost. They divide the domain in two layers (zones), with the upper one containing all the hot combustion products and the lower one filled with cold, ambient air [18]. By considering the conservation of mass and energy, parameters such as layer height and temperature can be calculated. However, these models are likely to be imprecise in their predictions, due to variable averaging in the two zones. Using a field model instead, the resolution is improved by dividing the domain into many three-dimensional control volumes (cells), and the physical changes in each cell is calculated using the fundamental equations of fluid dynamics expressing the conservation of mass, momentum and energy [18]. The process of solving these equations with digital computers is known as CFD. This topic is further described in the next sections, concluded by an introduction to the CFD tools FLACS and FDS.

Computational Fluid Dynamics (CFD)

McGrattan and Miles [19] presents CFD as follows:

> *The starting point for CFD models is the set of partial differential equations that assert conservation of mass, momentum and energy within the fire and throughout the space surrounding it. These equations are solved numerically to yield time-varying predictions of temperature, gas velocity, gas species concentrations and so forth, on a three dimensional mesh of control volumes that spans the geometry being modelled.*

Introducing the governing conservation equations for fluid dynamics is thereby a natural place to start. Their derivations can be found in several textbooks on fluid dynamics, for instance "Computational Fluid Dynamics: the basics with applications" by John D. Anderson, JR [20]. The author specifies that different forms of the equations exists, depending on the flow model on which the fundamental physical principles are applied.

2.2.1 Governing equations

Continuity equation

The continuity equation is derived by applying on a system the fundamental physical principle of *mass conservation*. If it is applied to a infinitesimally small fluid element fixed in space, the resulting form of the continuity equation is the differential conservation form [20] as seen in Equation (2.21):

$$\frac{\partial \rho}{\partial t} + \nabla \cdot (\rho \mathbf{u}) = 0 \ , \tag{2.21}$$

where $\mathbf{u}$ is the local velocity vector and $\nabla\cdot$ is the vector operator called the *divergence*:

$$\nabla \cdot \mathbf{u} = \frac{\partial u}{\partial x} + \frac{\partial v}{\partial y} + \frac{\partial w}{\partial z} \ .$$

Momentum equation

When deriving the three momentum equations, the fundamental physical principle applied to the system is *Newton's second law*, namely that $\mathbf{F} = m\mathbf{a}$. If doing so on a infinitesimally small fluid element fixed in space, the result is the momentum equation on differential, conservation form as stated in Equation (2.22) collected and adapted from McGrattan and Miles [19]:

$$\frac{\partial(\rho\mathbf{u})}{\partial t} + \nabla \cdot (\rho\mathbf{u}\mathbf{u}) = -\nabla p + \rho\mathbf{f} + \nabla \cdot \tau \ , \tag{2.22}$$

where $\mathbf{f}$ represents the body force vector acting on a unit mass of the fluid element, and τ represents shear and normal stresses. The notation ∇p refers to the pressure *gradient*:

$$\nabla p = \frac{\partial p}{\partial x} + \frac{\partial p}{\partial y} + \frac{\partial p}{\partial z} \ .$$

Energy equation

The last fundamental physical principle, on which the derivation of the energy equation is based, is *energy conservation.* There are many ways of expressing this phenomena, which due to its many forms and long expressions are not included here. They are thoroughly presented in Anderson's [20] book on CFD.

Concluding the governing equations

In the CFD literature, one often encounter the term Navier-Stokes equations. Historically, the three momentum equations made up the Navier-Stokes equations, but more recently the term has been expanded to include the continuity and energy equation, and thereby consist of the entire system of equations [20]. The set of five equations now consist of six unknowns (ρ, p, u, v, w and h), meaning that one more equation is needed to close the system. The sixth equation is provided by the equation of state:

$$pM = \rho RT \ , \tag{2.23}$$

where ρ is density, p is pressure, M is molecular weight, T is temperature, and R is the ideal gas constant, approximately 8.314 $\mathrm{J} \cdot \mathrm{K}^{-1}\mathrm{mol}^{-1}$.

This introduces the temperature T as a seventh unknown, which is solved by the thermodynamic relation, $dh = c_p dT$.

When dealing with fire as opposed to dealing with only fluid flow, the objective is usually not to account for the total mass, but for the different species involved, such as fuel, oxygen and products, and the mass conservation equation is thereby often written as a set of transport equations for the mass fractions of the individual species, w_α [19]. An example of the transport equation is presented in Equation (2.24):

$$\frac{\partial(\rho w_\alpha)}{\partial t} + \nabla \cdot (\rho w_\alpha \mathbf{u}) = \nabla \cdot (\rho D_\alpha \nabla w_\alpha) + \dot{m}_\alpha''' \ , \tag{2.24}$$

where D_α is the diffusion coefficient for species α, and $\dot{m}_\alpha'''$ is the source/sink term (rate of production/destruction of species α per unit volume).

2.2.2 Turbulence modelling

In the previous section a closed equation system for laminar flame problems was defined and ready to be solved, and can in principle be transferred to a turbulent flame problem and solved numerically with no modifications, by the method referred to as Direct Numerical Simulation (DNS) [14]. Capturing both the large-scale convection transport of heat and combustion processes, as well as the small-scale diffusive processes in turbulent flows would, however, require a very fine mesh, and thereby a huge amount of computational time [19]. A significant contribution to the computational time is also the time-dependency of the Navier-Stokes solution to turbulent flows, as the solution is not steady [14].

DNS is thereby still not possible for large-scale fire simulations, even with the powerful computers we have today. Even if it was possible, the level of detail in such a solution would be overwhelming, and one would likely have to do a lot of time-averaging to obtain the results of interest [14]. By instead using turbulence models, these averaged properties are obtained directly, and thrown in for good measure is a great reduction in computational time. Some of these models are further described in the next sections.

Reynolds-Averaged Navier-Stokes (RANS)

The information in this section is collected from McGrattan and Miles [19] unless stated otherwise.

For many fire simulations, the approach is to solve a statistically time-averaged form of the governing equations, known as Reynolds-Averaged Navier-Stokes (RANS) . Due to large density variations in combustion processes, a density-weighted average known as the *Favre average*, is also often used. In this context, however, it will suffice to only introduce one averaging method, as the two are very similar.

The idea when Reynolds-averaging is to divide the arbitrary flow property ϕ into a time-averaged component (denoted by an overbar) and a fluctuating component (denoted by a prime), as previously defined by Equation (2.11):

$$\phi(\mathbf{x},t) = \bar{\phi}(\mathbf{x},t) + \phi'(\mathbf{x},t) \ ,$$

and substituting these into the original set of equations. The result is a set of similar equations, see for instance the momentum equation:

$$\frac{\partial(\rho\bar{\mathbf{u}})}{\partial t} + \nabla\cdot(\rho\bar{\mathbf{u}}\bar{\mathbf{u}}) = -\nabla p + \rho\mathbf{f} + \nabla\cdot\bar{\tau} - \nabla\cdot\rho\overline{\mathbf{u'u'}} \ . \tag{2.25}$$

At first glance, the main difference is the overbar on the flow variables, but there is also an extra term on the right-hand side, $\rho\overline{\mathbf{u'u'}}$, known as the *Reynolds stress.* This brings up again the problem of more unknowns than equations, and it is where the term *turbulent transport models* comes up, as they are used to close the set of equations. The idea is that the Reynolds stress is interpreted as turbulent transport, assuming that the fluctuations can thereby be modelled with diffusive terms:

$$\rho\overline{\mathbf{u'}\phi'} = -\rho\nu_T\nabla\bar{\phi} \ , \tag{2.26}$$

where ν_T is called the turbulent exchange coefficient, which essentially is what the turbulence models need to determine [14]. The most widely used turbulence model today is a so-called two-equation model, known as the *k-ε model.* Using this model, two additional transport equations (Equations 2.27 and 2.28, collected and adapted from Warnatz et al. [14]) are solved for the turbulent kinetic energy, k, and its rate of dissipation, ε:

$$\frac{\partial(\rho\bar{k})}{\partial t} + \nabla \cdot (\rho\bar{\mathbf{u}}\bar{\mathrm{k}}) - \nabla \cdot (\rho\nu_T \nabla\bar{k}) = G_k - \rho\bar{\varepsilon} \tag{2.27}$$

and

$$\frac{\partial(\rho\bar{\varepsilon})}{\partial t} + \nabla \cdot (\rho\bar{\mathbf{u}}\bar{\varepsilon}) - \nabla \cdot (\rho\nu_T \nabla\bar{\varepsilon}) = (C_1 G_k - C_2\rho\bar{\varepsilon})\frac{\bar{\varepsilon}}{\bar{k}} \ , \tag{2.28}$$

where C_1 and C_2 are empirical constants dependent on the nature of the problem considered, and G_k is a complicated function of the stress tensor [14]. Knowing these, as well as the empirically determined constant $C_\nu = 0.09$, allows the calculation of ν_T by Equation (2.29):

$$\nu_T = C_\nu \frac{\bar{k}^2}{\bar{\varepsilon}} \ . \tag{2.29}$$

Large Eddy Simulation (LES)

The information in this section is collected from Warnatz et al. [14] unless stated otherwise.

Looking at the largest to the smallest length scales, the scales become more and more independent of geometry, and at some point they can be described by an isotropic model. The intermediate scale above which the flow is geometry-dependent and below which it is isotropic, is called the *filter scale* or *grid scale*. Different methods of turbulence modelling defines this scale differently. For RANS, this scale is the largest length scale, making the fluctuating component of the model account for dynamics of a wide range of scales. DNS, however, sets the filter scale below the Kolmogorov length scale, making the model compute all scales. Between these two methods is the ever increasing use of Large Eddy Simulation (LES), who sets the filter scale somewhere in between, above which it solves the Navier-Stokes equations numerically, and below which turbulence models, such as the k-ε model, are invoked.

2.2.3 Boundary conditions and sources

The equations in the previous sections can be used for all fluid flow cases as well as combustion, even though the flow field in different cases are very different. The reason for this is that *boundary conditions*, and initial conditions, dictate a particular solution to the equations [20]. There are the physical boundary conditions, such as the no-slip condition, saying that if a fluid is flowing past a stationary surface, its velocity at the surface is zero [20]. Another example is mass inlet boundaries, such as air entrainment to the computational domain by natural ventilation or by a mechanical fan [19]. The proper numerical implementation of these boundary conditions, is one of the main subjects in CFD.

Another important subject is the source terms. How are the species transformed from reactants to products? How is soot produced and oxidized? How is convection and radiation heating the surroundings? For these purposes, different simulation tools employ different models. As an example, combustion models such as the Eddy Break-Up model or the Eddy Dissipation Concept (EDC), which is the one used in FLACS and FDS, assumes that the consumption of fuel is controlled by the rate of molecular mixing of reactants, which in turn is proportional to the rate of dissipation of turbulent eddies [19].

2.2.4 Numerical solution

Up until now, several continuous partial differential equations (PDEs) have been presented, being exact representations of the flow conditions at any point in time and space. They do, however, not have any closed form solution in most cases, and need to be approximated. This is where the numerical techniques of CFD enters the picture, and by different discretisation methods, the approximations of the flow parameters can be carried out. The term discretisation means prescribing values of the continuous function on a finite number of points or volumes of the domain [20]. This is why, in a fire simulation, the domain is divided into several smaller control volumes, constituting what is known as a *mesh* or *grid*. An example of a grid point P and its neighbouring points on a two-dimensional grid can be seen in Figure 2.4, based on a figure from Anderson [20, p. 126].

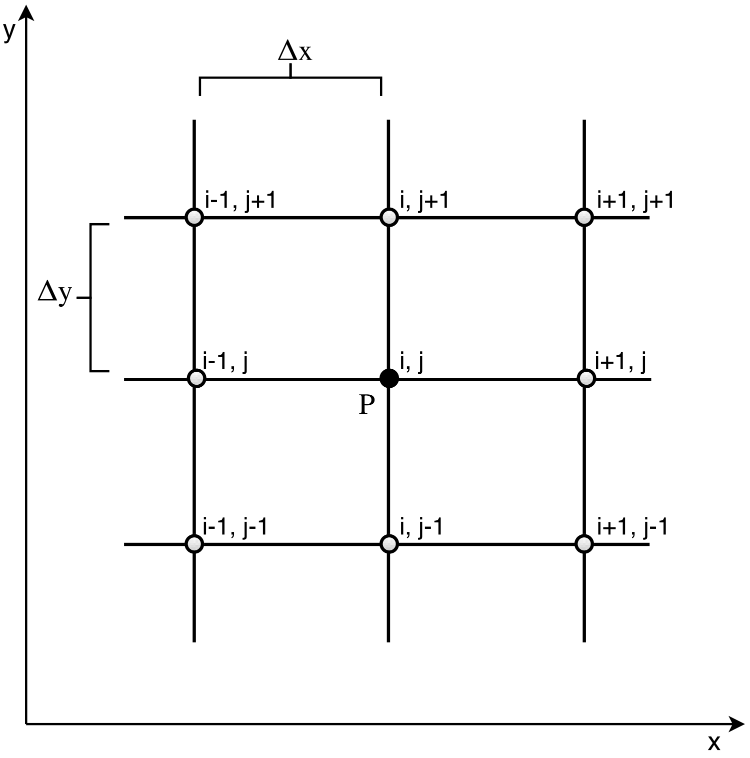

Figure 2.4: Illustration of a two-dimensional grid used for the numerical solution of PDEs at discrete grid points. Point P uses values from its neighbouring points to obtain a solution. Based on a figure from Anderson [20, p. 126]

A method for discretisation of the PDEs is called *finite differences*, and employs a Taylor series expansion at each grid point to generate appropriate finite difference expressions to approximate the partial derivatives of the governing equations [18]. The PDEs are thereby replaced with a system of algebraic equations which can be solved for the flow field variables at the grid points only, by means of a solution algorithm such as the SIMPLE scheme [20].

2.2.5 FLACS

The information in this section about FLACS is collected from the user manual provided with the software [21].

FLACS (FLame ACceleration Simulator) is a CFD code, whose full proprietary rights are held by Gexcon AS. It is developed especially to be applied in process safety issues such as dispersion of flammable of toxic gas, gas and dust explosions, propagation of blast and shock waves, and pool and jet fires. Some scenarios require specialised versions of FLACS, such as FLACS-Fire, which is the software used in this work.

The code Favre-averages the transport equations for mass, momentum, enthalpy, turbulent kinetic energy (k), rate of dissipation of turbulent kinetic energy (ε), mass-fraction of fuel (w_f) and mixture-fraction (ξ) on a structured Cartesian grid, discretizes them using a finite volume method, and solves them using the SIMPLE scheme for compressible flows, and SIMPLEC for non-compressible flows.

The software consists of a pre-processor, CASD (Computer Aided Scenario Design), where the scenarios are defined. It is possible to build geometry using rectangular and cylindrical boxes, or load an existing geometry into the program. In CASD, the user also defines all the input information about grid, fuel, ignition point and so on by using banners in a sidebar. Next, there is a run manager to start and manage the simulations and watch the results as they are ready, and finally a post-processor, FLOWVIS, to plot and visualize the results.

Included in FLACS-Fire are several models to accurately predict parameters of interest, such as combustion rate, radiation and smoke/soot mass or volume fraction. Some models are set as default, but to save computational time, the user may choose to use another model included in the software, or to disregard the associated parameter altogether.

2.2.6 Fire Dynamics Simulator (FDS)

This section is based on the user guide [22] and the technical reference guide [23] provided with the program.

FDS is a free CFD model of fire-driven fluid flow, developed by the National Institute of Standards and Technology (NIST) and VTT Technical Research Centre of Finland, which solves numerically a form of the governing equations appropriate for low-speed, thermally driven flow by the LES-method.

The pre-processing with FDS can be carried out in the separate user interface program Pyrosim, or by simply coding the scenario in an FDS input file, defined with a simple text editor such as Notepad. In this file, all the information about geometry (input as rectangular boxes), grid, fuel, HRR and so on, is specified using namelist formatted records, and the parameters can be integers, reals, character strings or logicals. Next, FDS is the solver, and finally the plotting of results is carried out in the separate accompanying visualisation program, Smokeview.

2.3 Ceiling jets

– Steady flow under horizontal, unconfined ceilings

The information in this section is collected from Alpert's article on ceiling jets [1], unless stated otherwise.

Due to buoyancy, the hot gas of combustion products rises above the fire and impinges on the ceiling, which causes the flow to turn and move horizontally. This causes smoke to spread to other areas further away from the fire, introducing a serious health risk to humans, by issues such as inhalation of poisonous gases, or increased evacuation time due to vision restrictions. It is thereby of great interest to quantify this flow of hot gases with regards to parameters such as temperature and smoke layer height, to be able to provide the most efficient smoke detection system.

A *ceiling jet* is defined as "the relatively rapid gas flow in a shallow layer beneath the ceiling surface that is driven by the buoyancy of the hot combustion products from the plume". The concept can be seen in Figure 2.5, based on a figure from Alpert [1, p. 430], showing an axisymmetric ceiling jet flow at different radial positions, r, beneath an unconfined ceiling with height H above the fire with a HRR of $\dot{Q}$. The device at radial position r is there to illustrate a detector, measuring parameters such as temperature or smoke concentration. As the jet flows radially along the ceiling, the layer grows thicker because of room air entraining at the lower boundary.

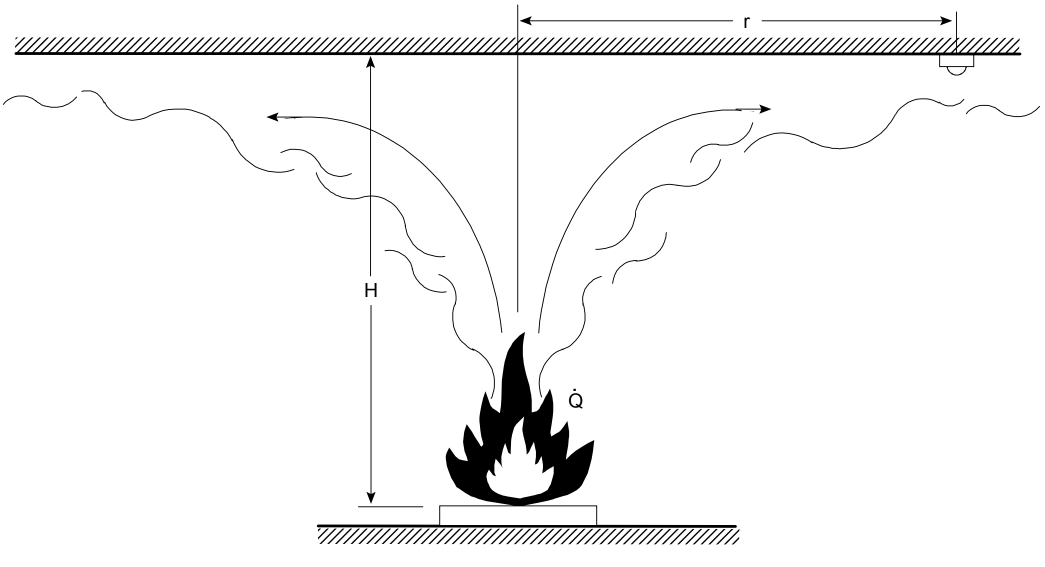

Figure 2.5: Illustration of an idealized axisymmetric ceiling jet at different radial positions, r, beneath an unconfined ceiling of height H, resulting from a fire of size $\dot{Q}$. Based on a figure from Alpert [1, p. 430]

The situation in Figure 2.5 is idealized, and exists only at the beginning of a fire. Later, the combustion gases will accumulate into a stagnant layer of hot gases in the upper part of the compartment, increasing in thickness as time passes by. This is due to continued entraining of colder air at the lower boundary, causing the temperature of the layer to drop and thereby reducing its velocity.

Already in 1972, Alpert started developing a theory to predict gas velocities, gas temperatures and thickness of a steady fire-driven ceiling jet flow. Several idealizations were made, but the correlations should according to Alpert still give reasonable estimates over radial distances of one or two ceiling heights.

2.3.1 Ceiling jet thickness

The thermal thickness of the ceiling jet, ℓ_T, was defined by Alpert [1] as "the distance below the ceiling where the excess temperature above the ambient value, ΔT, drops to 1/e (= 1/2.718...) of the maximum excess temperature". This temperature criterion and other parameters are visualized schematically in Figure 2.6, based on a figure from Motevalli and Marks [3, p. 302] where $\delta_{T_{max}}$ is the boundary layer thickness, located at the temperature maxima. According to Alpert, experiments show that they occur at distances below the ceiling (z) of 1-2 % of the ceiling height for r/H ratios up to 2, and a smaller percentage at higher ratios.

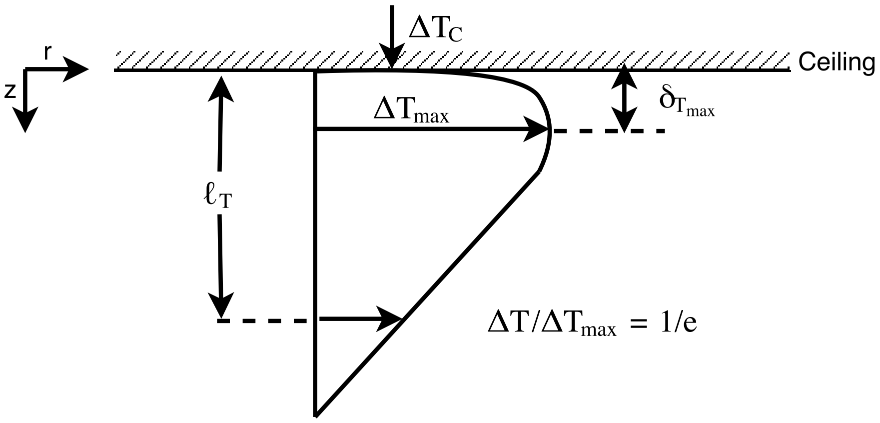

Figure 2.6: Schematic illustration of several temperature parameters in a ceiling jet; boundary layer thickness, $\delta_{T_{max}}$, with corresponding maximum temperature, the ceiling temperature, ΔT_C, and ceiling jet thickness, ℓ_T. Also included is Alpert's temperature criterion for determining ceiling jet thickness; $\Delta T/\Delta T_{max}$ = 1/e. Based on a figure from Motevalli and Marks [3, p. 302]

Based on experiments conducted by Motevalli and Marks [3], Alpert's theory was refined, and the following correlation for thermal ceiling jet thickness ℓ_T was developed:

$$\frac{\ell_T}{H} = 0.112\left[1 - \exp\left(-2.24\frac{r}{H}\right)\right] \qquad \text{for } 0.26 \leq \frac{\mathrm{r}}{\mathrm{H}} \leq 2.0\ . \tag{2.30}$$

Similarly, a momentum ceiling jet thickness, ℓ_V, was developed based on velocity measurements, but since velocities are not measured in the current work, this is not further elaborated.

2.3.2 Temperatures in a weak plume-driven flow field

To quantify the maximum excess temperature at any radial position in a ceiling jet produced by a steady fire, Alpert's correlations are widely used. They are based on fire tests of many different solid and liquid fuels and ceiling heights, with measurements along a wide range of radial positions. For the case of a weak plume, i.e. the flame height, L, is much less than the ceiling height above the fire, H, the correlations are as follows:

$$T - T_\infty = 16.9 \frac{\dot{Q}^{2/3}}{H^{5/3}} \qquad \text{for r/H} \leq 0.18 \tag{2.31}$$

and

$$T - T_\infty = 5.38 \frac{\dot{Q}^{2/3}/H^{5/3}}{(r/H)^{2/3}} \qquad \text{for r/H} > 0.18 \ , \tag{2.32}$$

where temperature T and ambient temperature T_∞ is in °C or K, total HRR $\dot{Q}$ is in kW, and radial position r and ceiling height H is in m. Equation (2.31) applies for the impingement point, where the upward flow towards the ceiling turns to move horizontally. In other words, it is used to calculate the temperature at the ceiling height above the fire, and is thereby independent of radial position. Equation (2.32) applies outside this turning region, as the flow moves horizontally along the ceiling away from the impingement area.

2.3.3 Temperatures in a strong plume-driven flow field

The ceiling jet resulting from a fire with flame height comparable to the ceiling height, or even impinging on the ceiling and extending radially away from the impingement point, is a ceiling jet from a strong fire plume. Strong fire plumes have high excess temperatures or density defects compared to ambient levels, and does not show proportionality between plume radius and ceiling height [4]. In the correlations for weak plume-driven flows as presented in Section 2.3.2, the excess temperature was a function of r/H after a certain radial distance, and can thereby not be used for strong plumes. Heskestad [4] derived an expression for the plume radius at the ceiling level, b, replacing H as a characteristic length scale for the correlations, such that the excess temperature is rather a function of r/b. This plume radius is expressed by Equation (2.33):

$$b = 0.42 \left[(c_p \rho_\infty)^{4/5} T_\infty^{3/5} g^{2/5} \right]^{-1/2} \frac{T_p^{1/2} \dot{Q}_c^{2/5}}{\Delta T_p^{3/5}} \ , \tag{2.33}$$

where $\dot{Q}_c$ is the convective HRR in unit W, which can be assumed to be 70 % of the total HRR, $\dot{Q}$ [4]. The constant g is the gravitational acceleration, which is equal to approximately 9.81 $\mathrm{m \cdot s^{-2}}$ near the Earth's surface. The subscript p refers to the plume centerline, such that ΔT_p is the temperatures directly above the fire, and all temperatures in the equation are in unit K. ΔT_p can be calculated using Equation (2.34) [24]:

$$\Delta T_p = 9.1 \left(\frac{T_\infty}{g c_p^2 \rho_\infty^2} \right)^{1/3} \dot{Q}_c^{2/3} (h - h_0)^{-5/3} \ , \tag{2.34}$$

where h is the height above the fire source and h_0 is the elevation of the virtual origin of the fire source, namely the point at which the plume *appears* to originate, see Figure 2.7 which also illustrates the plume centerline temperature and plume radius.

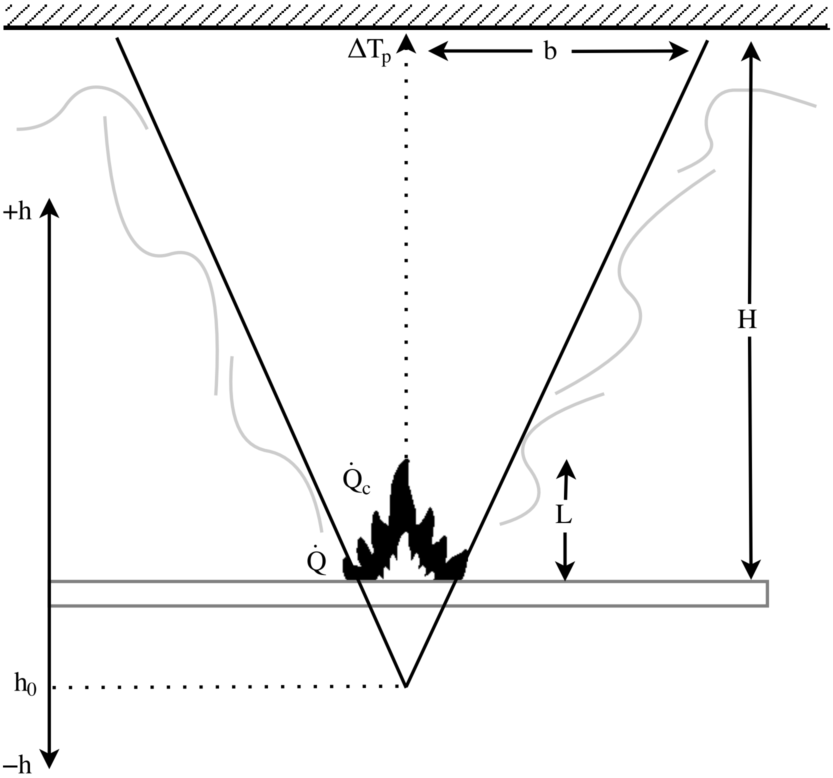

Figure 2.7: Illustration of fire plume characteristics; radius, b, centerline temperature, ΔT_p, and virtual origin, h_0, of a plume resulting from a fire with convective HRR $\dot{Q}_c$ and flame height L.

The virtual origin is only of great importance for predictions near the fire source, and can be assumed to be zero for prediction at high elevations above the fire source [24]. This is the case for the current work, seeing as it is the temperature at the ceiling level which is of interest. In Equation (2.34), h_0 is therefore set to 0, and h is set to the location of the maximum temperature.

With the plume radius b defined, it can be used as the characteristic length scale in the correlation for excess temperature. This is defined by Heskestad and Hamada [4] as in Equation (2.35):

$$\frac{\Delta T}{\Delta T_p} = 1.92 \left(\frac{r}{b}\right)^{-1} - \exp\left[1.61\left(1 - \frac{r}{b}\right)\right] \qquad \text{for } 1 \leq \frac{\mathrm{r}}{\mathrm{b}} \leq 40 \; . \tag{2.35}$$

2.3.4 Heskestad flame height correlation

To identify whether or not the ceiling jets are weak or strong plume-driven, it is necessary to quantify the physical height of the flame, relative to the height of the room. Heskestad [24] defines the mean flame height (L) as the distance above the fire source where intermittency (fraction of time that the flame is above this elevation) has declined to 0.5. His correlation for flame height as defined in Equation (2.36) is widely used, for instance implemented in FDS.

$$\frac{L}{D} = -1.02 + 3.7(\dot{Q}^{+})^{2/5} \; . \tag{2.36}$$

In Equation 2.36, D represents the diameter of the fire source or the effective diameter of a non-circular fire source, which is the case in the current study. Therefore, an effective diameter is used, such that $\pi D^2/4 =$area of fire source. In Equation (2.36), the superscript $+$ represents a non-dimensional quantity, making $\dot{Q}^+$ the non-dimensional HRR, defined by Equation (2.37) [24]:

$$\dot{Q}^+ = \frac{\dot{Q}}{\rho_\infty c_p T_\infty \sqrt{g} D^{5/2}} \ . \tag{2.37}$$

$\dot{Q}^+$ is a representation of the Froude number, relating the jet momentum flow to the buoyant force of the fire, i.e. for low $\dot{Q}^+$ the fire is buoyancy controlled, and for high ones it is momentum controlled [15].

Other definitions of flame height exists, such as temperature thresholds or visual height according to the human eye. In the current work, as measurements are not available, flame heights are calculated by Equation (2.36), thereby following the definition of Heskestad.

Chapter 3

Method and Data

3.1 Experimental work

Empirical correlations, such as Alpert's equations mentioned in Section 2.3, are continuously under development and need to be validated to see that they actually are an appropriate picture of the physical conditions they represent. The same goes for evaluating fire models, and CFD codes such as FLACS and FDS, which are updated regularly. The method of evaluation is comparing physical parameters obtained by simulation or empirical correlations with the same parameters obtained experimentally.

As one of only eight institutions in the world, the Western Norway University of Applied Sciences (HVL) in Haugesund offers a master's degree concerning Fire Safety, and thereby holds a big fire laboratory where fire experiments are conducted. A student enrolled at this programme, Nichlas Lyche, was conducting experiments in the fire laboratory in conjunction with his master's thesis, and kindly invited me along to take part in initial testing and receive results from the actual experiments for comparison with simulations. The experiments are therefore fully conducted by Nichlas Lyche, and the results belong to him.

3.1.1 Experimental setup

The experiments were conducted indoors in the fire laboratory at HVL, where the test facility is built according to the ISO standard 9705 "Room Corner Test". This room is however not used in the current work, as instead a wooden scaffolding was built to support a 2.44x2.44 m ceiling just below the exhaust hood outside the ISO room. To be able to measure the ceiling jet temperature as far as possible away from the fire, the burner was placed under one corner of the ceiling, so that the fire centre was 0.90 m away from the corner, while thermocouples were placed diagonally towards the opposite corner of the ceiling, the first one 0.40 m away from the fire centre and the others with 0.25 m apart. The ceiling height is adjusted by building up the burner with pallets. The over all setup is visualized in Figure 3.1 which, for readability, is without positions and dimensions.

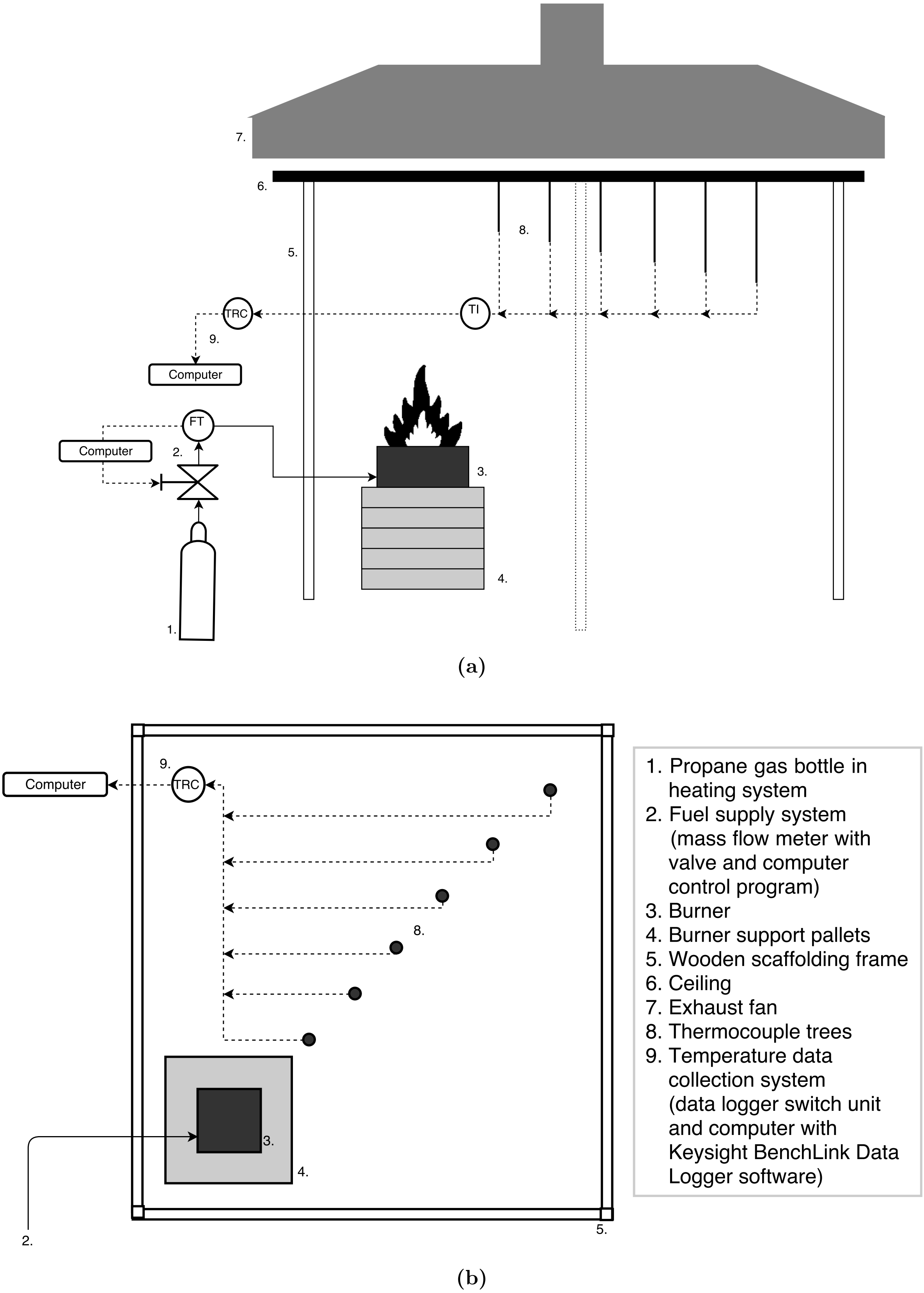

Figure 3.1: Schematic presentation of the experimental setup for temperature measurement of ceiling jets, seen from (a) the side corner and (b) from the top of the ceiling, with numbered elements and corresponding description in the legend.

Fuel supply

The fuel used in the experiments was pure propane gas (C_3H_8), provided to the burner by means of a fuel supply system consisting of a mass flow controller connected to a data program controlling the valve going in to the flow controller, see Figure 3.2. Hereby, the conductor of the experiments can set a desired flow rate in the computer program, making sure that the valve is in the right position by controlling that the mass flow is as desired.

The mass flow controller is of the type Brooks Delta II Mass Flow model SLA5853 (Figure 3.2a) with an accuracy of ±1.0 % of rate. The computer program used to control the system is the software accompanied by the mass flow controller, called Data Logger and Controller Brooks 52xx (Figure 3.2b). The valve is a pressure regulator by GOK, art.no 51 033-00 (Figure 3.2c).

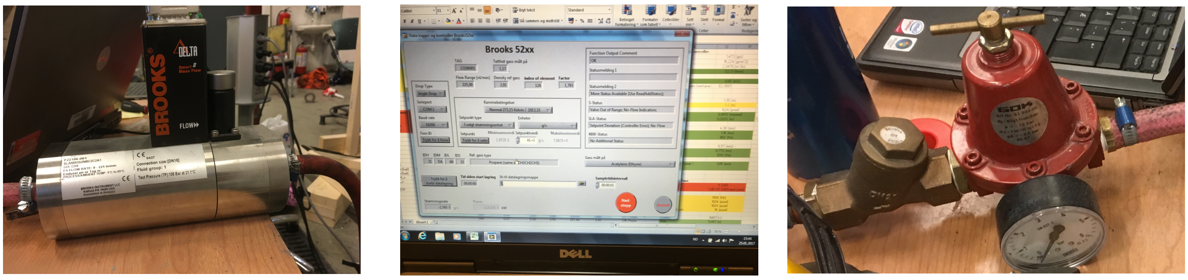

(a) **(b)** **(c)**

Figure 3.2: Fuel supply system for the ceiling jet experiments, consisting of a mass flow controller (a) with accompanying computer program (b) controlling a valve (c).

When gas is drained from the bottle, the pressure inside decreases, causing a temperature drop with ice forming on the outside of the bottle and in the tubes connecting it to the fuel supply system. This causes the system to act poorly, and it was decided to keep as much as possible of the bottle and the tubes in a heating system, see Figure 3.3. This was the drum of an old washing machine filled with water, with only the heat element still operative.

Figure 3.3: Propane gas bottle placed in heating system for optimal performance during the ceiling jet experiments.

Burners

Two different sandbox burners were used in the experiments. The largest (see Figure 3.4a) had a surface of 0.5x0.5 m and a height of 0.26 m, while the smaller (see Figure 3.4b) had a surface of 0.3x0.3 m and a height of 0.11 m. They were both filled with cat litter sand for optimal distribution of propane gas to the surface of the burners. The black substances on top of the burner is material originating from rubber tires, generally used as filling in artificial grass for soccer fields. In these experiments they were used to generate black smoke detectable for camera, as the PhD-student David R.U. Johansen was doing research on smoke movement in the same experiments. Measurements for the current work were started after the clearing of smoke from these rubber substances, which was quite fast (less than a minute).

(a) **(b)**

Figure 3.4: Two different sized sandbox burners used in the ceiling jet experiments, with surface area (a) 0.5x0.5 m and (b) 0.3x0.3 m.

Ceiling height

To vary the ceiling height in different experiments, the height of the burners was adjusted by putting stone pallets underneath, resulting in heights from 0.25 m to 1.52 m above the floor. The stated ceiling heights, measured from the rim of the burner to the ceiling surface, thereby vary from 1.12 m to 2.39 m.

Heat release rate

The size of the fire was to be varied from 44 kW to 176 kW by inputting different mass flow rates to the computer program in the fuel supply system. These mass flows are calculated by Equation (2.20), where the heat of combustion for propane, Δh_C, can be found in literature. In the current work, it is chosen to use the fuel information in appendix B in Turns [15], where the lower heating value (the heat of combustion assuming that none of the water in the products has condensed) of propane is listed as 46.357 MJ/kg. The resulting mass flow rates are listed in Table 3.1.

Table 3.1: Mass flows used to achieve corresponding HRRs during the ceiling jet experiments, calculated according to Equation (2.20).

$\dot{Q}$, kW	**$\dot{m}$, kg/s**
44	$9.49155 \cdot 10^{-4}$
65	$1.40216 \cdot 10^{-3}$
80	$1.72574 \cdot 10^{-3}$
120	$2.58861 \cdot 10^{-3}$
176	$3.79662 \cdot 10^{-3}$

Temperature measurements

To measure temperatures at a wide area below the ceiling, a total of 45 thermocouples (TCs) were placed at various heights in six different radial positions, and thereby grouped in six so-called thermocouple trees, hereby referred to as TC1, TC2 and so on. The placement of the TCs relative to the ceiling and the fire centre is listed in Table 3.2. How it actually looked from below is pictured in Figure 3.5.

The first TC of each tree was placed at the distance below the ceiling assumed to represent the boundary layer thickness, and thereby hold the maximum temperature of the ceiling jet. Knowing that this boundary layer thickness occur at z=1-2 % of H (see Section 2.3.2), it was decided to keep the first TCs of each tree at a distance 2 cm below the ceiling, throughout all the experiments.

To capture the entire temperature profile of each ceiling jet, the distances between the first and second TC had to be varied, so that experiments expected to have a thicker ceiling jet had a larger distance between the first and second TC. The experiments were therefore grouped into three groups of TC arrangements, marked in Table 3.2 with colours red, green and blue.

Due to the fact that ceiling jets increase in thickness as they move radially away from the fire source, it was decided to increase the number of TCs by one for each tree, such that TC1 had five TCs and TC6 had ten. Because of availability, 26 TCs were of size 1.5 mm and 19 of size 1.0 mm, all of which are of unknown type.

Table 3.2: Information about thermocouple placements in the ceiling jet experiments.

Thermo-couple tree	**Radial distance from fire centre, cm**	**Number of TCs**	**Placement of TCX-1 (distance below ceiling), cm**	**Placement of TCX-2 (distance below ceiling), cm**			**Distance between further TCs, cm**
TC1	45	5	2	5	8	13	2.5
TC2	70	6	2	5	8	13	2.5
TC3	95	7	2	5	8	13	2.5
TC4	120	8	2	6	10	15	2.5
TC5	145	9	2	7	10	15	2.5
TC6	170	10	2	7	11	15	2.5

Figure 3.5: Picture towards the roof showing the thermocouple trees, for temperature measurements at different radial positions and distances below the ceiling.

Temperatures were recorded every five seconds by a Keysight 34972A Data Aquisition/Switch Unit (see Figure 3.6), with accompanying computer software Keysight BenchLink Data Logger. The unit has an accuracy of 1 °C, and temperatures were time averaged over an interval of two minutes after steady state was reached. No additional repetitions were carried out.

Figure 3.6: Temperature recorder Keysight 34972A Data Aquisition/Switch Unit used for temperature recording in the experiments.

3.1.2 Overview of performed experiments

Table 3.3 summarizes the ceiling jet experiments performed by Nichlas Lyche at HVL, including the different fire sizes, ceiling heights, burner sizes and TC arrangement. To ease the transition to simulations in FLACS, which require a job number with six digits, each experiment is assigned with a six-digit ID, according to the following system:

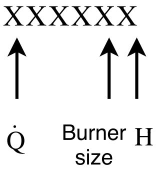

where $\dot{Q}$ is varied from 44 kW (0) to 176 kW (4), H is varied by adjusting the burner height above the floor from 0.25 m (0) to 1.52 m (5) and burner size varies between area 0.25 m^2 (0) and 0.09 m^2 (1). These IDs are also listed in Table 3.3, and will be used when comparing and discussing results.

Table 3.3: Overview of all the experiments performed, with corresponding fire size (HRR), burner area and ceiling height. The different colours represent different arrangements of TCs, where the red one is the narrowest, green is somewhat wider and blue is the widest. Each experiment is assigned a six-digit ID for easy comparison with FLACS simulations.

Fire HRR ($\dot{Q}$), kW	**Ceiling height (H), m**											
	1.12		1.52		1.74		1.94		2.14		2.39	
44	000015	000005		000004	000013						000010	000000
65	100015	100005				100003	100012	100002		100001	100010	100000
80	200015	200005					200012	200002			200010	200000
120		300005	300014				300012	300002			300010	300000
176			400014	400004			400012	400002			400010	400000
Burner area, m^2	0.09	0.25	0.09	0.25	0.09	0.25	0.09	0.25	0.09	0.25	0.09	0.25

3.2 Simulations

3.2.1 Grid sensitivity analysis

It is important to use the optimal grid size for the simulations, which leads to sufficiently accurate results without spending a disproportional amount of time. This was achieved in both FLACS and FDS by varying the grid size from coarse to finer, optimally until the results did not change at all; a so called grid independent result, or at least until the results were sufficiently close to the experimental and empirical results.

The FLACS user manual [21] recommends the following procedure for setting up the grid for dispersion simulations, which will be analogous to fire simulations:

1. Cover the computational domain with a uniform grid.
2. Refine the grid in the region of a jet perpendicular to the jet axis, that is, if a jet flows upwards (in the +Z direction), refine the grid in x- and y-direction close to the jet.
3. Stretch the grid outside the region of interest towards the boundaries.
4. Smooth transitions between larger and smaller grid sizes.

This procedure was performed in FLACS on one of the performed experiments (ID 000004), starting with a coarse uniform grid with little refinement and gradually refining the grid. The tests performed are summarized in Table 3.4, with a visualisation of grids available in Figure 3.7.

Table 3.4: Description of the grids used in grid sensitivity analysis for FLACS, with grid size, degree of refinement and total number of grid cells.

Grid number	Size of uniform grid, m	Core region of interest	Refined grid size, m	Stretching	Total number of grid cells	Figure 3.7 reference
1	0.1	Under the ceiling, refinement in z-direction only.	0.025	None	43200	3.7a
2	0.05	Under the ceiling, refinement in z-direction only.	0.025	z-direction: below burner surface towards floor and above ceiling towards upper boundary.	194936	3.7b
3	0.025	Everything between burner surface and ceiling, uniform grid with no further refinement.	-	z-direction: below burner surface towards floor and above ceiling towards upper boundary. x- and y-direction: outside burner area and monitor region, towards boundaries.	599675	3.7c
4	-	Everything between burner surface and ceiling. Refinement in region perpendicular to the jet-axis.	0.02	All except refinement region is only slightly stretched towards boundaries.	764640	3.7d
5	0.02	Everything between burner surface and ceiling, uniform grid with no further refinement.	-	z-direction: below burner surface towards floor and above ceiling towards upper boundary. x- and y-direction: outside burner area and monitor region, towards boundaries.	1009400	3.7e

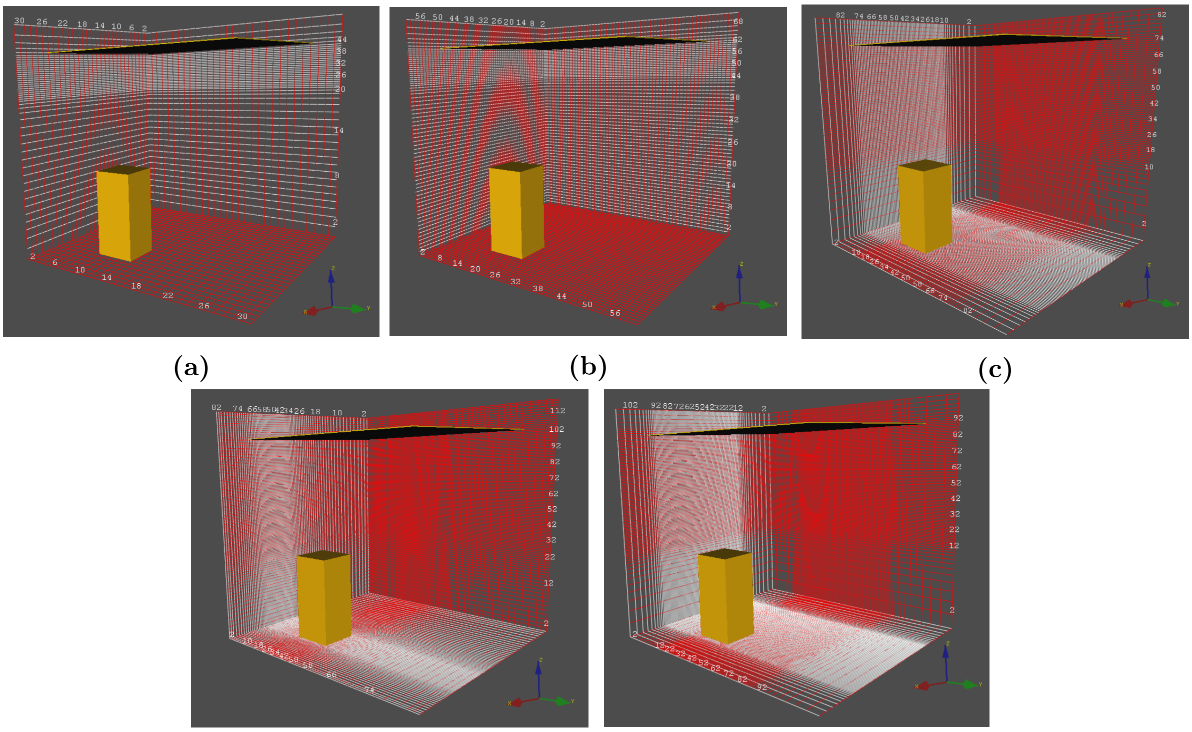
(a)
(b)
(c)
(d)
(e)

Figure 3.7: Grids used in the FLACS grid sensitivity analysis, moving from the coarsest (a) to the finest (e).

Due to limited experience with FDS, it was in these cases decided to keep a uniform grid over the whole domain, with sizes 0.1 m, 0.05 m, 0.025 m and 0.02 m, resulting in total number of grid cells 27000, 216000, 1728000 and 3375000.

3.2.2 FLACS simulations

Once a grid size was decided upon, a total of 33 simulations were executed in FLACS, where all properties of the performed experiments were mimicked by varying several parameters when defining the scenarios in the pre-processor CASD.

Geometry

The geometry of the experiments was recreated in FLACS by the use of two solid boxes, one to represent the roof and one for the pallets plus burner volume. Their placements in the 3x3x3 m domain were calculated based on placements and dimensions from the experimental setup, using the pythagorean theorem for all items along the diagonal. Their placements in the xy-plane can be seen in Figure 3.8, which also includes the placement of the TC-trees.

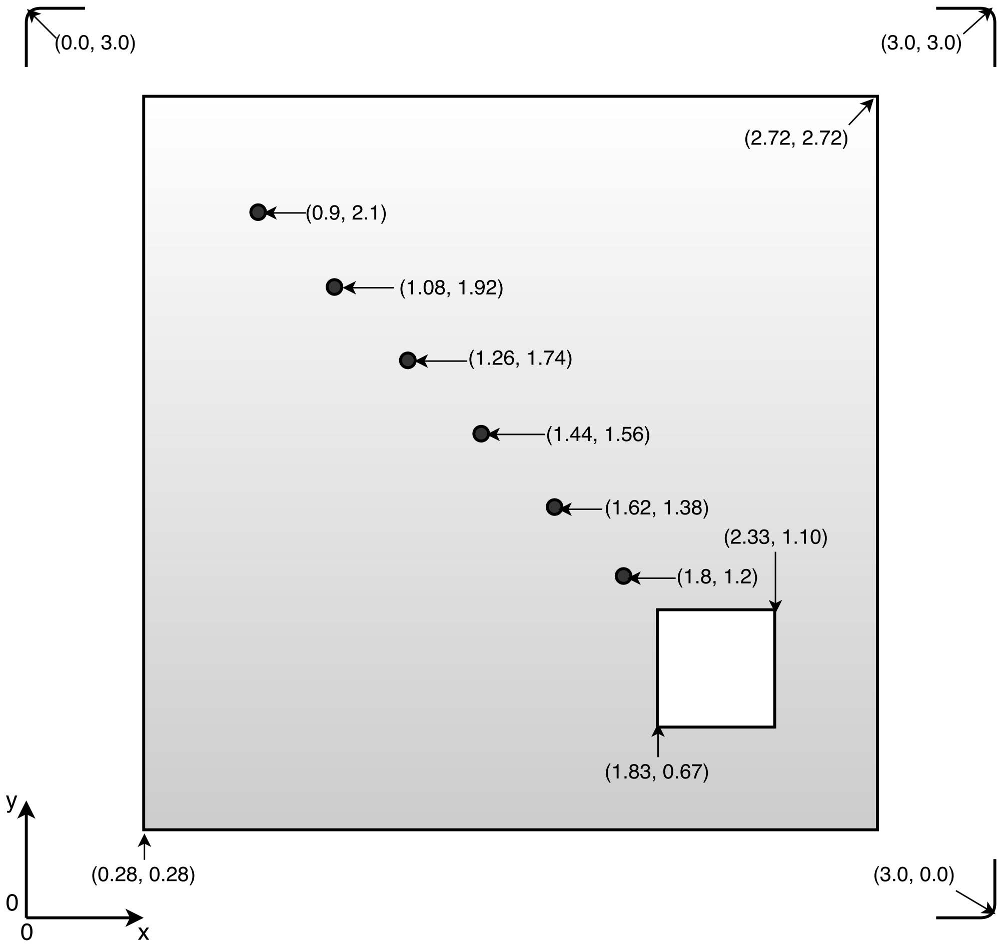

Figure 3.8: Calculated positions for the placement of geometry and thermocouple trees within the computational domain for the cases with burner area 0.25 m^2.

The roof box had dimensions 2.44x2.44x0.01 m, fixed at position (0.28, 0.28, 2.65), while the pallet/burner box, placed at position (1.825, 0.675, 0) for the cross-sectional burner area of 0.5x0.5 m and at position (1.925, 0.775, 0) for the cross-sectional burner area of 0.3x0.3 m, had varying z-dimension to account for the different ceiling height of the experiments. The reason for the slight offset between these positions and the calculated positions as seen in Figure 3.8, is the fact that walls should be aligned with grid lines in FLACS. This is due to the program's porosity calculations, where walls are automatically moved to the nearest grid line, potentially causing problems such as holes between geometry objects. This is mostly a problem for more complex geometries, but even in this simple geometry it is best to follow these guidelines for optimal simulations.

Scenario

The fire scenarios were defined in CASD, using the sidebar for scenario settings, see Figure 3.9, where each tab of the menu can be opened by clicking the arrow on the left hand side. Moving through each tab, the TC arrangement, fuel supply, initial conditions and so on, were set to match the experiments. The next few paragraphs go systematically through these tabs, explaining which parameters were changed, and which were kept as default. An example of the resulting scenario file for FLACS input (cs000004.dat3) can be viewed in Appendix A.

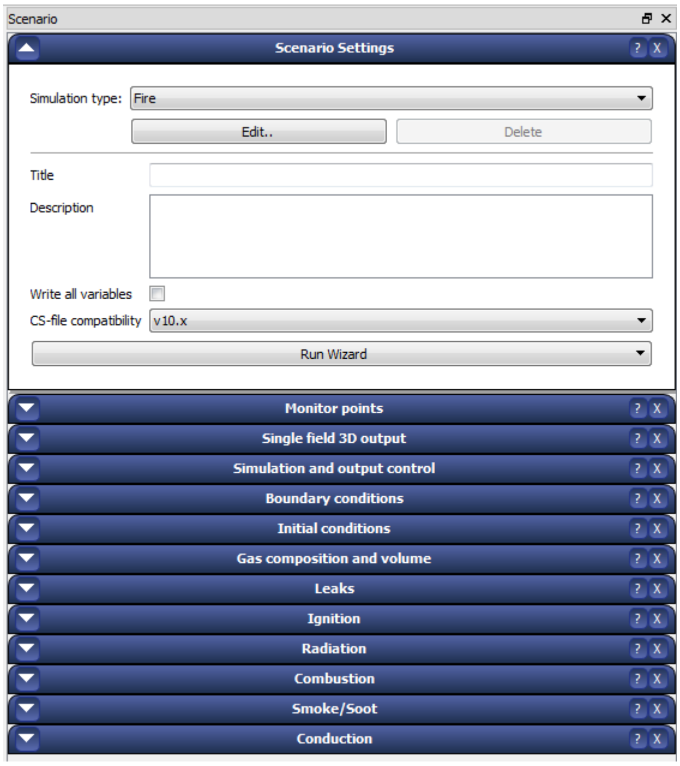

Simulation type: Fire

Title

Description

Write all variables ☐

CS-file compatibility v10.x

Figure 3.9: Scenario Settings sidebar in FLACS's pre-processor CASD. The simulation type is set to 'fire', displaying the default settings which are usually changed during such simulations.

Monitor points

The monitor points are the spatial locations where one or more variables are to be monitored during simulations. In the current work, the main variable of interest is temperature, and the monitor points are in this case supposed to act as the TCs of the simulations. A total of 45 monitor points were therefore placed according to the positions for TC trees in Figure 3.8, and with distances from the ceiling as according to Table 3.2, with some small adjustments to fit inside the control volumes, and not directly on a grid line.

In addition to temperature, these points were also set to monitor other variables, such as velocities, turbulence intensity, soot and so on, to have a basis for comparison for, and maybe then a better understanding of, the temperature results. The complete list of monitored variables is as follows:

- Turbulent length scale
- Temperature
- Turbulence velocity
- Velocity vector
- Mass fraction of SOOT
- Volume fraction of SOOT
- Radiative heat flux
- Convective heat flux
- Total heat flux
- Wall incident heat flux

Single field 3D output

The same variables that can be measured in monitor points, can also be monitored in three dimensions, to allow the user to make plots of spatial distribution of variables, i.e. plot of a two-dimensional cut plane, or a three-dimensional volume plot.

In the current work, the same variables as for the monitor points were chosen, see list in previous paragraph, for the same reasons mentioned above. These output does, however, produce very large files, taking up a lot of disc space. Due to the use of many separate computers in the simulations, and deleting files as they were no longer of interest, this was not a problem in the current work.

Simulation and output control

In this tab, several parameters concerning issues such as size and duration of the simulation are chosen. In the current work, only two values were changed from default, namely TMAX and DTPLOT. TMAX is the simulation maximum time in seconds, and was in all cases set to 20, to allow the flame to be stabilized after ignition and have a good basis for time averaged temperature results. DTPLOT is the time interval for field output in seconds, which was set to 0.2 to obtain a clear picture of the flame's behaviour.

Boundary conditions

The boundary conditions were not changed in the current work, keeping the default 'open' boundary condition for fire simulations, NOZZLE, in all cases.

Initial conditions

The initial values for temperature, turbulence, pressure and so on, are set under this tab. The only non-default value was in this case the initial temperature, which was set to 17 °C, instead of the default value 20 °C.

Gas composition and volume

To make sure that the fuel in the simulations was equivalent to the experiments, the 'Volume fraction' option under this tab was double-clicked and set to 1 for propane, indicating pure propane as fuel.

Leaks

To act as the burner in the simulations, an area fuel leak was defined under this tab. This can be achieved by clicking 'Add', and filling in information about the leak, or by using the so-called 'Leak Wizard'. The latter is more intuitive and user friendly, and was therefore used in the current work. A window pops up, in which one fills out information about the leak.

The position of the leak was set to (1.825, 0.675, $2.64-H$) in the cases with 0.5x0.5 m burners, and (1.925, 0.775, $2.64-H$) in the cases with 0.3x0.3 m burners. This was to ensure that the flame center was in the same position in all cases. The slight offset from calculated positions was to align the leak with grid lines. The leak box size was set to 0.5x0.5 m or 0.3x0.3 m, and the direction was set to +Z, making sure that the gas flows upwards in the domain.

Next was deciding on one of the six different leak types available in FLACS. In the current work, the choice was between 'Diffuse' and 'Jet', and a comparison between the two in some initial testing revealed that the 'Jet' option resulted in much more unstable flames than 'Diffuse', and was therefore ruled out.

The leak rate was entered manually, allowing for a second window with options for area leak shape (elliptic or rectangular), where rectangular was chosen, and leak profile (Gaussian, uniform or parabolic), where a uniform profile was chosen. Lastly, a window with information about leak outlet appears, where leak area was set to 0.25 m^2 or 0.09 m^2, mass flow was entered according to Table 3.1, relative turbulence intensity was set to 0.05 (medium intensity), turbulence length scale was set to 0.05 or 0.03 m (10 % of burner diameter), temperature was set to ambient (17 °C), and leak duration was set to a very large number (1000 seconds), making sure that fuel would be supplied throughout the simulation.

Ignition

A three-dimensional region of size 0.5x0.5x0.5 m directly above the burner was chosen as ignition region, with ignition occurring after 1 second of fuel leakage. This was to make sure that there would be enough fuel in the domain for ignition to take place.

Radiation

Because of its accuracy, the default radiation model used in FLACS-Fire is the Discrete Transfer Method (DTM) model. This calculates radiation in the three-dimensional domain, while the other model, the Six-Flux model, accounts only for heat radiation in the six Cartesian directions [21]. Consequently, the DTM takes a huge part of the computational time, and consumes a lot of disc space. A third, not recommended option, is to switch off the radiation model altogether, causing inaccurate results.

In the current work, the DTM model was chosen as radiation model, leaving all associated parameters as default values.

Combustion

Under this tab, the Eddy Dissipation Concept was chosen as combustion model, because it is the default model recommended by FLACS. Also under this tab, an option FIRESWITCH can be set. Due to problems with flame extinction during initial testing, this option was set to '[2] EDC for coupled pool fires' during all simulations, eliminating the problem.

Smoke/Soot

The most detailed model, the Formation-Oxidation model, is the default one and was therefore chosen in the current work.

Conduction

The default conduction option 'None' was chosen, as the conduction model in FLACS-Fire is not yet validated [21].

3.2.3 FDS simulations

The same number of cases simulated with FLACS (33) were to be simulated in FDS for comparison. Due to no previous experience with FDS before the current work, it was decided to use only very simple setup files, written in the Windows built in text editor 'Notepad', based on one of the example files provided with the software. The next few paragraphs goes through the structure of the setup files, to account for the different elements of the experiments. An example of such a file (000004.fds) can be seen in Appendix B.

Simulation and output control

The line `&HEAD` holds the ID of the simulation, given the same six-digit ID as in FLACS, see Table 3.3. The FDS simulation will then produce output files with this name. Also in the same line is the title of the simulation, set to a short description of the equivalent experiment. Next is the `&TIME` line, where the maximum simulation time was set to 20 seconds.

Grid and domain

The `&MESH` line states the number of grid lines in x-, y- and z-direction and the size of the domain, which in the current work was set to 3x3x3 m.

Geometry

The `&OBST` lines are used to make solid obstacles in the simulations, and two boxes with positions and sizes analogous to the FLACS simulations were made, see geometry paragraph of Section 3.2.2. Due to a small error, the ceiling was placed at height 2.64 m in FDS, as opposed to 2.65 m in FLACS, but this was later found to be non-problematic.

Combustion

The next line, `&REAC` gives information about the chemical reaction taking place in the simulation, so the fuel was set to 'PROPANE', and soot yield to 0.01, meaning that 1 % of the fuel mass would be converted to soot in the reaction. This value was chosen because of its use with a propane reaction in an example file provided with the program.

The next two lines, `&SURF` and `&VENT` are related to the position and size of the fire. HRR per unit area, 'HRRPUA', was varied to desired value as according to Table 3.5, while the position was set to the top of the pallet/burner box, analogously to FLACS.

Table 3.5: Values for HRR per unit area as input on fire size in FDS.

HRR, kW	HRRPUA, kW/m^2 (for 0.5 m burner)	HRRPUA, kW/m^2 (for 0.3 m burner)
44	176	488.89
65	260	722.22
80	320	888.89
120	480	1333.33
176	704	1955.56

Initial and boundary conditions

By the use of line `&MISC`, the ambient temperature was set to 17 °C, to override the default value of 20 °C. Using `&VENT` lines, the boundaries in all directions were set to 'OPEN'.

Monitor points and two-dimensional monitor regions

Analogous to in FLACS, 45 monitor points were created using the `&DEVC` line with ID corresponding to TC names and position according to calculated values. These were set to only monitor temperature, due to the format of the results being too complex if more than one variable was chosen. A single device was also set to monitor CPU (=central processing unit) time, to be able to compare computational time for the different simulations.

Otherwise, several two-dimensional monitor methods are available in FDS, and in the current work it was decided to use boundary files (`&BNDF`) to monitor several variables at all solid boundaries, such as the ceiling. These variables were radiative, convective and net heat flux, as well as wall temperature and burning rate.

The second method for two-dimensional monitoring is by the use of slice files (`&SLCF`), used to monitor quantities at all points of a plane in the domain. In the current work, it was decided to monitor u-, v- and w-velocities in the x- and y-plane over the burner, as well as in the z-plane at the location of the maximum temperatures (2 cm under the ceiling). This was to be able to calculate turbulence intensity in case this would be of interest when analysing the results.

3.3 Post-processing of results

FLACS monitor point outputs are stored in binary r1-files named with the format r1000000.dat3. To be able to use these results for further post-processing such as plotting, the data must be converted to ASCII format. This is achieved using the 'r1file' program by FLACS, and for the file r1000000.dat3, monitor point temperatures can be extracted by typing in the cmd-window of Windows:

```
r1file r1000000.dat3 name=NT force output=000000
```

This creates a temperature file 000000.NT, with temperatures at all monitor points for all timesteps, and was done for all FLACS simulations in the current work.

FDS monitor point outputs are stored in csv-files with no further need of formatting, and the experimental results are stored in DAT-files, also ready for post-processing.

To ease the process of treating the results of experiments and simulations, a MATLAB function `avg_temp.m` was created, see Appendix C. To use the code, one needs to input an existing file name of a certain format (.DAT, .NT or .csv) containing temperature results, as well as the thermocouple placement ('green', 'red' or 'blue', see Tables 3.2 and 3.3) and method ('exp' for experimental, 'FLACS' or 'FDS'). The code will then calculate average temperatures at all locations and place these in a matrix of systematic order, as given below:

TC1-1	TC2-1	TC3-1	TC4-1	TC5-1	TC6-1
TC1-2	TC2-2	TC3-2	TC4-2	TC5-2	TC6-2
TC1-3	TC2-3	TC3-3	TC4-3	TC5-3	TC6-3
TC1-4	TC2-4	TC3-4	TC4-4	TC5-4	TC6-4
TC1-5	TC2-5	TC3-5	TC4-5	TC5-5	TC6-5
0	TC2-6	TC3-6	TC4-6	TC5-6	TC6-6
0	0	TC3-7	TC4-7	TC5-7	TC6-7
0	0	0	TC4-8	TC5-8	TC6-8
0	0	0	0	TC5-9	TC6-9
0	0	0	0	0	TC6-10

Further, the code calculates the ceiling jet thickness at each radial position according to Alpert's temperature criterion, see Section 2.3.2. By storing the results in such a matrix, it is easy to use it further to plot results in MATLAB plots.

Another MATLAB function `plot_temp.m` was made, see Appendix D, to make such plots easily, without having to do any alterations to the MATLAB code for each case. One uses the resulting average temperature matrices from the `avg_temp.m` function on temperature results from experiments, FLACS simulations and FDS simulations, as well as a vector containing the maximum temperatures at each radial position according to Alpert's correlations, see Equations (2.31) and (2.32), which, combined with input about TC arrangement and desired plot title, produces a figure with several subplots of the arrangement as presented in Table 3.6.

Table 3.6: Layout of temperature subplots produced by post-processing code `plot_temp.m` in MATLAB.

	Maximum temperatures at all radial positions	
Temperatures at various distances below the ceiling (z) for thermocouple tree ...	TC1	TC2
	TC3	TC4
	TC5	TC6

Chapter 4

Results and Discussion

4.1 Grid analysis

4.1.1 FLACS simulations

A grid sensitivity analysis was performed in FLACS on case 000004 (with $\dot{Q}$=44 kW, H=1.52 m and burner area 0.25 m^2) on the different grids listed in Table 3.4, where grid number 1 is the coarsest and 5 is the finest. The results for grid numbers 2, 3 and 4 are given in Figure 4.1, whereas grid number 5 was stopped prematurely due to too extensive computing time, and grid number 1 produced no result at all, as it did not ignite at ignition time, one second after simulation start. This was probably due to dilution of the gas, i.e. the gas concentration was under the lower flammability limit in the cells of ignition.

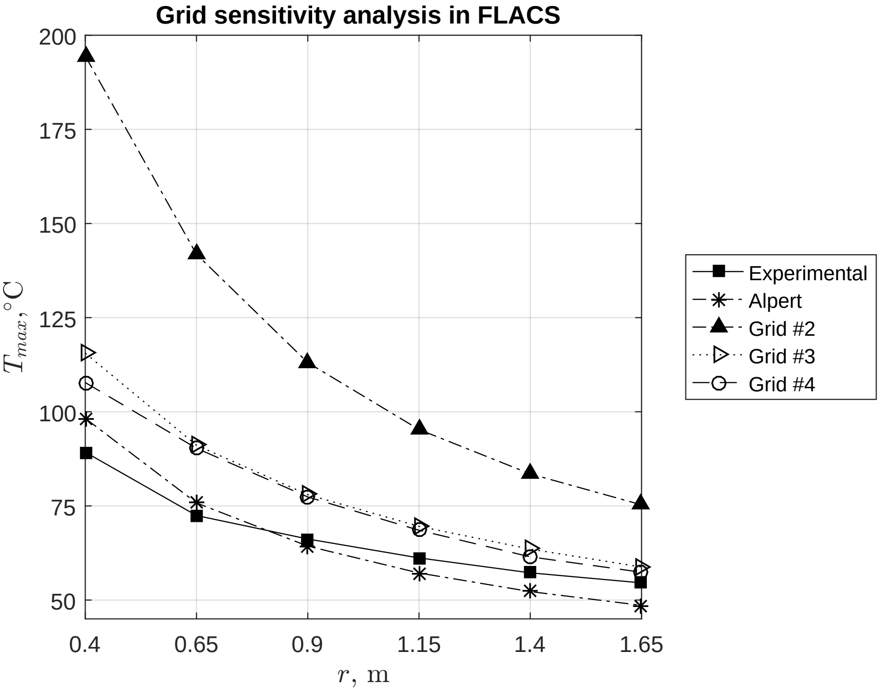

Figure 4.1: Maximum temperature results for case 000004 ($\dot{Q}$=44 kW, H=1.52 m and burner area 0.25 m^2) on three different grid resolutions in FLACS, compared to experimental and empirical values.

It is clear from Figure 4.1 that there is a significant improvement in temperature results from FLACS simulations compared to experimental values, when going from grid number 2 to grid number 3. By looking at 2D slice plots of the results in the post-processor Flowvis, it is possible to compare the velocity vectors and turbulence level of the two simulations. Figure 4.2 shows the temperature field and velocity vectors for the two grid sizes in the fire center at times (a) 9.4 s and (b) 9.8 s, whereas Figure 4.3 shows the turbulence velocity field, i.e. the root mean square of velocity fluctuations [21], at the same position and times.

With the coarser grid, on the left hand side of Figure 4.2, the velocity vectors point straight upwards in the z-direction until reaching the ceiling, where they turn to move horizontally. The flame is stable, with no visible fluctuation from one timestep to the next. This is however not the case in the simulation with the finer grid, on the right hand side of Figure 4.2, where a clear sideways flame movement is visible. At the first timestep, the velocity vectors show a slight tilt towards the negative x-direction, while at the next timestep, they are tilting slightly towards the positive x-direction. This behaviour continues throughout the simulation time, and indicates a higher degree of mixing than in the case where there is no fluctuation in the x-direction.

This indication is further enhanced by Figure 4.3, showing the turbulence velocity. The intensity of the turbulence is clearly more spread throughout the fire plume in the right hand side, while it is centred at the ceiling level on the left hand side. The sideways fluctuation in x-direction from one timestep to another is also clear in this figure.

More fluctuation, and thereby more turbulence, causes a higher degree of mixing and transportation of heat. So instead of accumulating turbulence and heat below the ceiling, the finer grid allows for heat transfer to the lower parts of the compartment, causing the ceiling temperatures to drop drastically, as seen in Figure 4.1.

These fluctuations from side to side as seen in Figures 4.2 and 4.3, might represent the physical oscillations that occur in any fire, or they might be a result of computational instability. There does not exist an analysis method to distinguish between the two, although there are some techniques to provide guidance on how to avoid many of the computational instabilities that are frequently encountered. However, the FLACS user manual [21] describes the phenomena as *puffing*, i.e. oscillatory behaviour of a flame, which occur in pool fires. This is the case in the current simulations, as the option FIRESWITCH was set to '2: EDC for coupled pool fires' (see Section 3.2.2). This effect is only captured with a small enough grid size, and is in the current work thereby only present in grid number 3 and not in grid number 2.

The effect of further refining the grid to 2 cm (grid number 4) is far less significant. In fact, the only noticeable difference is in the results near the flame center, where the temperature is slightly lower with the finer grid. This slightly improved result does, however, not make up for the extra computational time. An attempt was made to measure CPU time, but the simulation stopped due to some technical problems after 12 seconds of simulated fire. Since the simulation then had been running for almost a week, it was decided that this was too slow. All simulations were therefore to be run with grid number 3, differing only in the amount of stretching below the burner surface.

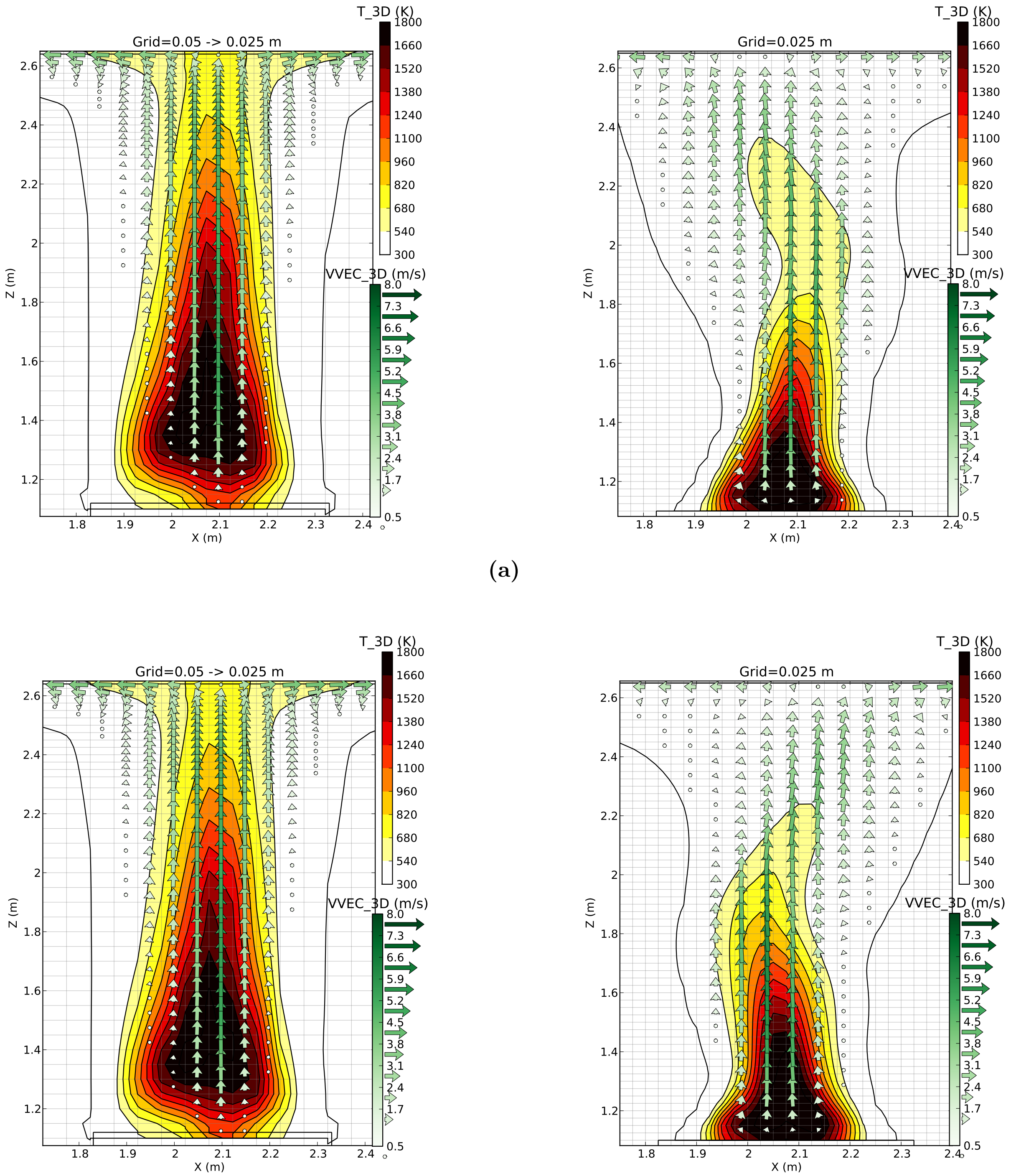

(a)

(b)

Figure 4.2: Two-dimensional slice plots of the fire plume's center temperatures and velocity vectors from FLACS simulations of case 000004 on grid 2 (0.05 m and 0.025 m under the ceiling) to the left, and grid 3 (0.025 m) to the right, at times (a) 9.4 s and (b) 9.8 s.

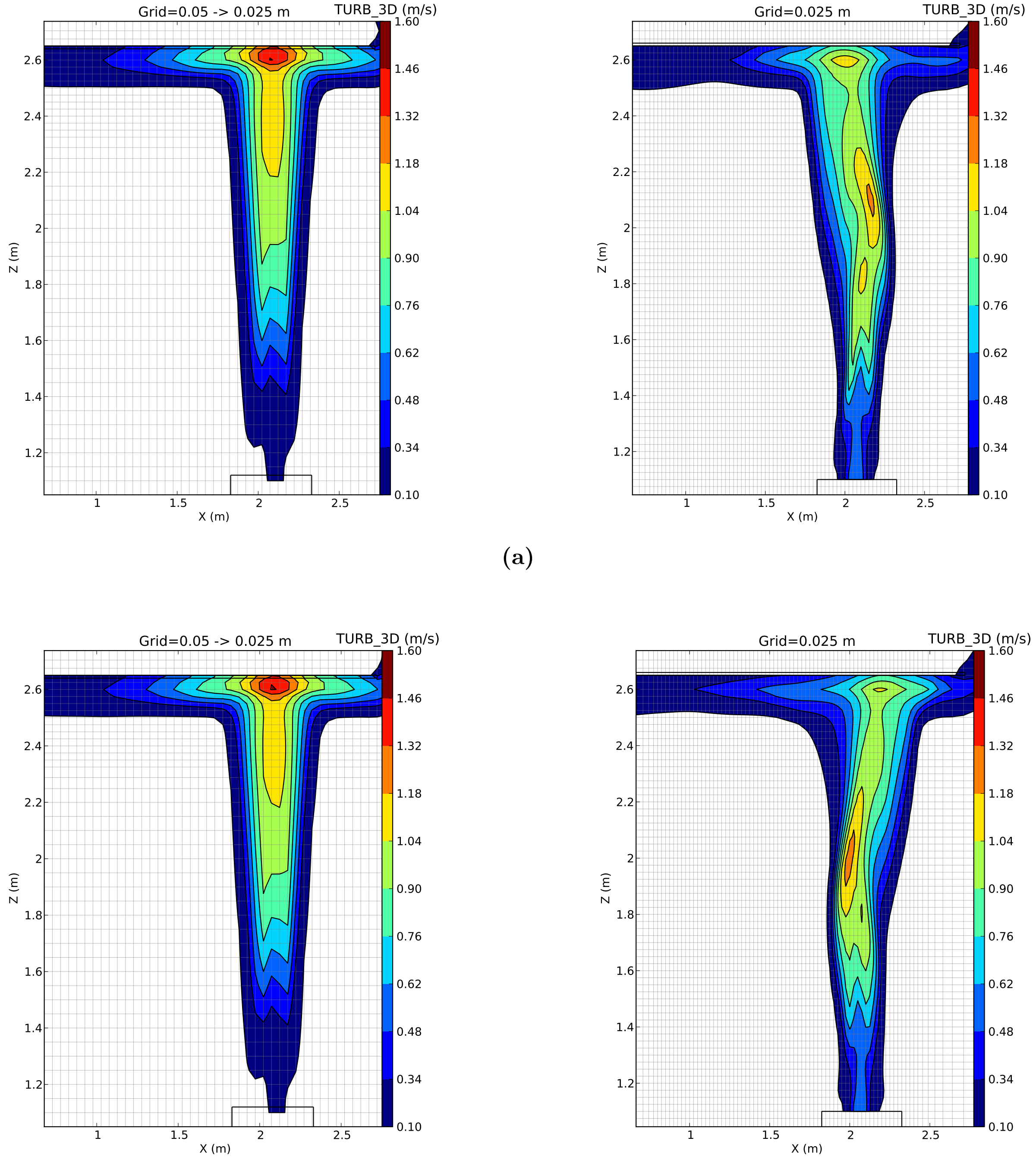

(a)

(b)

Figure 4.3: Two-dimensional slice plots of the plumes' center turbulence velocities from FLACS simulations of case 000004 on grid 2 (0.05 m and 0.025 m under the ceiling) to the left, and grid 3 (0.025 m) to the right, at times (a) 9.4 s and (b) 9.8 s.

4.1.2 FDS simulations

Similar as for FLACS, a grid sensitivity analysis was performed in FDS, comparing results for case 000004 ($\dot{Q}$=44 kW, H=1.52 m and burner area 0.25 m^2) on four different grid sizes from 0.02 m to 0.1 m, with results from the experiment and Alpert's correlation. The result is shown for the three finer grid sizes (0.05 m, 0.025 m and 0.02 m) in Figure 4.4. The coarsest grid (0.01 m) is not included, as several of the monitor points were gathered in the same cell, producing no temperature profile and thereby making no sense physically.

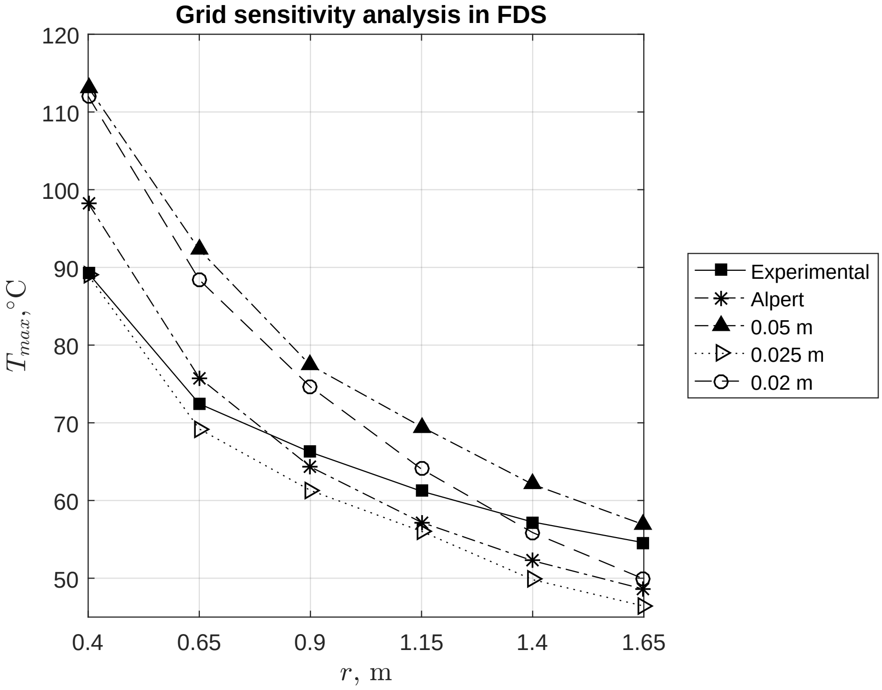

Figure 4.4: Maximum temperature results for case 000004 ($\dot{Q}$=44 kW, H=1.52 m and burner area 0.25 m^2) on different grid sizes in FDS, compared to experimental and empirical values.

The figure shows that there is a clear effect of going from a 0.05 m to a 0.025 m grid, giving about 20 °C lower temperatures at several radial positions. The effect is however not as drastic as for the FLACS simulations, where the temperature difference near the fire center is close to 80 °C for the two grid sizes. More surprising is the results for 0.02 m grid, as they again show higher temperatures, very similar to the 0.05 m grid in the first three data points. It is important to remember that for both FLACS and FDS, changes to the grid mean changes to the monitor points, as temperatures are measured in the entire cell in which the monitor point is located, and not in the exact point specified. This might explain the behaviour seen in Figure 4.4, where the results for 0.025 m grid overall resembles the experimental results the most. Even more so, they highly resemble the empirical results, where the largest deviation is only about 10 °C. It is important to bear in mind that the temperature results from the experiments by no means can be considered as the "correct" answer, as there are several uncertainties in the measurements. Figure 4.4 suggests that the empirical correlation might be more correct in this case, and that FDS in that case predicts the temperatures very well on a 0.025 m grid.

Based on the discussion above, it was decided to run all cases on a uniform 0.025 m grid. Later on, it was discovered that there exists an "FDS Mesh Size Calculator" online [25], created by one of the developers of FDS, Kristopher Overholt. Its purpose is to generate a `&MESH` line for input in an FDS file, but it also gives guidance on grid resolution and what will be considered a coarse, moderate or fine grid in any case. To do so, it uses a plume resolution index, $D^*/\delta x$, being the number of grid cells of length δx that span the characteristic diameter, D^*, of the fire. This characteristic diameter is defined as follows:

$$D^* = \left(\frac{\dot{Q}}{\rho_\infty c_p T_\infty \sqrt{g}} \right)^{2/5} . \tag{4.1}$$

When $D^*/\delta x = 4$, the grid is considered coarse, when $D^*/\delta x = 10$ it is considered moderate, and when $D^*/\delta x = 16$ it is considered a fine grid [25]. It is emphasised that this is only a rule of thumb, and that a grid sensitivity analysis should always be performed. It is still interesting to see if the grid chosen for the current work is considered coarse. The only variable in Equation (4.1) changing in the current work is the HRR ($\dot{Q}$), so a table with the five different HRRs with corresponding characteristic fire diameter, plume resolution index and grid characterisation is provided in Table 4.1.

Table 4.1: Characterisation of the grid chosen for FDS simulations (with $\delta x = 0.025$ m), based on plume resolution index $D^*/\delta x$, where D^* is characteristic fire diameter corresponding to the different HRRs, $\dot{Q}$.

$\dot{Q}$, kW	**D^*, m**	**$D^*/\delta x$**	**Grid characterisation (coarse, moderate, fine)**
44	0.28	11	Moderate
65	0.32	13	Moderate
80	0.35	14	Moderate/fine
120	0.41	16.5	Fine
176	0.48	19	Fine

From Table 4.1 it is clear that a grid size of 0.025 m is considered 'moderate' or 'fine' for all HRRs. A 'fine' grid for the case analysed in Figure 4.4 would require a grid size of $\delta x = 0.0175$ m, which was tested later on, giving almost identical results as grid size $\delta x = 0.02$ m, and thereby further away from experimental and empirical results. This should probably have been tested for more cases, but since the number of experiments is so big, and there are three parameters that vary, it would be too extensive to do a grid analysis on all cases. It is also important to remember that grid refinement means increased CPU-time, and refining only from 0.025 m to 0.02 m in FDS resulted in going from a CPU-time of $2.507 \cdot 10^4$ to $6.057 \cdot 10^4$ s, which is more than double. For all the reasons listed, a grid size of 0.025 m was considered to be fine enough for all cases.

4.2 Temperature fluctuations

The numerical temperatures in the grid sensitivity analysis are mean temperatures from a 20 second long simulation, excluding the first five seconds because of ignition processes and unsteady-state. It is, however, important to realise that the instantaneous temperatures fluctuate greatly, see for instance Figure 4.5, showing instantaneous and mean temperatures at the location of TC1-1 in FLACS and FDS versus mean experimental temperature for the 300010 case (with $\dot{Q}$=120 kW, H=2.39 m and surface area 0.09 m^2). It is clear that there are some very large fluctuations in both directions, from about 30 °C to 300 °C. The fluctuations are more dramatic for FDS than FLACS, especially in the direction towards lower temperatures, thereby resulting in a lower mean temperature closer to experimental value. In Figure 4.5 the dotted line for FDS is located directly below the solid line for experimental mean temperature. The standard deviations, σ, are 34.49 °C for FLACS and 42.76 °C for FDS.

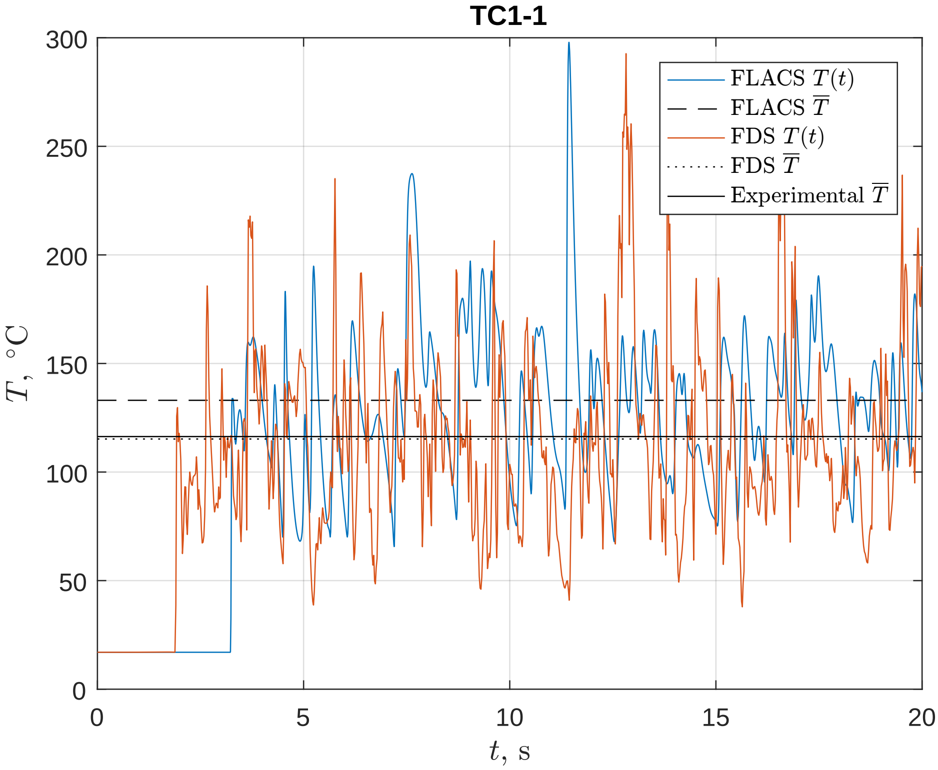

Figure 4.5: Instantaneous and mean temperatures in location TC1-1 for case 300010 ($\dot{Q}$=120 kW, H=2.39 m and surface area 0.09 m^2) from FLACS and FDS, compared to experimental mean temperature.

The experimental temperature, recorded every five seconds over two minutes, also show some fluctuation despite the assumption of steady state, see Figure 4.6. The values vary from slightly above 100 °C to slightly above 120 °C, corresponding to a standard deviation σ=5.01 °C, and thereby show far less variation than the numerical fluctuations. Looking at the plot, it is evident that the first five measurements are slightly lower than the rest, resulting in a lowering of the mean value by about 2 °C. This introduces a suspicion that the recordings were started before steady state was reached, and that experimental temperatures generally might be highly uncertain.

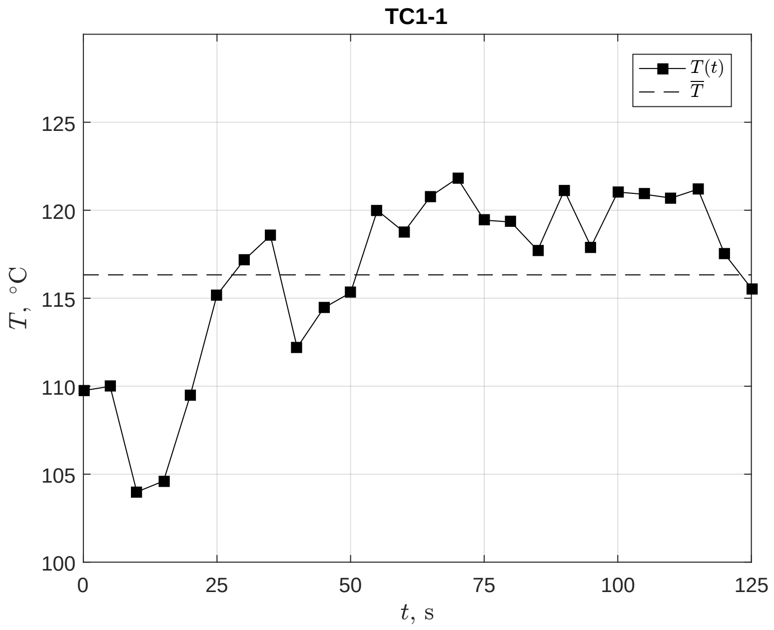

Figure 4.6: Instantaneous and mean experimental temperatures in location TC1-1 for 300010 ($\dot{Q}$=120 kW, H=2.39 m and surface area 0.09 m^2).

Figures 4.5 and 4.6 represent only one TC in one case, but as several more cases are researched, the same tendencies are found, to a variable degree; for TCs close to the ceiling and fire center, FDS fluctuates more than FLACS, resulting in lower mean temperature. Moving away from these locations, the behaviour looks a little different, see Figure 4.7 for location TC5-3, and Figure 4.8 for location TC6-10.

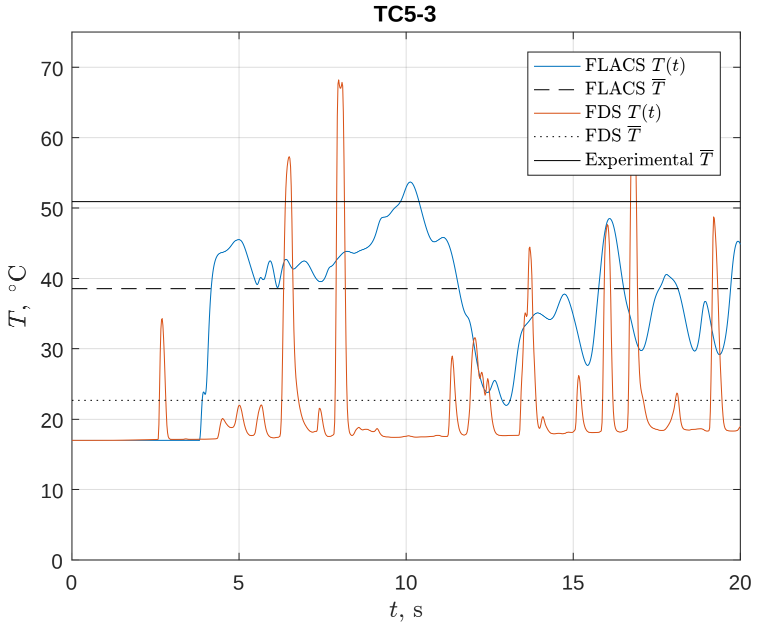

Figure 4.7: Instantaneous and mean temperatures in location TC5-3 for case 300010 ($\dot{Q}$=120 kW, H=2.39 m and surface area 0.09 m^2) from FLACS and FDS, compared to experimental mean temperature.

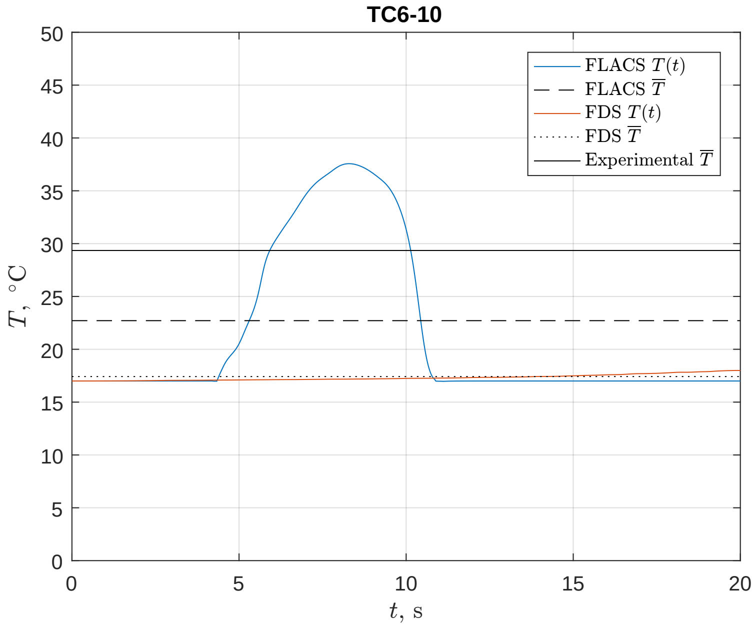

Figure 4.8: Instantaneous and mean temperatures in location TC6-10 for case 300010 ($\dot{Q}$=120 kW, H=2.39 m and surface area 0.09 m^2) from FLACS and FDS, compared to experimental mean temperature.

The fluctuations in location TC5-3 (Figure 4.7) are far less than in TC1-1, especially for FDS, where there are some large peaks towards high temperatures, but the 'baseline' is at room temperature, resulting in a very low mean temperature. FLACS exhibits more of a random fluctuation, with some peaks in both directions. Moving even further away, to location TC6-10 (Figure 4.8), which is the measuring point furthest from both fire center and ceiling, FDS shows no fluctuation at all, and is fixed at room temperature. FLACS exhibits an initial 'wave' of heat between five and ten seconds, followed by a settling towards room temperature for the rest of the simulation. Consequently, the mean temperature is higher for FLACS than for FDS, but still lower than the experimental mean. Looking at Figure 4.8 raises a suspicion that the temperature from FLACS would also settle at room temperature permanently, such that increasing the simulation time would lower the mean temperature drastically. In this way, the current calculated mean temperature from FLACS would not be representative. This behaviour is found for several cases.

The fluctuations and uncertainties presented in this section, are important to bear in mind when discussing the rest of the results, as from now on only mean temperatures are used.

4.3 Plume characterisation

For all experiments, flame heights were calculated using the Heskestad flame height correlation as given in Equation (2.36). The resulting flame heights were compared to the ceiling height to decide whether the ceiling jets resulted from a weak or strong fire plume. Since no rule of thumb was found, on which ratio classifies a strong jet, a decision had to be made based on comparisons of Alpert's temperature correlations (Equations 2.31, 2.32 and 2.35) with experiments and simulations. It was decided that all flame height to ceiling height ratios over 0.75 were to be considered strong, as well as all cases with $\dot{Q}$=176 kW. All other cases were to be considered as weak plume-driven ceiling jets. These results are summarised in Table 4.2, where the cases concluding with a strong plume also continue to list plume centerline temperature difference, ΔT_p, calculated by Equation (2.34) and plume radius, b, at the location of temperature maxima, calculated by Equation (2.33). These are thereby ready for use as input in the strong plume temperature correlation, Equation (2.35).

Table 4.2: Calculated values for Heskestad flame height, L, for all experiments, resulting flame height to ceiling height ratio, L/H, and a characterisation of whether the plume is considered weak or strong. For strong plumes, calculated plume centerline temperature difference (ΔT_p) and radius at location of thermal boundary layer (b) are also listed.

ID	**Heskestad flame height (L), m**	**L/H**	**Plume characterisation**	**ΔT_p, K**	**Plume radius (b) at thermal boundary layer, m**
000000	0.446	0.19	Weak	-	-
000004	0.446	0.29	Weak	-	-
000005	0.446	0.40	Weak	-	-
000010	0.676	0.28	Weak	-	-
000013	0.676	0.39	Weak	-	-
000015	0.676	0.60	Weak	-	-
100000	0.618	0.26	Weak	-	-
100001	0.618	0.29	Weak	-	-
100002	0.618	0.32	Weak	-	-
100003	0.618	0.36	Weak	-	-
100005	0.618	0.55	Weak	-	-
100010	0.848	0.35	Weak	-	-
100012	0.848	0.44	Weak	-	-
100015	0.848	0.76	Strong	269.47	0.171
200000	0.722	0.30	Weak	-	-
200002	0.722	0.37	Weak	-	-
200005	0.722	0.64	Weak	-	-
200010	0.952	0.40	Weak	-	-
200012	0.952	0.49	Weak	-	-
200015	0.952	0.85	Strong	309.48	0.177
300000	0.950	0.40	Weak	-	-
300002	0.950	0.49	Weak	-	-
300005	0.950	0.85	Strong	405.54	0.190
300010	1.180	0.49	Weak	-	-
300012	1.180	0.61	Weak	-	-
300014	1.180	0.78	Strong	241.84	0.227
400000	1.202	0.50	Strong	145.65	0.324
400002	1.202	0.62	Strong	206.89	0.281
400004	1.202	0.79	Strong	312.19	0.241
400010	1.433	0.60	Strong	145.65	0.324
400012	1.433	0.74	Strong	206.89	0.281
400014	1.433	0.94	Strong	312.19	0.241

4.4 Temperature comparisons

Temperatures were post-processed and plotted as described in Section 3.3. For all plots of temperature results from experiments versus simulations and empirical correlations, in the same order as given in Table 4.2, see Appendix E.

It is a clear tendency among the maximum temperatures at different radial positions, that Alpert's maximum ceiling jet temperature correlations result in temperatures slightly above experimental values, rarely deviating with more than 20 °C, and usually even less. Next are the temperatures from FDS, closely resembling the correlations, strengthening both of their validity. FLACS usually produces the highest maximum temperatures, giving cause for concluding that these are over-predicted. However, in a safety aspect, an over-prediction is 'better' than an under-prediction, because it leads to more conservative measures. Also important to remember, is the fact that devices are usually placed several centimetres below the ceiling surface, and that an over-prediction at one location might not be problematic if the temperatures are more accurate further below.

One possible explanation for the temperature differences between FLACS and FDS might be found by studying the heat flux at solid surfaces. Using Flowvis for FLACS and Smokeview for FDS, the three-dimensional domain can be studied with regards to *incident* net surface heat flux (convection and radiation), which for case number 000004 is visualised for time t=20 s in Figure 4.9, where (a) is from FLACS and (b) is from FDS. Due to a visualisation problem with thin walls in Flowvis, the heat flux is only visible on the top of the ceiling, although representing the same heat flux as from below [26].

From the figure it is clear that for both FLACS and FDS, the majority of heat falling on a surface happens from the fire to the burner surface, with the main difference between the two codes being the circular shape of the heat flux in FLACS versus the quadratic shape in FDS. Looking at the ceiling, however, there are some differences in net heat flux between the two codes. In FLACS, the total heat incident on the ceiling ranges from 2.5 up to 5 kW/m^2, which is more than for FDS, where it ranges from about 1 to 4 kW/m^2. Since the fires are defined with the same HRR for both simulation tools, this implies that more heat is transferred to the ceiling surface in FLACS, thereby resulting in higher temperatures along the ceiling. Also, the heat seems to be spread further radially along the ceiling in FLACS than in FDS.

In FLACS, there is an option of defining thermally active walls and adding materials by defining their properties [21]. The user guide of FDS [22] also states that properties like conductivity, density, specific heat and emissivity should always be specified for any solid material. Since these properties were unknown for the material used in the experiments, they were not specified in the current work. The solids were therefore left with default properties, such as an emissivity of ε=0.9 in FDS, and ε=0.85 in FLACS. These numbers are probably both a bit high, resulting in too much energy reflected and emitted as thermal radiation from the ceiling to the rest of the compartment.

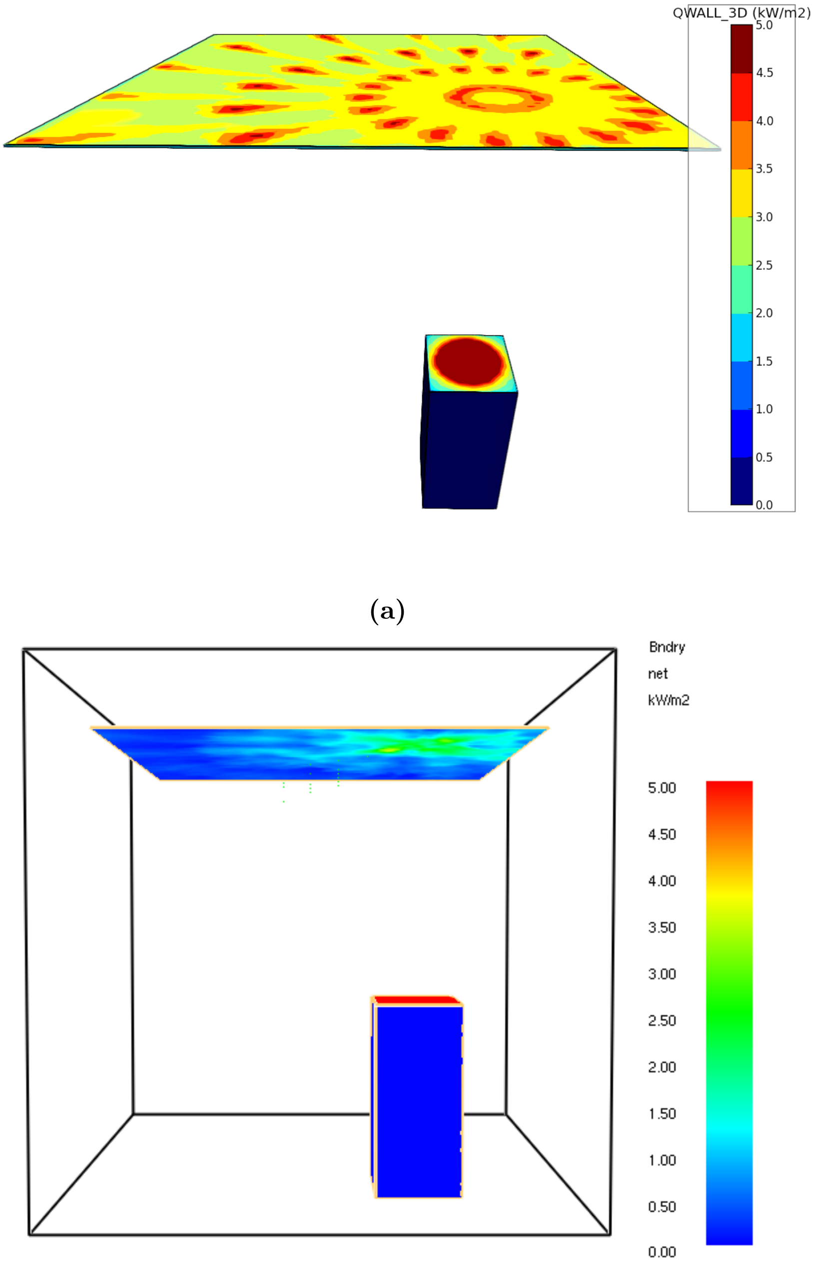

(a)

(b)

Figure 4.9: Net heat flux (convection and radiation) on surfaces for the 000004 case ($\dot{Q}$=44 kW, H=2.39 m and burner surface area 0.25 m^2) in (a) FLACS and (b) FDS.

The temperature difference might be explained by this difference in net heat flux in the two codes, as there are several methods and degree of sophistication for modelling of heat transfer. An important part of this modelling, is the level of turbulent mixing. The turbulence level in FLACS has already been investigated in the grid sensitivity analysis, but FDS has in the current work not yet been studied with regards to turbulence. FDS does not have an output value of turbulence velocity, turbulent kinetic energy, rate of dissipation etc., like FLACS does, so the turbulence level must be studied via velocities. Velocities are visualised with vectors along a slice in the xz-plane in Figure 4.10, where the legend in (a) has magnitudes of velocity in x-direction, and at time 19 s, while (b) is with magnitudes of velocity in z-direction, and at time 20 s. Due to the resolution of the images, the legend is not very clear. It is therefore important to know that there is a difference in the legend units between the two, before comparing them, as the u-velocity in (a) is in $\mathrm{m \cdot s^{-1}}$, while the w-velocity in (b) is in $10^{-2}\ \mathrm{m \cdot s^{-1}}$.

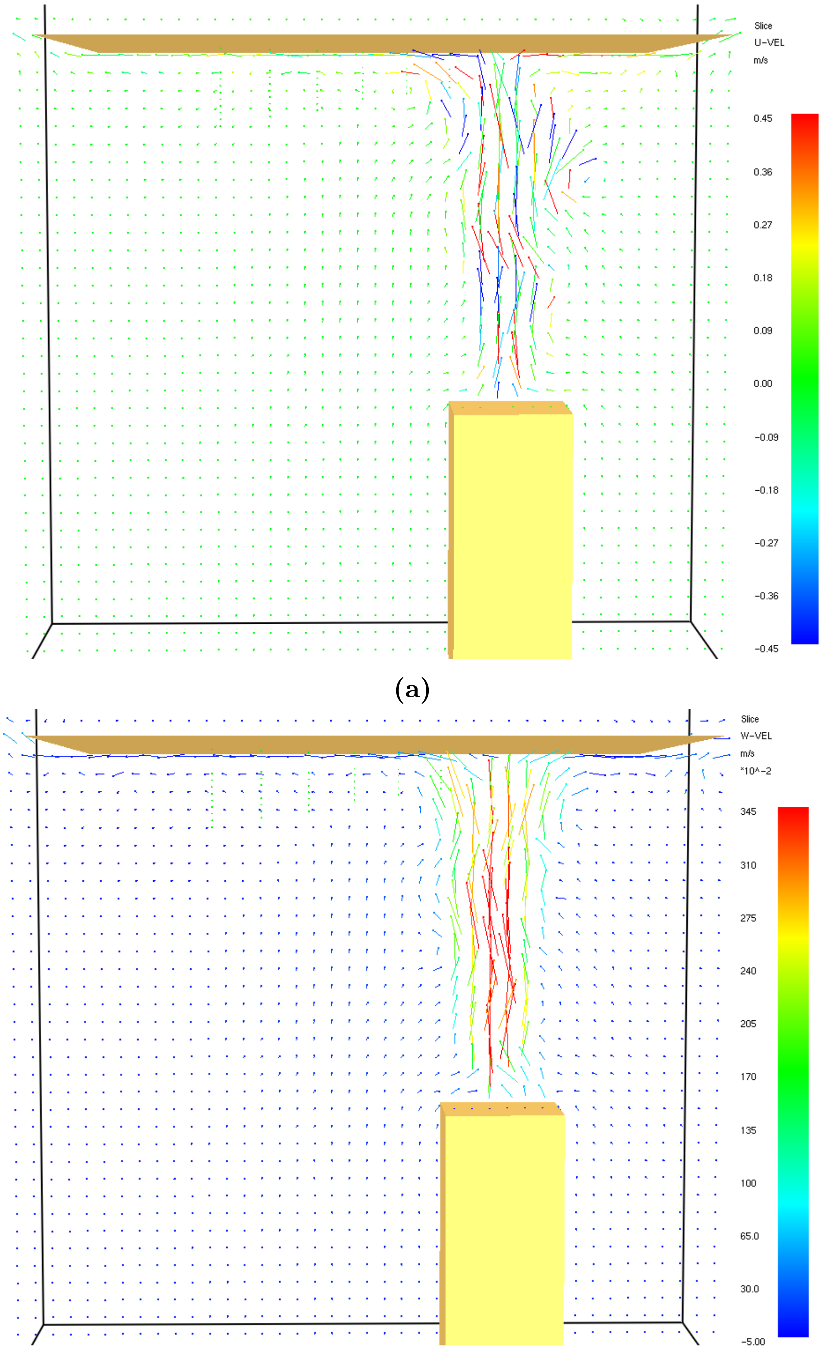

(a)

(b)

Figure 4.10: Two-dimensional slice plots of velocity for the 000004 case ($\dot{Q}$=44 kW, H=2.39 m and burner surface area 0.25 m^2) in FDS, where the different colours of the legend represent in (a) u-velocity and in (b) w-velocity. Velocity vectors are also included, and (a) is at time 19 s and (b) is at time 20 s.

Figure 4.10 shows that the velocity in z-direction is up to approximately ten times higher than in x-direction. The u-velocity profile suggest a high degree of fluctuation and random movement, as velocity in both positive and negative x-direction is represented to a high degree. Also, fluctuations in time is visible when comparing the vectors at the two different times. This indicates that the colder room air is well mixed with the hot combustion products in the plume. Whether or not there is *more* mixing here than it was with FLACS is difficult to say, but if that is the case, it might be the explanation for the lower ceiling heat flux and thereby lower temperatures with FDS.

In buoyancy driven fires, the contribution of buoyancy to turbulent mixing is important, and as described in the introduction chapter, Nam and Bill [6] solved the problem with temperature over-prediction by adding to the turbulence model a term for production of turbulence kinetic energy generated by buoyancy, as well as changing constants used in the turbulence model. This production of turbulence due to buoyant forces, is modelled in FLACS by a simple gradient model, and there are several constants used in the turbulence model. It might be an idea to look into these factors, to see if changing them will result in more accurate results.

Chatterjee et al. [11] also experienced an over-prediction of temperatures, but mostly for flames impinging on the ceiling. They suggested further investigation of several model features to improve accuracy. In the current work, it was not recorded if flames were impinging on the ceiling, but the flame height to ceiling height ratio (L/H) as given in Table 4.2, gives an indication on the degree of flame impingement. The cases with high L/H ratio are not found to give a higher degree of over-prediction than lower ones.

Up until now, only the maximum temperatures along the ceiling have been reviewed, but it is also important to examine the temperatures at different locations below the ceiling for all thermocouple trees. Closest to the fire (at TC1) the temperatures from FDS are very close to experimental values, although slightly above. In FLACS, the result differ more from experimental values. These differences are probably due to the modelling of mixing colder room air with the hot combustion products in the plume, as described above.

When moving away from the fire center, FDS does not capture the entire temperature spectre below the ceiling, since temperatures go from maximum ceiling jet temperature to room temperature almost immediately when leaving the boundary layer location. In FLACS, the temperatures far away from the fire center and ceiling surface closely resemble the experimental values in many cases. At these positions, the modelling of mixing will also play a great role on temperature distribution, as the hot combustion products mix with colder air under the roof and towards the floor, causing a wider temperature profile. It may seem that for distances far from the flame, this effect is better modelled in FLACS than in FDS. This is also indicated when looking at Figure 4.10 with velocities from FDS, where it seems like the degree of mixing due to the flow field is much higher in the plume than in the actual ceiling jet.

Despite some deviation in temperatures found experimentally and numerically, their temperature profiles in the z-direction usually have similar shape, as for instance case 300014 in Figure E.26, where all temperature results show similar curvature. In a few cases, however, the experiments show a curvature to the opposite direction than the numerical tools do, especially for temperatures far away from the flame (i.e. in TC5 and TC6), see for instance case 300012 in Figure E.25. Another common feature of these particular cases, is experimental ceiling jet thicknesses a lot higher than the prediction methods, including the empirical correlation. This might indicate an inaccuracy in experimental results, something that could have been avoided, or at least elaborated, with more repetitions of each experiment.

4.4.1 Effect of varying HRR

When analysing the effect on temperatures by only varying the HRR, $\dot{Q}$, it is useful to look at all results from ceiling height H=2.39 m, as this is the height at which all HRRs are tested, and in addition on both burners.

On burner the burner with surface area 0.25 m^2, hereby called burner 1, this means looking at the results from cases 000000, 100000, 200000, 300000 and 400000, see plots in Appendix E (Figures E.1, E.8, E.15, E.21 and E.27). For simple comparison of maximum temperatures, the top plot of all these figures are gathered below, in Figure 4.11.

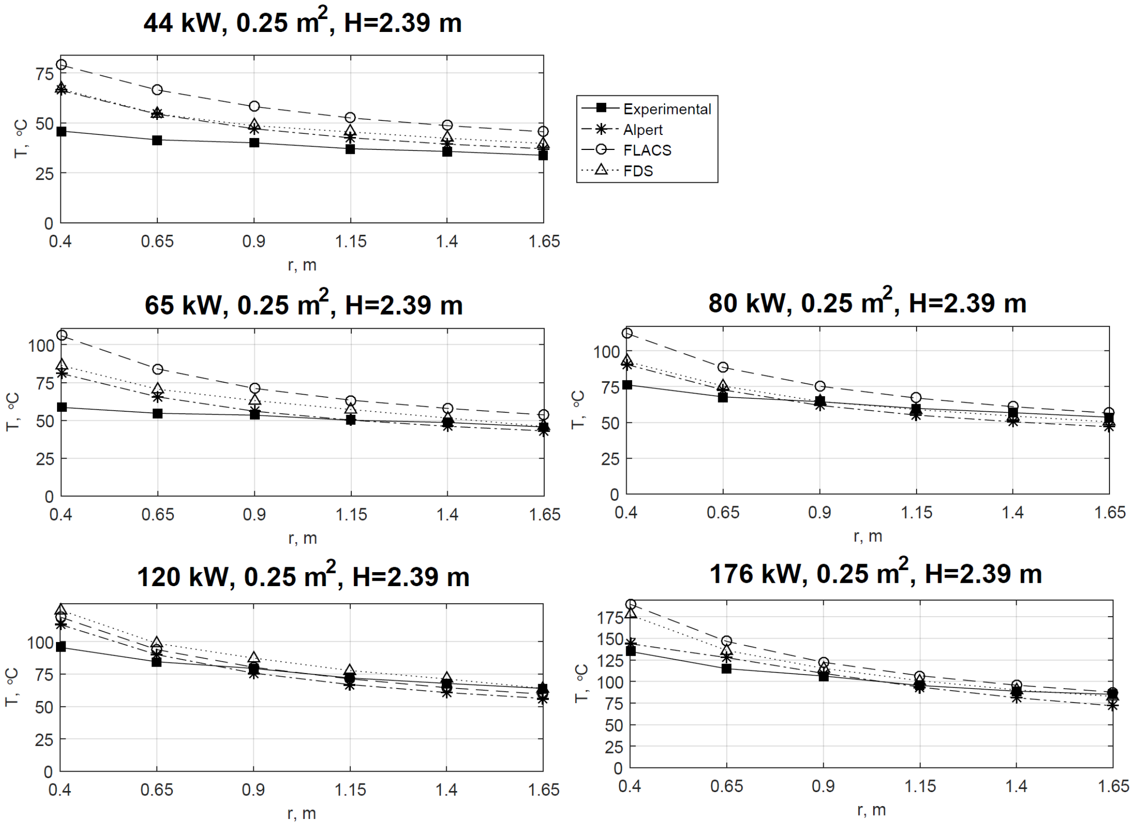

Figure 4.11: Maximum temperature results along the ceiling for the cases with H=2.39 m and burner surface area 0.25 m^2, with varying HRR, for comparison between experimental values, empirical correlation, FDS and FLACS.

When $\dot{Q}$ increases, the temperatures increase to a variable degree for all four methods. The results from FLACS show temperatures more similar to the other values as HRR is increased. The gap between experimental values and Alpert/FDS also decreases, thereby indicating better prediction at higher HRR for all four methods.

Before concluding with this however, it is important to also consider the temperatures at different heights under the ceiling (z). The results for the thermocouple tree closest to the fire center (TC1) and furthest away (TC6), are gathered in Figure 4.12.

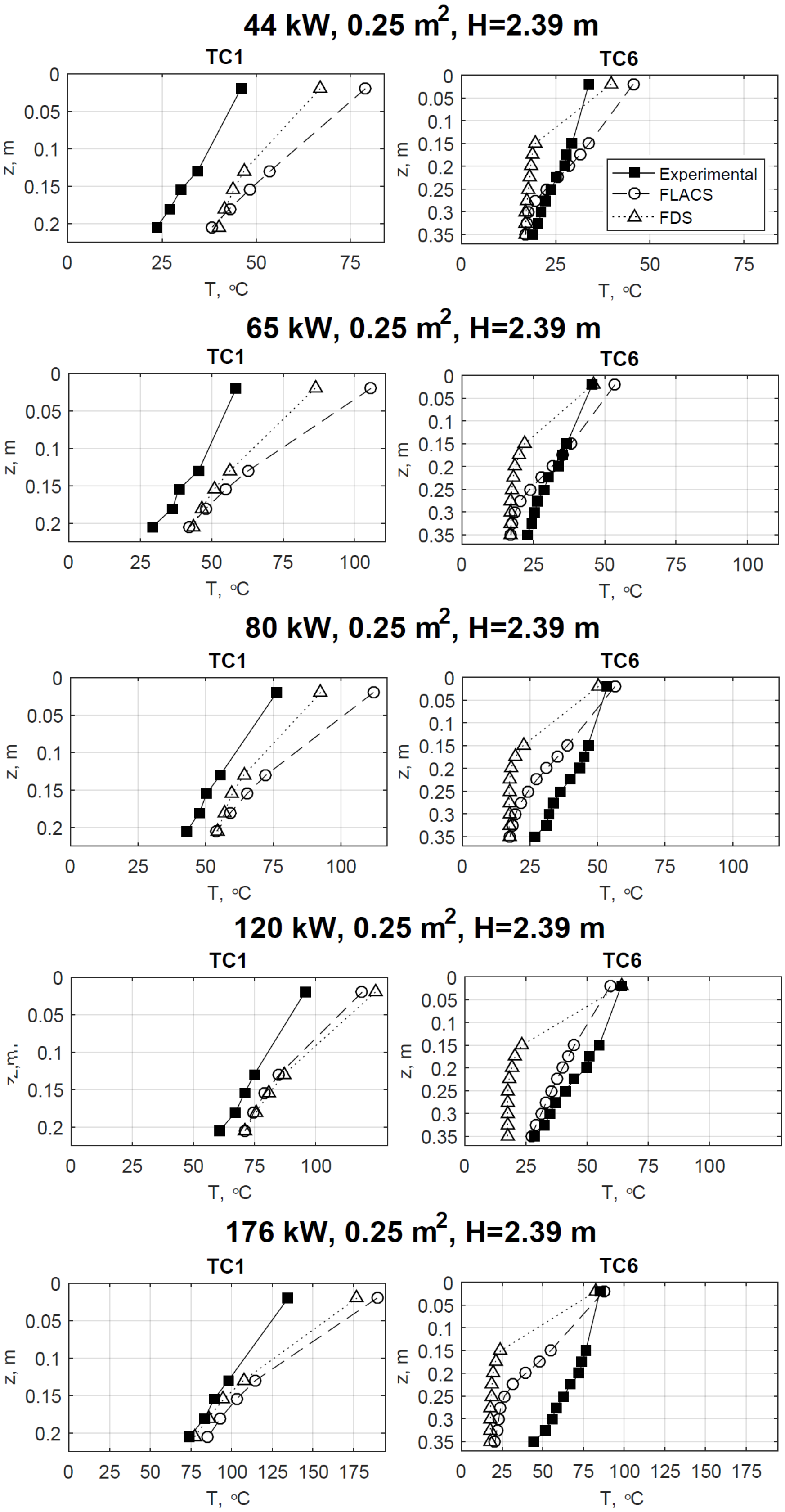

Figure 4.12: Temperature results for TC1 and TC6 in the cases with H=2.39 m and burner surface area 0.25 m^2, with varying HRR, for comparison between experimental values, FDS and FLACS.

Closer to the fire center, at TC1, FLACS approaches the results of FDS as $\dot{Q}$ is increased, indicating better prediction at higher $\dot{Q}$. Moving away from the fire center towards TC6, FLACS is far better at capturing the temperature profile in z-direction than FDS, a tendency more predominant in the cases with lower $\dot{Q}$.

Some of the tendencies listed above are also present for the cases with the same ceiling height, but with the burner of surface area 0.09 m^2 (hereby called burner 2), see cases 000010, 100010, 200010, 300010 and 400010 (Figures E.4, E.12, E.18, E.24 and E.30). FLACS still captures more of the ceiling jet than FDS, and also still over-predicts temperatures close to the ceiling for lower $\dot{Q}$, see Figure 4.13. Also here FDS and Alpert are closely related, and FLACS approaches these results as $\dot{Q}$ increases, an effect that is even more visible in these cases with burner 2, than it was with burner 1.

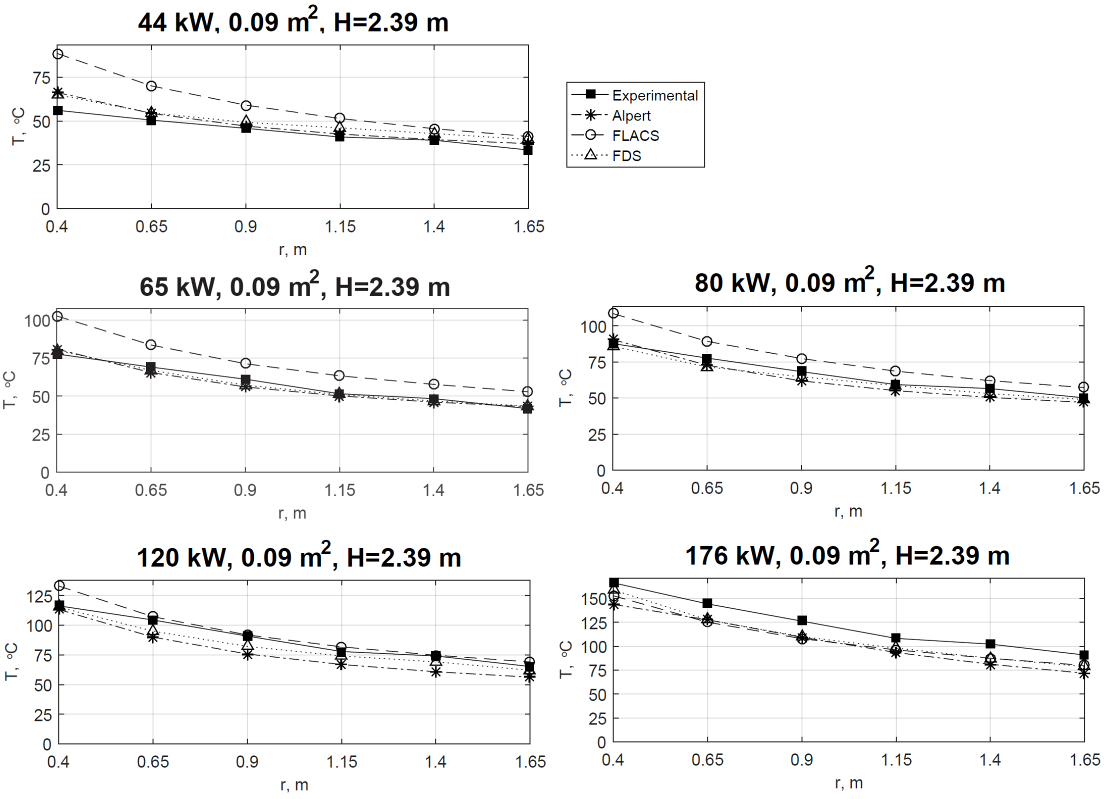

Figure 4.13: Maximum temperature results along the ceiling for the cases with H=2.39 m and burner surface area 0.09 m^2, with varying HRR, for comparison between experimental values, empirical correlation, FDS and FLACS.

The case for $\dot{Q}$=176 kW is worth a closer look, where for the first time experimental values are the highest, while the prediction methods are almost identically about 20 °C lower. This gives cause for thinking that there might have been something wrong with this experiment, such as a higher HRR or a lower ceiling height than the value stated. This problem with suspicion of wrong marking arise for several experiments, and would have been highly reduced by doing more repetitions of each experiment.

Applying burner 1 on lower ceiling height, H=1.94 m, as in cases 100002, 200002, 300002 and 400002 (Figures E.9, E.16, E.22 and E.28), shows the same tendencies for varying HRR as before, when it comes to maximum temperatures along the ceiling. However, at lower HHRs, FLACS does not seem to capture the entire ceiling jet below the ceiling to the same extent as before, see Figure 4.14. FLACS gives overall better predictions at higher $\dot{Q}$.

Case 300002 (with $\dot{Q}$=120 kW) shows a very large deviation between experimental values and the prediction methods, and is believed to be incorrectly marked to 120 kW instead of 44 kW, which would give empirical values very close to the experimental ones. This experiment should thereby to some extent be disregarded.

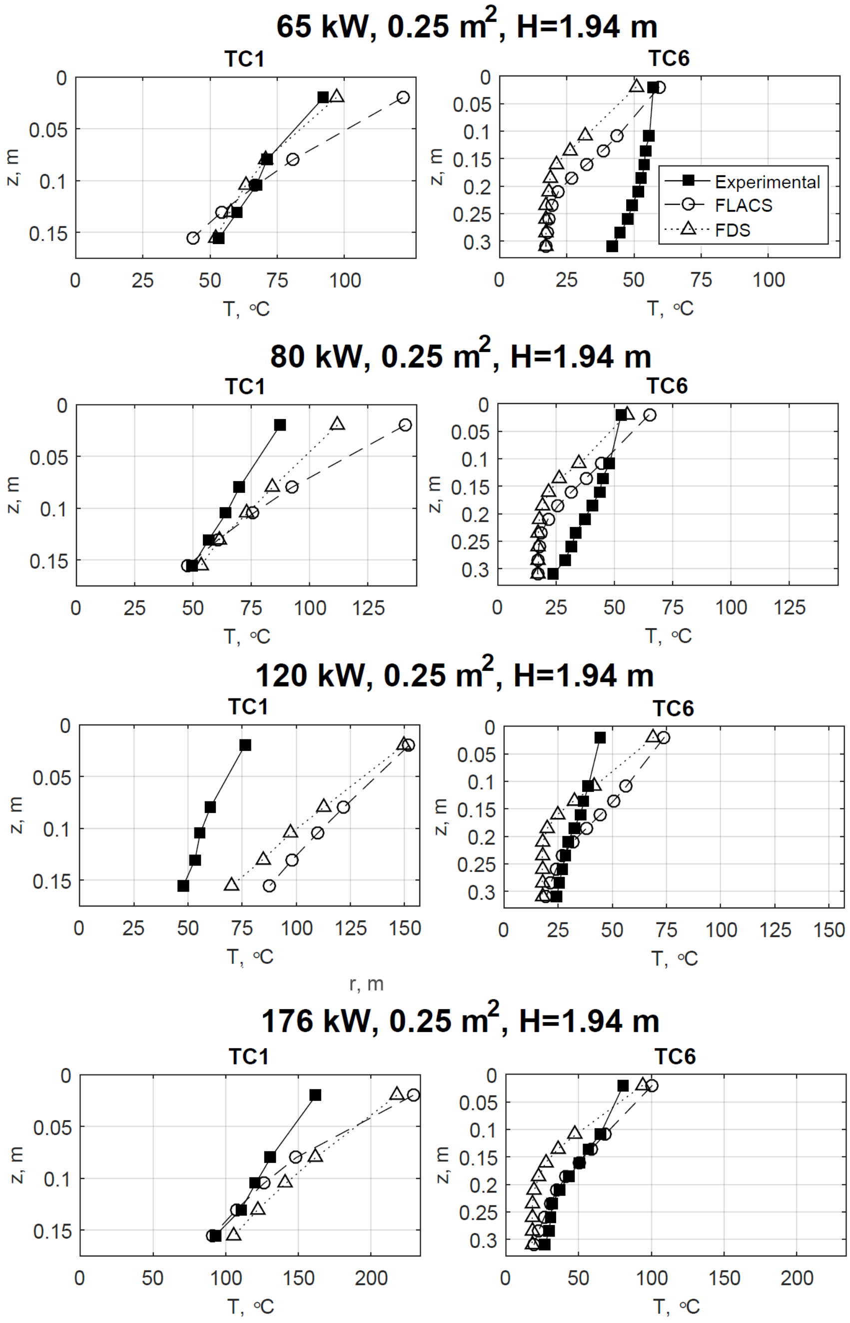

Figure 4.14: Temperature results for TC1 and TC6 in the cases with H=1.94 m and burner surface area 0.25 m^2, with varying HRR, for comparison between experimental values, FDS and FLACS.

Temperature results from varying HRR on burner 2 with H=1.94 m, namely cases 100012, 200012, 300012 and 400012, show similar trends, see Figures E.13, E.19, E.25 and E.31.

Lastly, at ceiling height H=1.12 m, the cases with burner 1 (000005, 100005, 200005 and 300005, see Figures E.3, E.11, E.17 and E.23) show some similarities to the other heights when varying $\dot{Q}$, but FLACS does not show the same degree of predictions improvement at higher HRRs as before. For all $\dot{Q}$, there is a great spread in the results from the four different methods. See for instance case 300005 (Figure E.23), where there is a temperature difference of about 50 °C between all methods for the point closest to the fire center and ceiling. This means that the difference between the highest and the lowest temperature is about 200 °C. FDS and Alpert are not as closely linked as before, as the correlation generally predicts higher temperatures than FDS. Spreading, although not as dramatic, is also present for the cases with burner 2 (000015, 100015 and 200015, see Figures E.6, E.14 and E.20).

4.4.2 Effect of varying ceiling height

To discuss the effect of narrowing in the distance between burner surface and ceiling, it is useful to study the results of cases with the same HRR and burner surface area, such as cases 100000, 100001, 100002, 100003 and 100005 (Figures E.7, E.8, E.9, E.10 and E.11). For the maximum temperatures along the ceiling, all three prediction methods show some degree of temperature rise when narrowing in the ceiling height, except the experimental results from H=1.74 m. Since it is not the case in other experiments, and since the experimental results also are located far below the prediction methods, this leads to a suspicion that there is something wrong with this experiment, such as a lower HRR than stated.

For all heights, as was the case when studying the effect of varying HRR, the results from experiments, correlations and FDS mostly gather around each other, while FLACS consequently over-predicts these maximum temperatures along the ceiling, see Figure 4.15. When the ceiling height is narrowed in, the flame height to ceiling heigh ratio increases, but no apparent trend for abilities of the correlations or models to predict maximum temperatures is visible from studying only this one HRR. For several other HRRs, however, experiments are only conducted for a small selection of ceiling heights and/or only with one burner, see Table 3.3, making it difficult to draw any conclusions on the effect of varying ceiling height.

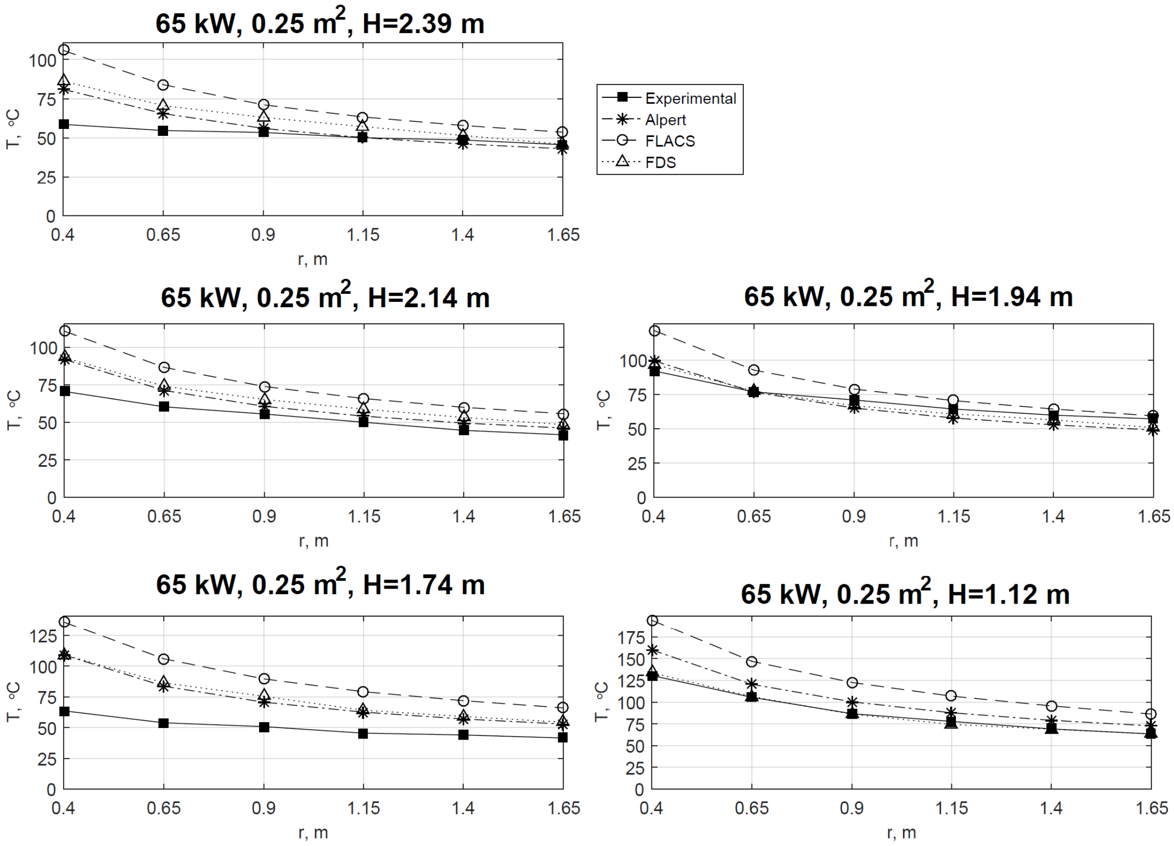

Figure 4.15: Maximum temperature results along the ceiling for the cases with $\dot{Q}$=65 kW and burner surface area 0.25 m^2, with varying ceiling height, for comparison between experimental values, empirical correlation, FDS and FLACS.

When looking at the variation of temperature in z-direction, FLACS still predicts temperatures far from the flames better than FDS, and the variation of H does not seem to affect prediction abilities for any of the methods, see Figure 4.16. However, when closely examining the temperatures near the flame in FLACS as H is decreased, the temperature difference in this TC tree seem to broaden. By this it is meant that maximum temperature closest to the ceiling (TC1-1) is increasing as the flame tip approaches the ceiling, but the lowest temperature in the TC closest to the ground (TC1-5) is actually decreasing. This is also present to some extent in the experiments and FDS. An explanation to this may be the fact that experiments are performed with different TC arrangements, such that TC1-5 is not in the same position for each case. This leads to thinking that results are not comparable for the different ceiling heights, unless looking very carefully at the values for z in each case. However, the observations made on general trends of prediction quality still applies.

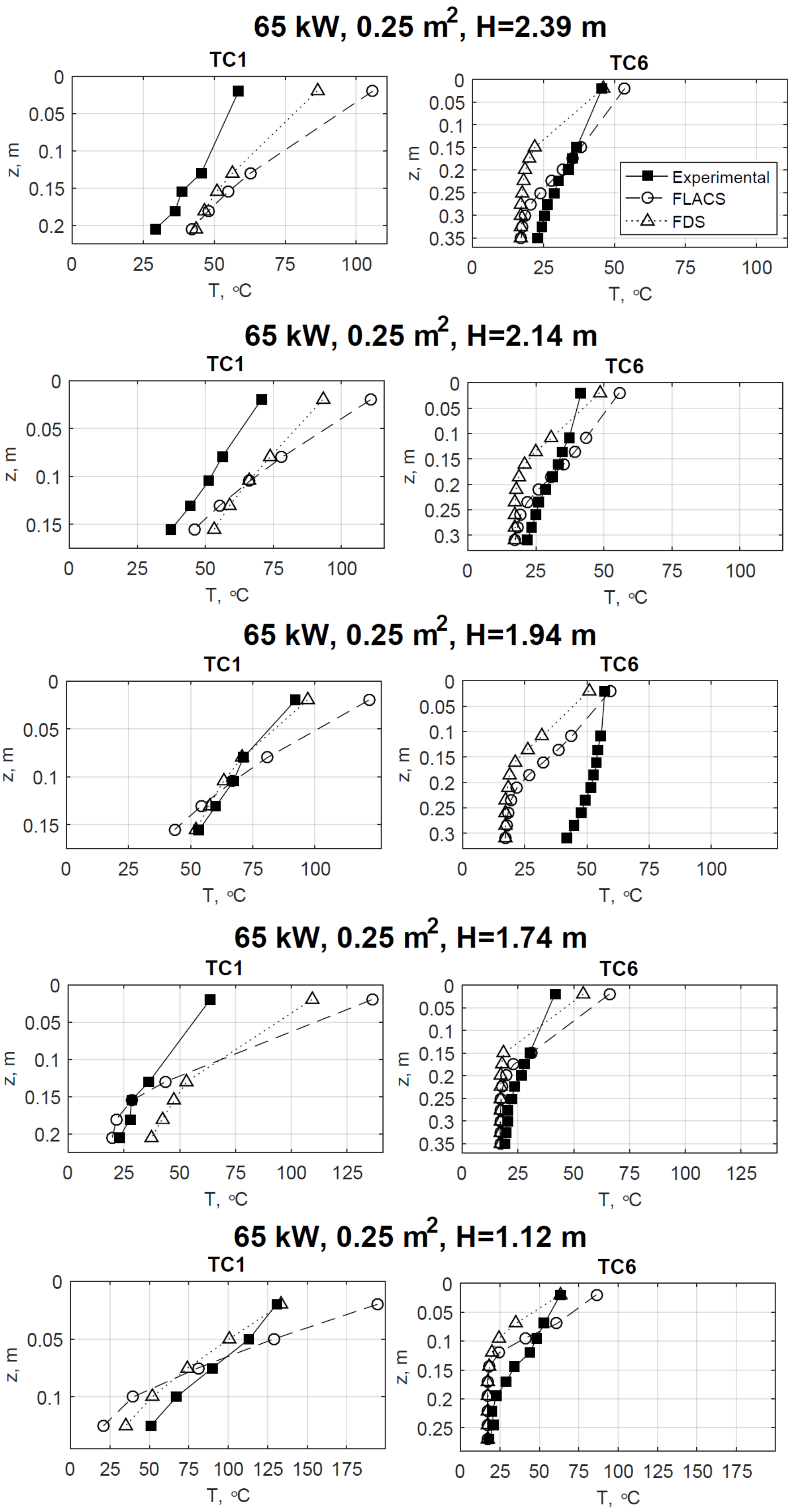

Figure 4.16: Temperature results for TC1 and TC6 in the cases with $\dot{Q}$=65 kW and burner surface area 0.25 m^2, with varying ceiling height, for comparison between experimental values, FDS and FLACS.

4.4.3 Effect of varying burner surface area

Returning to the cases with H=2.39 m, the effect of changing the burner surface area can be further studied. When comparing the results from the two different burners, it is clear that going from a bigger to a smaller burner area in all cases leads to higher experimental temperatures under the ceiling, see Figure 4.13 as opposed to Figure 4.11. Since the mass flow is the same when comparing two experiments of the same HRR, the smaller burner area will result in higher gas velocities, and thereby larger flame heights. According to the flame height correlation in Equation (2.36), the smaller burner will typically lead to a 20 cm increase in flame height. As the flame approaches the ceiling, temperatures along the ceiling and in TC1 are expected to increase.

The results from FDS and FLACS, however, do not follow a clear trend when going to a smaller burner surface area. For several $\dot{Q}$ they actually give lower temperature results when going from burner 1 to burner 2. This might be a result of an overestimation of the increased turbulence level in a fire from a smaller burner surface, causing more heat to be transferred to the surroundings at distances further below the ceiling. Since experimental values increase and numerical values decrease, the maximum temperature over-predictions decrease when going from a bigger to a smaller burner surface area. For the reasons mentioned, this improved prediction is probably based on the wrong physical principle.

When comparing results at different distances below the ceiling (z), there are also some differences between the two burners. Near the flame (at TC1) the numerical temperatures drop as the experimental temperatures rise, when going from the bigger to the smaller burner. This is probably due to the effect of turbulence in the numerical simulations, as mentioned before. Further away from the fire center (at TC6), experimental temperatures decrease slightly, while numerical results seem unchanged.

At lower ceiling height, H=1.94, experimental maximum temperatures continue rising for the smaller burner area, except from the case when $\dot{Q}$=65 kW, suggesting some error in this experiment. However, now numerical values also increase, suggesting that the effect of a taller flame overrules the effect of turbulence as the flame tip approaches the ceiling. According to Motevalli [27], the development of a turbulent plume requires a minimum height between burner surface and ceiling, suggesting that the turbulence level in the plume is lower in these cases. The same temperature rise is observed at TC1, while there are some inconsistencies for TC6, particularly for the experimental results. For some $\dot{Q}$, the temperatures decrease dramatically, while for others they increase slightly, with no apparent pattern.

For even lower ceiling heights, H=1.12 m, all temperatures generally rise to some extent or do not change noticeably when going from burner 1 to burner 2.

4.5 Ceiling jet thickness comparisons

The temperature criterion of Alpert ($\Delta T/\Delta T_{max} = 1/e$) is used to define the ceiling jet thicknesses for the experiments and simulations, by applying it for each radial position. The results are shown in plots in Appendix F. The empirical correlation by Alpert (Equation 2.30) is also included in these plots, but due to its area of validity, some plots are missing a point for the first radial distance from the fire center.

The correlation usually under-predicts the thickness to a variable degree compared to experiments, but is closer than numerical tools. It is important to realise that the correlation is continuous with regards to distance below ceiling, while measurements are made with distances of at least 2.5 cm between each other, resulting in a high probability of inaccuracy. Because of this, and the fact that the correlation in many cases is fairly close to experimental values, it is concluded that it gives sufficiently good prediction of ceiling jet thickness for the cases studied in the current work.

As a result of FDS's tendency of jumping from maximum to room temperature quite quickly below the thermal boundary layer, probably due to a shortcoming in the modelling of mixing hot combustion products with colder air, the temperatures below the thermal boundary layer are too low to be included in the temperature criterion. It thereby predicts the narrowest ceiling jet thickness of all three methods. This modelling of mixing seems to be more accurate in FLACS, which captures higher temperatures further below the ceiling, and thereby predicts ceiling jet thicknesses more accurately than FDS. If the maximum temperatures were not over-predicted with FLACS, the temperature criterion would be lower, and the resulting ceiling jet thicknesses would be even closer to correlations and experimental values.

4.5.1 Effect of varying HRR

The correlation for ceiling jet thickness is only dependent on r/H, and its results will thereby not be influenced by changing $\dot{Q}$ or burner surface area. To check if this is a correct representation of physical conditions, results from cases 000000, 100000, 200000, 300000 and 400000 are compared, see Figure 4.17.

When looking at the experimental results, Figure 4.17 shows that there is not much difference in ceiling jet thickness when going from 44 to 65 kW. For 80, 120 and 176 kW the plots look slightly different from the first two, although similar to each other. The two 'groupings' might have been recorded on different days, causing different ambient conditions. FDS does not capture any ceiling jet thickness at all, and by increasing HRR, no change (if not a slight worsening) in predictions is visible.

In FLACS, the results in ceiling jet thickness from one HRR to another show some inconsistencies, especially for the case with 120 kW. This case shows thicker ceiling jet than both 80 kW and 176 kW, causing some concern that something is wrong with this simulation. If disregarding this case, the change in ceiling jet thickness when varying HRR is minimal, also in FLACS.

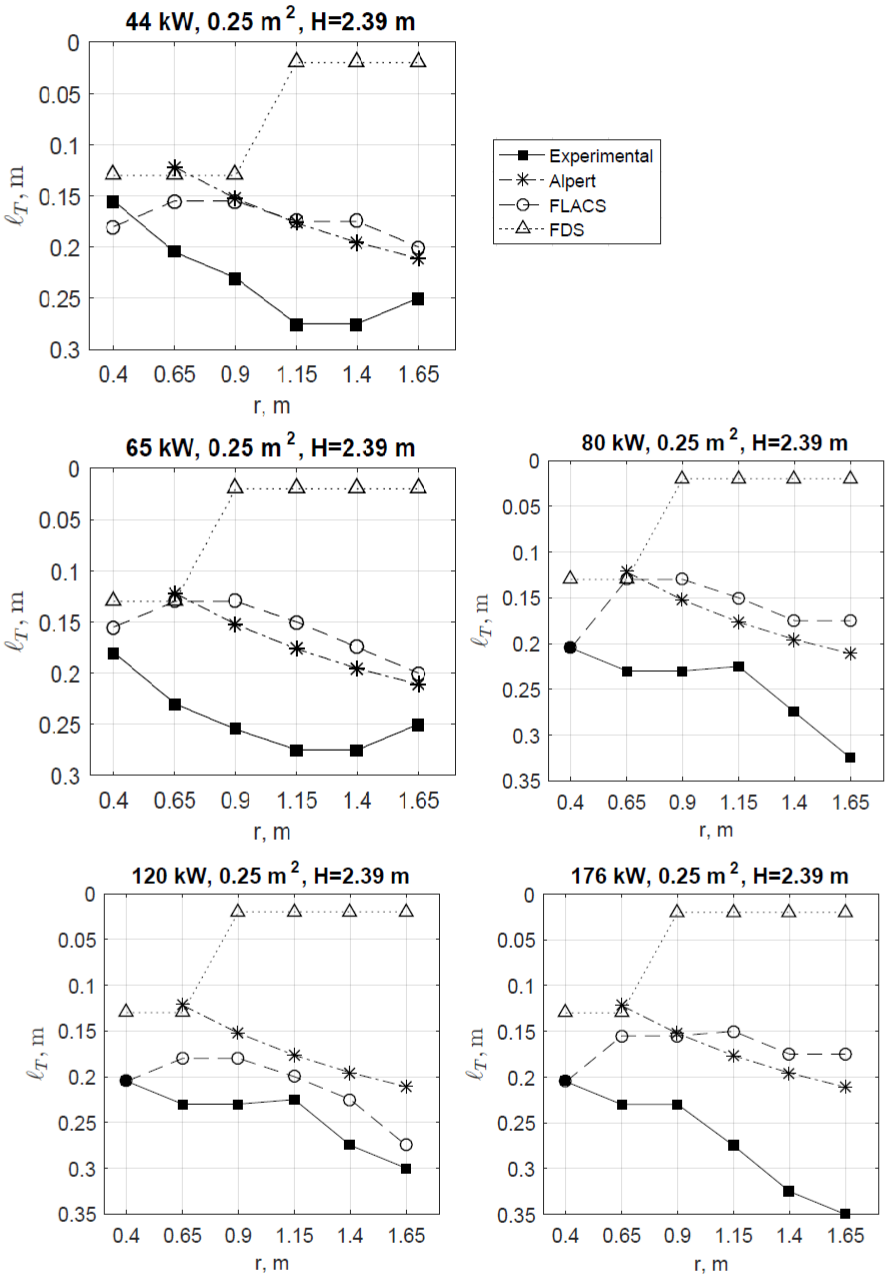

Figure 4.17: Ceiling jet thickness results for the cases with H=2.39 m and burner surface area 0.25 m^2, with varying HRR, for comparison between experimental values, Alpert's correlation, FDS and FLACS.

To verify if the variation of HRR does not affect the ceiling jet thickness, other cases are checked, such as the ones with the same ceiling height but with burner 2, see Figure 4.18.

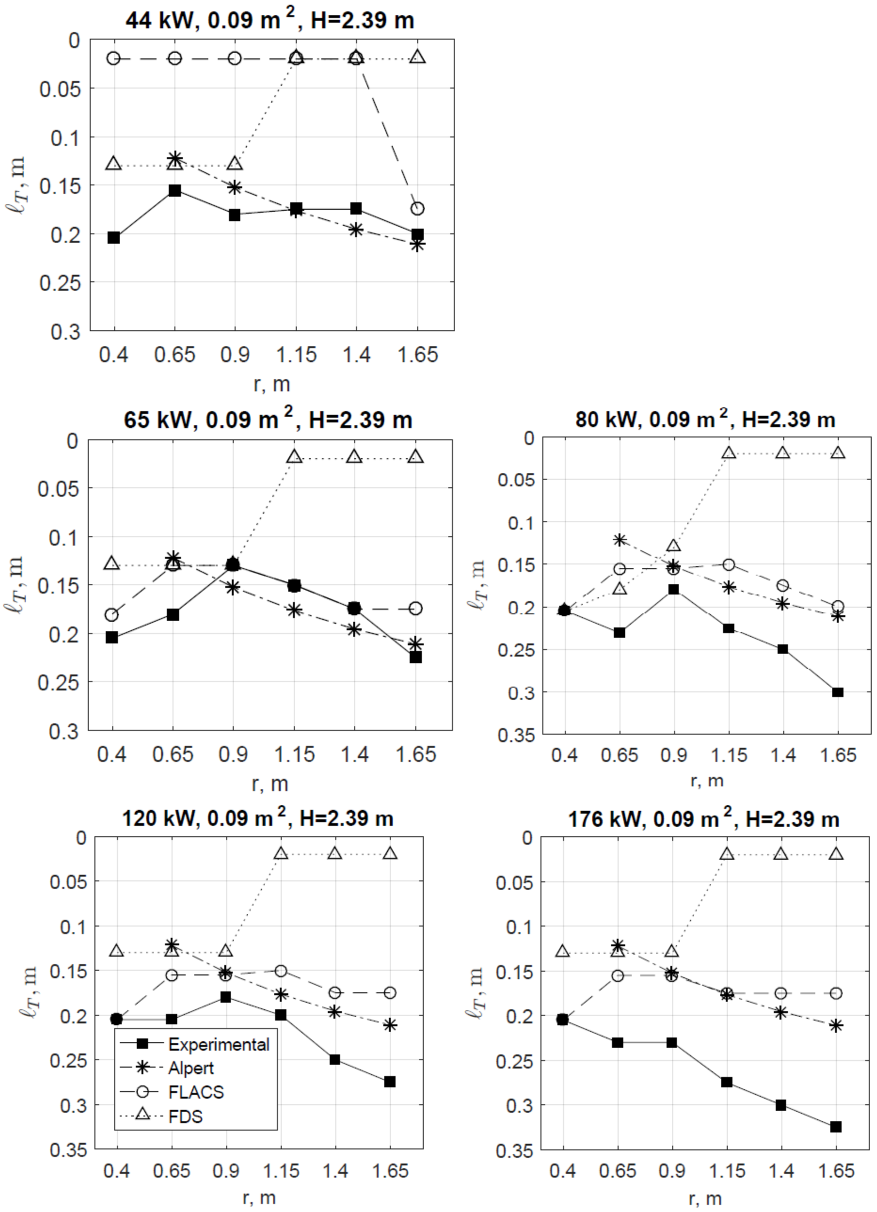

Figure 4.18: Ceiling jet thickness results for the cases with H=2.39 m and burner surface area 0.09 m^2, with varying HRR, for comparison between experimental values, Alpert's correlation, FDS and FLACS.

Figure 4.18 shows that there is a slight difference in experimental ceiling jet thickness when varying HRR, as it is somewhat thicker for higher $\dot{Q}$. However, looking at simulation results for both of the burners, there is very little difference between the thicknesses from one HRR to another, one exception being the results of case 000010 (see top plot of Figure 4.18) where FLACS does not catch any ceiling jet thickness at all for the first five radial positions. In the same case with burner 1, FLACS agrees well with other results, so it is believed that something have gone wrong with this one simulation in FLACS.

Based on the comparison between different HRRs for the same height and burner, it is evident that only experimental results differ noticeably. With the many sources of error in the experimental measurements in mind, it is reasonable to assume that ceiling jet thickness is not dependent on HRR, and the correlation is right not to include it as a variable.

4.5.2 Effect of varying ceiling height

FDS highly under-predicts the thicknesses for all cases with the ceiling height studied in the previous paragraphs. For lower ceiling heights it seems to approach the other methods in their results for ceiling jet thicknesses. Looking at results with the same HRR (65 kW) with burner 1, the effect on ceiling jet thickness result by changing the ceiling height becomes visible, see Figure 4.19.

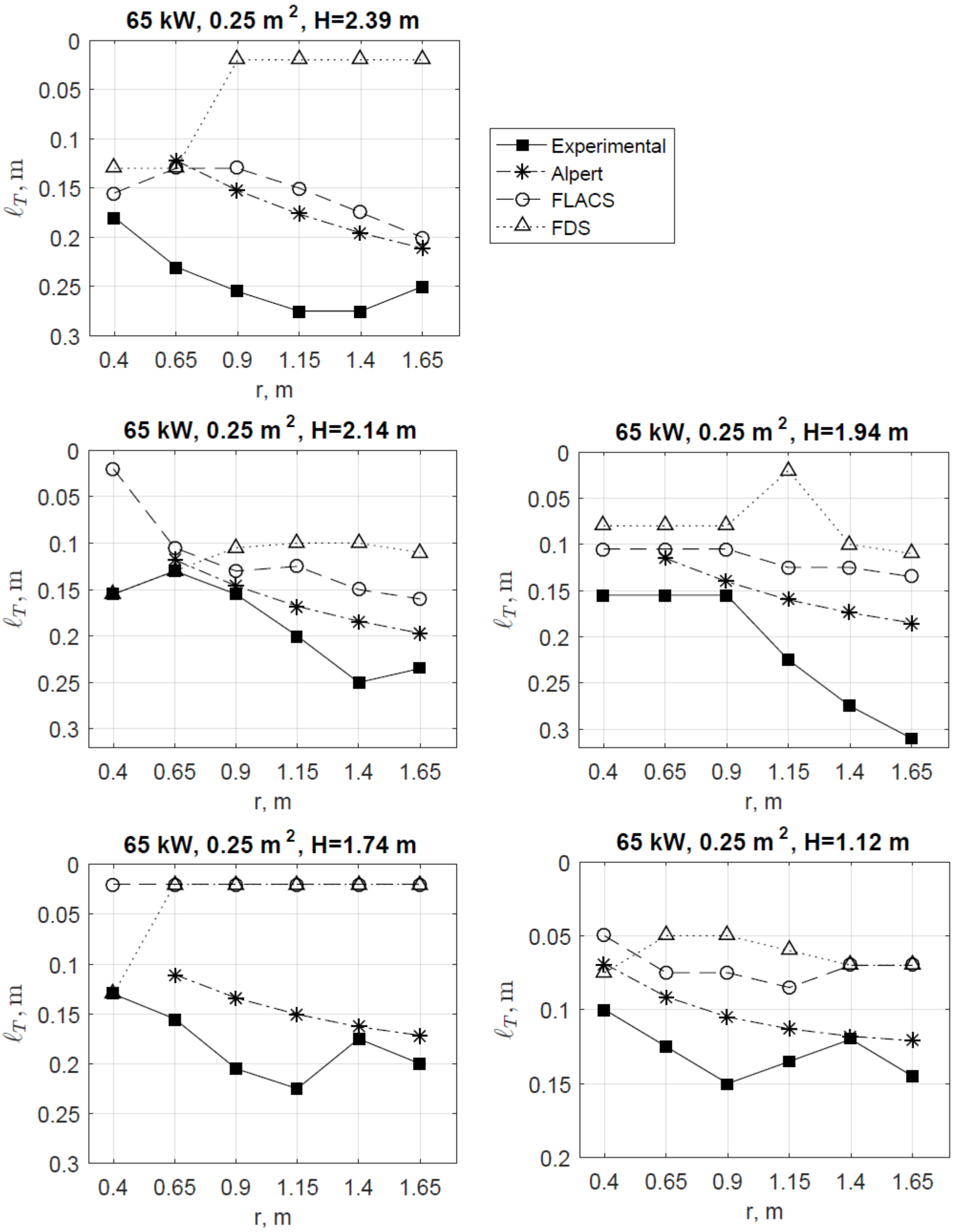

Figure 4.19: Ceiling jet thickness results for the cases with $\dot{Q}$=65 kW and burner surface area 0.25 m^2, with varying ceiling height, for comparison between experimental values, Alpert's correlation, FDS and FLACS.

In Figure 4.19 the correlation's dependency of r/H is visible; a shorter ceiling height leads to a narrower ceiling jet. This is generally the case for experimental results too, but with some points diverging in all directions. FDS generally gives results closer to the other methods when H decreases, and FLACS generally catches the ceiling jet thickness better than FDS. For the case with H=1.74 m, however, both simulation tools seem to not catch any ceiling jet thickness at all. In this particular case, the maximum temperatures from simulations and correlations seem to be a lot higher than experimental values (see Figure E.10), leading to a suspicion that there is an error in the experiment. This still does not explain the sudden decrease in ceiling jet thickness from numerical results. Looking at temperature results from this case, there is a significant temperature drop between the TC closest to the ceiling and the second one, causing the temperature criterion to be far higher than temperatures below the boundary layer. A plausible explanation for this is the fact that the experiment is performed on a 'blue' TC arrangement, meaning that there is a distance of 11 to 13 cm between the first two TCs of a tree. To capture the ceiling jet, this experiment should probably have been performed with a 'green' arrangement, as was the case for the two previous taller ceiling heights of Figure 4.19, or a 'red' one, which was the case for the lowest height.

4.5.3 Effect of varying burner surface area

When looking at the effect of varying HRR, it was already mentioned that changing the burner surface area had little or no effect on the ceiling jet thickness results. This is especially the case for higher $\dot{Q}$, but to an even greater extent it is more visible for numerical results than for experimental ones. Bearing in mind that there are many uncertainties in the experimental results, one may to some extent disregard the differences for the two burners, and conclude that the dimension of the burner does not affect the ceiling jet thickness. Numerical prediction abilities are thereby also not effected to a significant degree.

4.6 Choosing the right prediction tool

Depending on how accurate the results are required to be at which location, and the amount of time and funds available, different tools are the suitable choice. FDS is quicker than FLACS, and also free, but highly under-predict ceiling jet thicknesses. The correlations are free, quick and quite accurate, but does not offer any additional information on other parameters that may be of interest, like the CFD codes do.

4.7 Uncertainties

Throughout the discussions above, it has been stated several times that there are many uncertainties in the experimental measurements, but not a description or quantification of these. The latter is not an easy task in this work, as only some of the apparatuses has a known accuracy. However, knowing that they exist, and that the inaccuracy is magnified as more uncertainties are combined, is very important. Below is therefore a description on some of the uncertainties most likely to affect the results, and in some cases a suggestion on how to reduce them.

Setup

There is a minimum distance of 2.5 cm between all TCs. This means that the temperature at any point between two TCs might be within the temperature criterion, but since the temperature at the next TC is not, this is not captured as a part of the ceiling jet. It can thereby be up to 2.4999(...) cm thicker than what is estimated in the current work.

Knowing that there are three different TC arrangements also leads to difficulties when comparing temperatures from one case to another. The only solution to this would be to have several more TCs, distributed with a narrower distance between them, but due to limited resources, only the amount of TCs already possessed by HVL was used. It was therefore unknown which type they were, but the most common ones are type K, with a limit of error listed at ±2.2 °C or ± 0.75 % (whichever is greater) [28]. Due to this small limit of error, errors in experimental temperatures are more likely to be a result of the TCs placement than their inaccuracies.

In simulations, it was decided to put monitor points only at the same locations as in experiments. FLACS can, however, handle up to 8000 monitor points [21], and more points might have given a more complete picture of the ceiling jet, and more accurate thicknesses. Since the objective was to compare simulations with experiments, more monitor points would only cause confusion and difficulties when comparing, and was therefore ruled out.

Boundary layer is in this work assumed to extend from the ceiling to 2 cm below for all cases. This does, however, change with conditions and might be located elsewhere in some of the experiments, resulting in other maximum temperatures and thereby other temperature criteria for ceiling jet thickness. For instance, if the boundary layer is located at 1-2 % of the ceiling height, as mentioned in Section 2.3, the top TC representing the temperature maxima of each tree would have had to be moved when changing the distance between burner surface and ceiling. This is not as easy as it sounds, as the TCs were closely intertwined, and moving the top one with an accuracy of millimetres proved difficult. Also, on a tight schedule, taking the time of doing so must be compared to the effect in results. In several cases, one would have had to wait until everything had cooled sufficiently before being able to touch it.

Ceiling heights were varied by building up the burner surface with several, about 10 cm thick, stone pallets. This resulted in some inaccuracy when trying to obtain the desired height between burner surface and ceiling.

Even though only two minutes of fire was recorded for each experiment, some heating of the ceiling will have occurred, since it was not cooled or isolated in any way. Heated objects will cause movement of the surrounding fluid, due to density fluctuations. This will affect the flow pattern, as more and more heat is reflected down towards the burner surface, which is an effect not captured by FLACS, where mostly the flame transmits heat. In both numerical tools, it is possible to define material properties of an object, such as conductivity, density, specific heat and emissivity, where conductivity and specific heat can be functions of temperature. This was not defined for simulations in the current work, due to lack of information of such properties for the material used in the experiments.

Execution of experiments

Only one repetition was performed for each experiment, making the likelihood of some error going unnoticed very much present. If more than one repetition was done, a mean could be used to see how the different repetitions of an experiment deviate, and quantifying a margin of error. When comparing with experiments, one could check if the numerical results were within this margin of error. Also, it would have made it easier to identify if some experiments were marked with the wrong HRR, ceiling height or burner surface. However, performing 33 experiments in a short time frame must have been demanding enough, without having to repeat them.

HRR

According to Motevalli [27], most large-scale data have a fire source with HRR uncertainties ranging from 10 to 20 %. Even though the mass flow in the current work is constant, the resulting total HRR of the fire is dependent on several factors, such as air entrainment and turbulence. In the experiments, it is likely that combustion is not fully complete, due to lack of optimal air distribution to the fire, and thereby fuel rich conditions. Also, turbulence may cause local extinction of fires, although a level of turbulence greater than what was present for the experiments in the current work would probably be required.

The HRR of a fire is unlikely to be constant, neither for experiments or simulations, and fluctuations in different directions would cause a significant temperature difference. Hopefully, the mean values are still relatively comparable, something that probably should have been checked. For instance, the fuel supply program might have been able to provide a log of mass flow rates versus time, while FLACS logs HRR, and the two could have been compared.

To represent a certain HRR in FLACS, the mass flow was changed according to Table 3.1, based on calculations using Equation (2.20) with the lower heating value. This might have resulted in some deviation between obtained HRR and desired one.

According to Alpert [1], convection is the dominant mode of heat transfer for weak plumes impinging on the ceiling. His correlations were however made with total HRR, based on fuel mass loss rates and the estimates of heat of combustion available in the early 1970s. He argues that it would be desirable to use correlations based on convective HRR, $\dot{Q}_c$, instead. This might have been worth looking into in the current work, but as the experimental results were given with a total HRR instead of a convective one, this proved difficult, unless assuming that $\dot{Q}_c$ is 70 % of $\dot{Q}_{tot}$, which Heskestad [4] estimated.

Boundary conditions

Drafts were present in the laboratory, resulting in flame tilting in more than one direction. Tilting of the flame towards the TCs would result in a higher heat transfer to this direction, and tilting away from the TCs would do the opposite. Some level of flame tilting is believed to be almost impossible to avoid in the experiments, unless moving them to a location completely without drafts. The exhaust fan might also have contributed to this effect, but turning it off would go against the regulations at the laboratory, causing a dangerous environment for the participants. The draft also caused room temperature to fluctuate.

Small nuances in boundary conditions might have a huge effect on the comparability between simulations and experiments. The simulations were all performed with the same boundary conditions, such as an ambient temperature of 17 °C, which was definitely not the case experimentally, as they were conducted over several days with different temperature. A log of factors that might have influenced the results in any way, such as room temperature, the need for turning up the exhaust fan due to the filling of smoke, or heavy tilting of the flame in any directions, might have been useful to have a look at. The owner of the experimental results, Nichlas Lyche, kept a written log, but it was not made available for the current work.

Simulations

Some uncertainties have already been discussed for the simulations, such as not defining material properties for the ceiling, the fuel leak rate needed to obtain a certain HRR, the boundary conditions etc. Another aspect that is important to discuss, is the placement of monitor points in the grid and relative to the ceiling. For both FLACS and FDS, the temperature is measured as the mean value in the entire cell where the monitor point is located. This might have had an impact on the temperature results in the current work, as the top monitor points are placed in FLACS and FDS according to Figure 4.20, where the dotted lines represent grid lines in z-direction. Since the top TCs represent the maximum temperature, their monitor points should be located at the boundary layer location, 2 cm below the ceiling surface. In the figure, it is clear that they are actually measuring mean temperatures from 2.5 to 5 cm below the surface of the ceiling. The 'solution' to this problem is a smaller grid, but this was ruled out in the grid analysis, due to the extensive computational time.

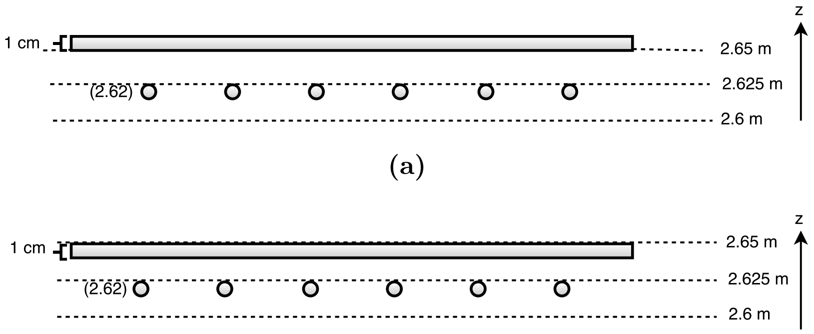

(a)

(b)

Figure 4.20: Placement of top TCs and ceiling relative to grid lines in z-direction for (a) FLACS and (b) FDS.

From Figure 4.20 it is clear that the ceiling was placed at different points in the two simulation tools, in FLACS above the grid line at 2.65 m, and in FDS below. First of all, this means that there is less distance between the top TC and the ceiling in FDS. Second, this means that the cell between the top TC and the ceiling is partially blocked in FDS, while in FLACS it is not. This might influence the results. For better comparison between the two methods, the ceiling should probably have been moved above the grid line in FDS. Later, this was tested for one case, resulting in no change in temperatures, and it is therefore assumed that all results from FDS are still valid and comparable to FLACS. A better solution to the issue with ceiling placement, would probably be to make the ceiling infinitely thin in both tools. In this manner, its placement relative to the grid line is not as important.

Most of the initial and boundary conditions were left as default in FLACS, which might have affected the results. A parameter analysis could be performed, to check if changing some parameters resulted in temperatures closer to experimental values. An attempt was made on changing the parameters associated with turbulence level in the leak, such as relative turbulence intensity and turbulence length scale, with no dramatic change in results. This analysis should probably have been conducted more systematically, and with more parameters.

Models

During simulations in both FLACS and FDS, there are many sub-models interacting with each other. For instance, the mixing of fuel and air is modelled by transport equations for mass, momentum, energy and turbulence models, and their individual performance may be affected to a various degree by the type of fluid flow simulated. How and where the combustion occurs is highly influenced by how the turbulence models mix fuel and oxidizer, for instance with excessive mixing either near the burner surface or far away from it [26].

Changing constants in the models may give results closer to the experimental values, but is mostly reserved for academic testing of the models' performance, and not for real cases.

While temperatures are measured directly in the experiments, they are calculated via modelling of enthalpy in the simulations. How this and other thermodynamic properties are modelled, and how they are used to calculate temperature, may have a significant effect on the results.

The combustion models of both FLACS and FDS assume that all fuel is completely reacted as soon as it is mixed with the oxidizer. Since the experimental fires are likely to be somewhat incomplete, as described in the paragraph about HRR, it makes sense that the simulations produces higher temperatures, as more fuel is reacted.

The degree of sophistication in combustion models may greatly influence the accuracy of results, but since a more detailed model would result in higher computation time, the simpler models in both FLACS and FDS are considered to give sufficiently accurate results [26].

Chapter 5

Conclusion

Temperature and thickness of ceiling jets from both weak and strong fire plumes have been studied with experimental work, empirical correlations and the two CFD codes FLACS and FDS. The major findings are listed below.

Prediction capabilities
For the ceiling jet's maximum temperature along the ceiling, experimental results, correlations and FDS are closely linked, while FLACS shows an over-prediction. FDS also shows more similarities with the experimental results for the temperatures near the flame, while FLACS over-predicts far more. However, FLACS captures the temperatures far away from the flame better than FDS, which drops to room temperature too quickly. As a result, FLACS is better at predicting ceiling jet thickness than FDS. The correlation shows thicknesses even closer to the experimental values, indicating better prediction with the correlation.

Effect of grid size
A grid refinement from 5 cm to 2.5 cm resulted in a temperature reduction in FLACS of 80 °C at the most, and thereby maximum ceiling jet temperatures much closer to the experimental values and Alpert's correlation. This is probably because of a higher degree of fire fluctuation from side to side, a phenomena which is only captured with a fine enough grid.

The same grid refinement also resulted in a temperature reduction in FDS, but further refinement resulted in higher temperatures. This is most likely due to the placement of monitor points and the fact that they monitor the temperature of the entire cell, not in an exact point.

Effect of varying conditions

- Higher HRR (heat release rate) resulted all over in higher temperatures, but had little effect on ceiling jet thickness, which only slightly and sporadically increased with increasing HRR. This corroborates that the ceiling jet thickness correlation does not include HRR as a variable. Prediction capabilities for the numerical methods were generally better at higher HRR.
- Lower ceiling height resulted in higher temperatures for all four methods, and a slightly narrower ceiling jet. There was no dramatic change in prediction capabilities for any of the methods, only a slight bettering of FDS results for lower ceiling heights.
- Smaller burner surface area resulted in higher experimental temperatures for all cases, due to larger flame heights, but in many cases both FLACS and FDS predicted lower temperatures. This was mostly the case for taller ceiling heights, suggesting that the effect of increased turbulent mixing might be greater than the effect of increased flame height in these cases. Ceiling jet thickness does not seem to change noticeably for any of the four methods when changing the burner size.

5.1 Suggestions for further work

To gain a full picture of the behaviour of ceiling jets, it would be useful to also measure velocities in addition to temperatures. This way, more information on turbulence level is available.

Also, as mentioned in Section 2.3.1, there exists an empirical correlation on ceiling jet thickness based on momentum, ℓ_V. This correlation's performance, as well as that of CFD codes, could with information about velocity be tested and compared to results obtained with the temperature based ceiling jet correlation.

Knowing if a ceiling jet is weak or strong plume-driven is difficult today, as there seems to not exists any clear limit on when a plume is considered weak or strong. In the current work a limit is set for a certain flame height to ceiling height ratio, or a certain HRR. If there existed a universal limit, this would ease the process of temperature prediction in ceiling jets.

In the current work, flame heights are calculated from an empirical correlation, and not measured. A suggestion for further work is to measure flame heights, compare with the flame height correlation, and check if this has an effect on the weak or strong plume characterization, and thereby on the empirical temperature prediction of ceiling jets.

Bibliography

[1] R. L. Alpert, “Ceiling Jet Flows,” in *SFPE Handbook of Fire Protection Engineering*, M. J. Hurley, Ed., 5th edition, Springer New York, 2016, pp. 429–454.

[2] Statistics Norway (SSB), *Fire and accident protection, 2015*, Jun. 2016. [Online]. Available: http://www.ssb.no/en/offentlig-sektor/statistikker/brann_kostra/aar/2016-06-23 (Accessed: 03.05.2017).

[3] V. Motevalli and C. H. Marks, “Characterizing The Unconfined Ceiling Jet Under Steady-State Conditions: A Reassessment,” *Fire Safety Science*, vol. 3, pp. 301–312, 1991.

[4] G. Heskestad and T. Hamada, “Ceiling Jets of Strong Fire Plumes,” *Fire Safety Journal*, vol. 21, pp. 69–82, January 1993.

[5] L. Y. Cooper, “Fire-Plume-Generated Ceiling Jet Characteristics and Convective Heat Transfer to Ceiling and Wall Surfaces in a Two-Layer Fire Environment: Uniform Temperature Geiling and Walls,” *Fire Science and Technology*, vol. 13, pp. 1–17, 1993.

[6] S. Nam and R. G. Bill, “Numerical Simulation of Thermal Plumes,” *Fire Safety Journal*, vol. 21, pp. 231–256, January 1993.

[7] T. Hara and S. Kato, “Numerical Simulation of Fire Plume-Induced Ceiling Jets Using the Standard kε Model,” *Fire Technology*, vol. 42, pp. 131–160, April 2006.

[8] K. McGrattan, S. Hostikka, R. McDermott, J. Floyd, C. Weinschenk, and K. Overholt, *Fire Dynamics Simulator Technical Reference Guide - Volume 3: Validation*, 6th edition. National Institute of Standards and Technology, 2016.

[9] N. O’Grady and V. Novozhilov, “Large Eddy Simulation of Sprinkler Interaction with a Fire Ceiling Jet,” *Combustion Science and Technology*, vol. 181, pp. 984–1006, Jun. 2009.

[10] V. Novozhilov, “Large Eddy Simulation of Transient Ceiling Jet in a Compartment Fire Environment,” in *Proceedings of the Fourteenth Australasian Fluid Mechanics Conference*, Adelaide, Australia: Department of Mechanical Engineering, Adelaide University, December 2001, pp. 367–370.

[11] P. Chatterjee, K. Meredith, B. Ditch, H. Yu, Y. Wang, and F. Tamanini, “Numerical Simulations of Strong-Plume Driven Ceiling Flows,” *Fire Safety Science*, vol. 11, pp. 458–471, 2014.

[12] *Fire - definition of fire in English | Oxford Dictionaries*. [Online]. Available: https://en.oxforddictionaries.com/definition/fire (Accessed: 13.09.2016).

[13] R. K. Eckhoff, *Explosion Hazards in the Process Industries*, 1st edition. Houston, TX: Gulf Publishing Company, 2005.

[14] J. Warnatz, U. Maas, and R. W. Dibble, *Combustion: Physical and Chemical Fundamentals, Modeling and Simulation, Experiments, Pollutant Formation*, 4th edition. Berlin/Heidelberg: Springer Berlin Heidelberg, 2006.

[15] S. R. Turns, *An Introduction to Combustion - Concepts and Applications*, 2nd edition, ser. McGraw-Hill Series in Mechanical Engineering. Boston: McGraw-Hill, 2000.

[16] J. W. Gooch, *Encyclopedic Dictionary of Polymers*, 2nd edition. Springer New York, 2011. [Online]. Available: http://link.springer.com/referenceworkentry/10.1007/978-1-4419-6247-8_4970 (Accessed: 08.11.2016).

[17] W. McCabe, J. Smith, and P. Harriott, *Unit Operations of Chemical Engineering*, 7th edition. Boston: McGraw-Hill Education, 2004.

[18] G. H. Yeoh and K. K. Yuen, *Computational Fluid Dynamics in Fire Engineering: Theory, Modelling and Practice.* Burlington: Butterworth-Heinemann, 2009.

[19] K. McGrattan and S. Miles, "Modeling Fires Using Computational Fluid Dynamics (CFD)," in *SFPE Handbook of Fire Protection Engineering*, M. J. Hurley, Ed., 5th edition, New York, NY: Springer New York, 2016, pp. 1034–1065.

[20] J. D. Anderson, *Computational Fluid Dynamics: The Basics With Applications*, 1st edition, ser. McGraw-Hill Series in Mechanical Engineering. New York: McGraw-Hill, 1995.

[21] Gexcon AS, *FLACS v10.4 User's Manual.* Gexcon AS, 2015.

[22] K. McGrattan, S. Hostikka, R. McDermott, J. Floyd, C. Weinschenk, and K. Overholt, *Fire Dynamics Simulator User's Guide*, 6th edition. National Institute of Standards and Technology, 2016.

[23] K. McGrattan, S. Hostikka, R. McDermott, J. Floyd, C. Weinschenk, and K. Overholt, *Fire Dynamics Simulator Technical Reference Guide - Volume 1: Mathematical Model*, 6th edition. National Institute of Standards and Technology, 2016.

[24] G. Heskestad, "Fire Plumes, Flame Height, and Air Entrainment," in *SFPE Handbook of Fire Protection Engineering*, M. J. Hurley, Ed., Springer New York, 2016, pp. 396–428.

[25] K. Overholt, *FDS Mesh Size Calculator*, March 2008. [Online]. Available: http://www.koverholt.com/fds-mesh-size-calc/ (Accessed: 02.05.2017).

[26] B. Lilleberg, *Private communication*, May 2017.

[27] V. Motevalli and S. Riahi, "Transient Ceiling Jet Temperature and Velocity Profiles in the Presence of an Upper Layer: Comparison with Predictions by LAVENT and JET Computer Fire Models," *Journal of Fire Sciences*, vol. 26, pp. 109–131, March 2008.

[28] REOTEMP Instrument Corporation, *Thermocouple Accuracy - Thermocouple Accuracy Comparison Chart*, 2011. [Online]. Available: http://www.thermocoupleinfo.com/thermocouple-accuracies.htm (Accessed: 19.05.2017).

Appendices

Appendix A

Scenario (cs-)file for FLACS input

```
VERSION 0.5
%TEMPLATE="_v9.1/scenario/default+1"
%!TEMPLATE_NAME="Fire"
%!SIMULATOR="fire"
%!TITLE=""
%!DESCRIPTION=""
%!WRITE_ALL_VARIABLES="false"
%!VERSION="v10.x"

SINGLE_FIELD_VARIABLES
  NLT        "LT        " 1          "(m)       " N
    "Turbulent length scale"
  NT         "T         " 1          "(K)       " N
    "Temperature"
  NTURB      "TURB      " 1          "(m/s)     " N
    "Turbulence velocity"
  NVVEC      "VVEC      " 3          "(m/s)     " N
    "Velocity vector"
  NU         "U         " 0          "(m/s)     " N
    "Velocity component x-direction"
  NV         "V         " 0          "(m/s)     " N
    "Velocity component y-direction"
  NW         "W         " 0          "(m/s)     " N
    "Velocity component z-direction"
  SOOT       "SOOT      " 1          "(-)       " N
    "Mass fraction of SOOT"
  VFSOOT     "VFSOOT    " 1          "(-)       " N
    "Volume fraction of SOOT"
  NQRAD      "QRAD      " 1          "(kW/m2)   " N
    "Radiative heat flux"
  NQCONV     "QCONV     " 1          "(kW/m2)   " N
    "Convective heat flux"
  NQ         "Q         " 1          "(kW/m2)   " N
    "Total heat flux"
  QWALL      "QWALL     " 1          "(kW/m2)   " N
    "Wall incident heat flux"
EXIT SINGLE_FIELD_VARIABLES

MONITOR_POINTS
%!NAME="TC1-1"
INSERT 1   1.8      1.2      2.62
DIRECTION   0        0        0
%!NAME="TC1-2"
INSERT 2   1.8      1.2      2.56
DIRECTION   0        0        0
%!NAME="TC1-3"
INSERT 3   1.8      1.2      2.535
DIRECTION   0        0        0
%!NAME="TC1-4"
INSERT 4   1.8      1.2      2.51
DIRECTION   0        0        0
```

```
%!NAME="TC1-5"
INSERT 5   1.8      1.2      2.485
DIRECTION   0        0        0
%!NAME="TC2-1"
INSERT 6   1.62     1.38     2.62
DIRECTION   0        0        0
%!NAME="TC2-2"
INSERT 7   1.62     1.38     2.56
DIRECTION   0        0        0
%!NAME="TC2-3"
INSERT 8   1.62     1.38     2.535
DIRECTION   0        0        0
%!NAME="TC2-4"
INSERT 9   1.62     1.38     2.51
DIRECTION   0        0        0
%!NAME="TC2-5"
INSERT 10   1.62     1.38     2.485
DIRECTION   0        0        0
%!NAME="TC2-6"
INSERT 11   1.62     1.38     2.46
DIRECTION   0        0        0
%!NAME="TC3-1"
INSERT 12   1.44     1.56     2.62
DIRECTION   0        0        0
%!NAME="TC3-2"
INSERT 13   1.44     1.56     2.56
DIRECTION   0        0        0
%!NAME="TC3-3"
INSERT 14   1.44     1.56     2.535
DIRECTION   0        0        0
%!NAME="TC3-4"
INSERT 15   1.44     1.56     2.51
DIRECTION   0        0        0
%!NAME="TC3-5"
INSERT 16   1.44     1.56     2.485
DIRECTION   0        0        0
%!NAME="TC3-6"
INSERT 17   1.44     1.56     2.46
DIRECTION   0        0        0
%!NAME="TC3-7"
INSERT 18   1.44     1.56     2.435
DIRECTION   0        0        0
%!NAME="TC4-1"
INSERT 19   1.26     1.74     2.62
DIRECTION   0        0        0
%!NAME="TC4-2"
INSERT 20   1.26     1.74     2.54
DIRECTION   0        0        0
%!NAME="TC4-3"
INSERT 21   1.26     1.74     2.515
DIRECTION   0        0        0
%!NAME="TC4-4"
INSERT 22   1.26     1.74     2.49
DIRECTION   0        0        0
%!NAME="TC4-5"
INSERT 23   1.26     1.74     2.465
DIRECTION   0        0        0
%!NAME="TC4-6"
INSERT 24   1.26     1.74     2.44
DIRECTION   0        0        0
%!NAME="TC4-7"
INSERT 25   1.26     1.74     2.415
DIRECTION   0        0        0
%!NAME="TC4-8"
INSERT 26   1.26     1.74     2.39
DIRECTION   0        0        0
%!NAME="TC5-1"
INSERT 27   1.08     1.92     2.62
DIRECTION   0        0        0
%!NAME="TC5-2"
```

```
INSERT 28   1.08     1.92     2.54
DIRECTION   0        0        0
%!NAME="TC5-3"
INSERT 29   1.08     1.92     2.515
DIRECTION   0        0        0
%!NAME="TC5-4"
INSERT 30   1.08     1.92     2.49
DIRECTION   0        0        0
%!NAME="TC5-5"
INSERT 31   1.08     1.92     2.465
DIRECTION   0        0        0
%!NAME="TC5-6"
INSERT 32   1.08     1.92     2.44
DIRECTION   0        0        0
%!NAME="TC5-7"
INSERT 33   1.08     1.92     2.415
DIRECTION   0        0        0
%!NAME="TC5-8"
INSERT 34   1.08     1.92     2.39
DIRECTION   0        0        0
%!NAME="TC5-9"
INSERT 35   1.08     1.92     2.365
DIRECTION   0        0        0
%!NAME="TC6-1"
INSERT 36   0.9      2.1      2.62
DIRECTION   0        0        0
%!NAME="TC6-2"
INSERT 37   0.9      2.1      2.53
DIRECTION   0        0        0
%!NAME="TC6-3"
INSERT 38   0.9      2.1      2.505
DIRECTION   0        0        0
%!NAME="TC6-4"
INSERT 39   0.9      2.1      2.48
DIRECTION   0        0        0
%!NAME="TC6-5"
INSERT 40   0.9      2.1      2.455
DIRECTION   0        0        0
%!NAME="TC6-6"
INSERT 41   0.9      2.1      2.43
DIRECTION   0        0        0
%!NAME="TC6-7"
INSERT 42   0.9      2.1      2.405
DIRECTION   0        0        0
%!NAME="TC6-8"
INSERT 43   0.9      2.1      2.38
DIRECTION   0        0        0
%!NAME="TC6-9"
INSERT 44   0.9      2.1      2.355
DIRECTION   0        0        0
%!NAME="TC6-10"
INSERT 45   0.9      2.1      2.33
DIRECTION   0        0        0
EXIT MONITOR_POINTS

PRESSURE_RELIEF_PANELS
EXIT PRESSURE_RELIEF_PANELS

SINGLE_FIELD_SCALAR_TIME_OUTPUT
NLT 1 2 3 4 5 6 7 8 9 10 11 12 13 14 15 16 17 18 19 20
 21 22 23 24 25 26 27 28 29 30 31 32 33 34 35 36 37 38 39 40
 41 42 43 44 45
NT 1 2 3 4 5 6 7 8 9 10 11 12 13 14 15 16 17 18 19 20
 21 22 23 24 25 26 27 28 29 30 31 32 33 34 35 36 37 38 39 40
 41 42 43 44 45
NTURB 1 2 3 4 5 6 7 8 9 10 11 12 13 14 15 16 17 18 19 20
 21 22 23 24 25 26 27 28 29 30 31 32 33 34 35 36 37 38 39 40
 41 42 43 44 45
NVVEC 1 2 3 4 5 6 7 8 9 10 11 12 13 14 15 16 17 18 19 20
 21 22 23 24 25 26 27 28 29 30 31 32 33 34 35 36 37 38 39 40
```

```
 41 42 43 44 45
NU 1 2 3 4 5 6 7 8 9 10 11 12 13 14 15 16 17 18 19 20
 21 22 23 24 25 26 27 28 29 30 31 32 33 34 35 36 37 38 39 40
 41 42 43 44 45
NV 1 2 3 4 5 6 7 8 9 10 11 12 13 14 15 16 17 18 19 20
 21 22 23 24 25 26 27 28 29 30 31 32 33 34 35 36 37 38 39 40
 41 42 43 44 45
NW 1 2 3 4 5 6 7 8 9 10 11 12 13 14 15 16 17 18 19 20
 21 22 23 24 25 26 27 28 29 30 31 32 33 34 35 36 37 38 39 40
 41 42 43 44 45
SOOT 1 2 3 4 5 6 7 8 9 10 11 12 13 14 15 16 17 18 19 20
 21 22 23 24 25 26 27 28 29 30 31 32 33 34 35 36 37 38 39 40
 41 42 43 44 45
VFSOOT 1 2 3 4 5 6 7 8 9 10 11 12 13 14 15 16 17 18 19 20
 21 22 23 24 25 26 27 28 29 30 31 32 33 34 35 36 37 38 39 40
 41 42 43 44 45
NQRAD 1 2 3 4 5 6 7 8 9 10 11 12 13 14 15 16 17 18 19 20
 21 22 23 24 25 26 27 28 29 30 31 32 33 34 35 36 37 38 39 40
 41 42 43 44 45
NQCONV 1 2 3 4 5 6 7 8 9 10 11 12 13 14 15 16 17 18 19 20
 21 22 23 24 25 26 27 28 29 30 31 32 33 34 35 36 37 38 39 40
 41 42 43 44 45
NQ 1 2 3 4 5 6 7 8 9 10 11 12 13 14 15 16 17 18 19 20
 21 22 23 24 25 26 27 28 29 30 31 32 33 34 35 36 37 38 39 40
 41 42 43 44 45
QWALL 1 2 3 4 5 6 7 8 9 10 11 12 13 14 15 16 17 18 19 20
 21 22 23 24 25 26 27 28 29 30 31 32 33 34 35 36 37 38 39 40
 41 42 43 44 45
EXIT SINGLE_FIELD_SCALAR_TIME_OUTPUT

SINGLE_FIELD_3D_OUTPUT
NLT
NT
NTURB
NVVEC
NU
NV
NW
SOOT
VFSOOT
NQRAD
NQCONV
NQ
QWALL
EXIT SINGLE_FIELD_3D_OUTPUT

SIMULATION_AND_OUTPUT_CONTROL
     TSTART                          -1
     TMAX                            20
     LAST                            -1
     LOAD                            -1
     CFLC                            20
     CFLV                            2
     STEP                            ""
     KEYS                            ""
     MODD                            1
     DTPLOT                          0.2
     GRID                            "CARTESIAN"
     INCOMPRESSIBLE                  0
     WALLF                           1
     HEAT_SWITCH                     1
EXIT SIMULATION_AND_OUTPUT_CONTROL

BOUNDARY_CONDITIONS
     XLO                             "NOZZLE"
     XHI                             "NOZZLE"
     YLO                             "NOZZLE"
     YHI                             "NOZZLE"
     ZLO                             "NOZZLE"
     ZHI                             "NOZZLE"
```

```
EXIT BOUNDARY_CONDITIONS

INITIAL_CONDITIONS
     UP-DIRECTION                   0              0              1
     GRAVITY_CONSTANT               9.8
     CHARACTERISTIC_VELOCITY        0
     RELATIVE_TURBULENCE_INTENSITY  0
     TURBULENCE_LENGTH_SCALE        0
     TEMPERATURE                    17
     AMBIENT_PRESSURE               100000
     AIR                            "NORMAL"
     GROUND_HEIGHT                  0
     GROUND_ROUGHNESS               0.0002
     REFERENCE_HEIGHT               10
     CANOPY_HEIGHT                  0
     LATITUDE                       0
     SURFACE_HEAT_P1                0              0              0
     SURFACE_HEAT_P2                0              0              0
     MEAN_SURFACE_HEAT_FLUX         0
     PASQUILL_CLASS                 "NONE"
     GROUND_ROUGHNESS_CONDITION     "RURAL"
EXIT INITIAL_CONDITIONS

GAS_COMPOSITION_AND_VOLUME
     POSITION_OF_FUEL_REGION        0              0              0
     DIMENSION_OF_FUEL_REGION       0              0              0
VOLUME_FRACTIONS
     METHANE                        0
     ACETYLENE                      0
     ETHYLENE                       0
     ETHANE                         0
     PROPYLENE                      0
     PROPANE                        1
     BUTANE                         0
     PENTANE                        0
     HEXANE                         0
     HEPTANE                        0
     OCTANE                         0
     NONANE                         0
     DECANE                         0
     HENDECANE                      0
     DODECANE                       0
     HYDROGEN                       0
     CO                             0
     H2S                            0
     H2O                            0
     CO2                            0
     USERSPEC_1                     0
     USERSPEC_2                     0
     USERSPEC_3                     0
EXIT VOLUME_FRACTIONS


     EQUIVALENCE_RATIOS_(ER0_ER9)   1e+30          0
EXIT GAS_COMPOSITION_AND_VOLUME

LEAKS
INSERT 1
     TYPE                           "DIFFUSE:AreaLeak(profile=Uniform,shape=Rectangular)"
     POSITION                       1.825          0.675          1.12
     SIZE                           0.5            0.5            0
     OPEN_SIDES                     "+Z"
     START_TIME                     0
     DURATION                       1000
OUTLET
     AREA                           0.25
     MASS_FLOW                      0.0009491555
     VELOCITY                       5
     RELATIVE_TURBULENCE_INTENSITY  0.05
     TURBULENCE_LENGTH_SCALE        0.05
```

```
     TEMPERATURE                    17
     DIRECTION_COSINES              0              0              0
EXIT OUTLET


VESSEL
     PRESSURE                       0
     TEMPERATURE                    0
     VOLUME                         0
     HEAT_EXCHANGE_COEFFICIENT      0
     WALL_TEMPERATURE               0
EXIT VESSEL


EXIT LEAKS

IGNITION
     POSITION_OF_IGNITION_REGION    1.825          0.675          1.12
     DIMENSION_OF_IGNITION_REGION   0.5            0.5            0.5
     TIME_OF_IGNITION               1
EXIT IGNITION

RADIATION
     RADIATION_MODEL                "DISCRETE TRANSFER METHOD"
     RADIATION_START                "WHEN IGNITED"
     RADIATION_START_TIME           0
     RADIATION_START_RAMP           0
     EMISSIVITY                     0.85
     ABSORPTION_COEFFICIENT_MODEL   "DANISH-COUPLED-WSGGM"
     ABSORPTION_COEFFICIENT         0
     SCATTERING_COEFFICIENT         0
     MEAN_BEAM_LENGTH_MODEL         "DOMAIN BASED"
     DTM_LOOP_MAX                   25
     DTM_TOLERANCE                  0.001
     DTM_MOD_ITER                   100
     DTM_MOD_TIME                   -1
     DTM_RAY_DISTRIBUTION           "STAGGERED"
     DTM_RAYS                       100
     DTM_VERBOSE                    1
     DTM_FULL_FLUX                  0
     DTM_BUFFER_SIZE                -1             0.01           -1
EXIT RADIATION

COMBUSTION
     COMBUSTION_MODEL               "EDDY DISSIPATION CONCEPT (EDC)"
     EXTINCTION                     0
     FIRESWITCH                     2
EXIT COMBUSTION

SOOT
     SOOT_MODEL                     "FORMATION - OXIDATION"
     SOOT_YIELD                     0.01
EXIT SOOT

CONDUCTION
     CONDUCTION_TYPE                "NO CONDUCTION"
EXIT CONDUCTION

EXIT
```

Appendix B

Scenario (.fds) file for FDS input

```
&HEAD CHID='000004', TITLE='Q=44 kW, h=1.12m, b=0.5m'  /
&TIME T_END=20. /

&MESH IJK=120,120,120, XB=0.0,3.0,0.0,3.0,0.0,3.0 /


&OBST XB= 0.28, 2.72, 0.28, 2.72, 2.64, 2.65 /
&OBST XB= 1.83, 2.33, 0.67, 1.17, 0.00, 1.12 /


&REAC SOOT_YIELD=0.01,FUEL='PROPANE'/
&SURF ID='fire', HRRPUA=176. /
&VENT XB= 1.83, 2.33, 0.67, 1.17, 1.12, 1.12, SURF_ID='fire' /


&MISC TMPA=17. /
&VENT MB='XMIN', SURF_ID='OPEN' /
&VENT MB='XMAX', SURF_ID='OPEN' /
&VENT MB='YMIN', SURF_ID='OPEN' /
&VENT MB='YMAX', SURF_ID='OPEN' /
&VENT MB='ZMIN', SURF_ID='OPEN' /
&VENT MB='ZMAX', SURF_ID='OPEN' /

&BNDF QUANTITY='RADIATIVE HEAT FLUX' /
&BNDF QUANTITY='CONVECTIVE HEAT FLUX' /
&BNDF QUANTITY='NET HEAT FLUX' /
&BNDF QUANTITY='WALL TEMPERATURE' /
&BNDF QUANTITY='BURNING RATE' /


&DEVC XYZ=1.80,1.20,2.62, QUANTITY='TEMPERATURE', ID='TC1-1' /
&DEVC XYZ=1.80,1.20,2.56, QUANTITY='TEMPERATURE', ID='TC1-2' /
&DEVC XYZ=1.80,1.20,2.535, QUANTITY='TEMPERATURE', ID='TC1-3' /
&DEVC XYZ=1.80,1.20,2.51, QUANTITY='TEMPERATURE', ID='TC1-4' /
&DEVC XYZ=1.80,1.20,2.485, QUANTITY='TEMPERATURE', ID='TC1-5' /

&DEVC XYZ=1.62,1.38,2.62, QUANTITY='TEMPERATURE', ID='TC2-1' /
&DEVC XYZ=1.62,1.38,2.56, QUANTITY='TEMPERATURE', ID='TC2-2' /
&DEVC XYZ=1.62,1.38,2.535, QUANTITY='TEMPERATURE', ID='TC2-3' /
&DEVC XYZ=1.62,1.38,2.51, QUANTITY='TEMPERATURE', ID='TC2-4' /
&DEVC XYZ=1.62,1.38,2.485, QUANTITY='TEMPERATURE', ID='TC2-5' /
&DEVC XYZ=1.62,1.38,2.46, QUANTITY='TEMPERATURE', ID='TC2-6' /

&DEVC XYZ=1.44,1.56,2.62, QUANTITY='TEMPERATURE', ID='TC3-1' /
&DEVC XYZ=1.44,1.56,2.56, QUANTITY='TEMPERATURE', ID='TC3-2' /
&DEVC XYZ=1.44,1.56,2.535, QUANTITY='TEMPERATURE', ID='TC3-3' /
&DEVC XYZ=1.44,1.56,2.51, QUANTITY='TEMPERATURE', ID='TC3-4' /
&DEVC XYZ=1.44,1.56,2.485, QUANTITY='TEMPERATURE', ID='TC3-5' /
&DEVC XYZ=1.44,1.56,2.46, QUANTITY='TEMPERATURE', ID='TC3-6' /
&DEVC XYZ=1.44,1.56,2.435, QUANTITY='TEMPERATURE', ID='TC3-7' /
```

```
&DEVC XYZ=1.26,1.74,2.62, QUANTITY='TEMPERATURE', ID='TC4-1' /
&DEVC XYZ=1.26,1.74,2.54, QUANTITY='TEMPERATURE', ID='TC4-2' /
&DEVC XYZ=1.26,1.74,2.515, QUANTITY='TEMPERATURE', ID='TC4-3' /
&DEVC XYZ=1.26,1.74,2.49, QUANTITY='TEMPERATURE', ID='TC4-4' /
&DEVC XYZ=1.26,1.74,2.465, QUANTITY='TEMPERATURE', ID='TC4-5' /
&DEVC XYZ=1.26,1.74,2.44, QUANTITY='TEMPERATURE', ID='TC4-6' /
&DEVC XYZ=1.26,1.74,2.415, QUANTITY='TEMPERATURE', ID='TC4-7' /
&DEVC XYZ=1.26,1.74,2.39, QUANTITY='TEMPERATURE', ID='TC4-8' /

&DEVC XYZ=1.08,1.92,2.62, QUANTITY='TEMPERATURE', ID='TC5-1' /
&DEVC XYZ=1.08,1.92,2.54, QUANTITY='TEMPERATURE', ID='TC5-2' /
&DEVC XYZ=1.08,1.92,2.515, QUANTITY='TEMPERATURE', ID='TC5-3' /
&DEVC XYZ=1.08,1.92,2.49, QUANTITY='TEMPERATURE', ID='TC5-4' /
&DEVC XYZ=1.08,1.92,2.465, QUANTITY='TEMPERATURE', ID='TC5-5' /
&DEVC XYZ=1.08,1.92,2.44, QUANTITY='TEMPERATURE', ID='TC5-6' /
&DEVC XYZ=1.08,1.92,2.415, QUANTITY='TEMPERATURE', ID='TC5-7' /
&DEVC XYZ=1.08,1.92,2.39, QUANTITY='TEMPERATURE', ID='TC5-8' /
&DEVC XYZ=1.08,1.92,2.365, QUANTITY='TEMPERATURE', ID='TC5-9' /

&DEVC XYZ=0.90,2.10,2.62, QUANTITY='TEMPERATURE', ID='TC6-1' /
&DEVC XYZ=0.90,2.10,2.53, QUANTITY='TEMPERATURE', ID='TC6-2' /
&DEVC XYZ=0.90,2.10,2.505, QUANTITY='TEMPERATURE', ID='TC6-3' /
&DEVC XYZ=0.90,2.10,2.48, QUANTITY='TEMPERATURE', ID='TC6-4' /
&DEVC XYZ=0.90,2.10,2.455, QUANTITY='TEMPERATURE', ID='TC6-5' /
&DEVC XYZ=0.90,2.10,2.43, QUANTITY='TEMPERATURE', ID='TC6-6' /
&DEVC XYZ=0.90,2.10,2.405, QUANTITY='TEMPERATURE', ID='TC6-7' /
&DEVC XYZ=0.90,2.10,2.38, QUANTITY='TEMPERATURE', ID='TC6-8' /
&DEVC XYZ=0.90,2.10,2.355, QUANTITY='TEMPERATURE', ID='TC6-9' /
&DEVC XYZ=0.90,2.10,2.33, QUANTITY='TEMPERATURE', ID='TC6-10' /


&DEVC XYZ=1.80,1.20,2.62, QUANTITY='CPU TIME' /


&SLCF PBY=0.92, QUANTITY=U-VELOCITY, VECTOR=.TRUE. /
&SLCF PBY=0.92, QUANTITY=V-VELOCITY /
&SLCF PBY=0.92, QUANTITY=W-VELOCITY /

&SLCF PBX=2.08, QUANTITY=U-VELOCITY, VECTOR=.TRUE. /
&SLCF PBX=2.08, QUANTITY=V-VELOCITY /
&SLCF PBX=2.08, QUANTITY=W-VELOCITY /

&SLCF PBZ=2.62, QUANTITY=U-VELOCITY, VECTOR=.TRUE. /
&SLCF PBZ=2.62, QUANTITY=V-VELOCITY /
&SLCF PBZ=2.62, QUANTITY=W-VELOCITY /


&TAIL /
```

Appendix C

MATLAB code for post-processing temperature results

```matlab
function [avg_temp,CJT]=temp_data(filename,TC_arrangement,method)
% [avg_temp,CJT]=temp_data(filename,TC_arrangement,method)
%
% Takes as input a valid filename (.LOG, .NT or .csv), termocouple
% (TC) arrangement(='green','red' or 'blue') and method ('exp',
% 'FLACS' or 'FDS'). It treats the file according to the method,
% reads values and returns the time-averaged temperatures with
% corresponding ceiling jet thickness, according to a temperature
% criterion.

% Open the file, read data (without headers) into matrix 'tempdata'.
if strcmp(method,'exp')
    % Read data file, replace comma with dot and save to a
    % temporary file, which is later deleted.
    raw_data = fileread(filename);
    raw_data = strrep(raw_data, ',', '.');
    file1 = fopen('temporary', 'w');
    fwrite(file1, raw_data, 'char');
    fclose(file1);
    file2 = fopen('temporary');
    d = textscan(file2, '%f%f%f%f%f%f%f%f%f%f%f%f%f%f%f%f%f%f%f'...
        '%f%f%f%f%f%f%f%f%f%f%f%f%f%f%f%f%f%f%f%f%f%f%f%f%f%f%f', ...
        'HeaderLines',5, 'Delimiter','\n', 'CollectOutput',1);
        fclose(file2);
        delete('temporary')
        tempdata = cell2mat(d);
elseif strcmp(method,'FLACS')
    file2 = fopen(filename);
    d = textscan(file2, '%f%f%f%f%f%f%f%f%f%f%f%f%f%f%f%f%f%f%f'...
        '%f%f%f%f%f%f%f%f%f%f%f%f%f%f%f%f%f%f%f%f%f%f%f%f%f%f%f', ...
        'HeaderLines',5,'Delimiter','\n', 'CollectOutput',1);
        fclose(file2);
        tempdata = cell2mat(d);
elseif strcmp(method,'FDS')
    tempdata=csvread(filename,2);
end

% Time vector
time = tempdata(:,1);

% Defining the point at which flame is stabilized. For simulations,
% this is after roughly 5 seconds, while for experiments all values
% are after steady state is reached.
if strcmp(method,'FLACS')
    steady=find(time>5,1);
    % FLACS stores temperatures in Kelvin by default, they are here
    % changed to Celsius:
    tempdata(:,2:46)=tempdata(:,2:46)-273.15;
```

```
elseif strcmp(method,'FDS')
    steady=find(time>5,1);
else
    steady=1;
end

% Define temperatures in thermocouple trees (TCX). Due to a 'wrong'
% placement of TC3-3 in experiments, TC3 is treated separately.
TC1 = tempdata(steady:end,2:6);
TC2 = tempdata(steady:end,7:12);
if strcmp(method,'FLACS')|strcmp(method,'FDS')
    TC3 = tempdata(steady:end,13:19);
elseif strcmp(method,'exp')
    TC3(:,1:2) = tempdata(steady:end,13:14);
    TC3(:,3) = tempdata(steady:end,19);
    TC3(:,4:7) = tempdata(steady:end,15:18);
end
TC4 = tempdata(steady:end,20:27);
TC5 = tempdata(steady:end,28:36);
TC6 = tempdata(steady:end,37:46);

% Time average of each thermocouple, placed in a matrix. Empty
% spaces in the matrix are set to zero by default.
avg_temp(1:5,1) = mean(TC1);
avg_temp(1:6,2) = mean(TC2);
avg_temp(1:7,3) = mean(TC3);
avg_temp(1:8,4) = mean(TC4);
avg_temp(1:9,5) = mean(TC5);
avg_temp(1:10,6) = mean(TC6);

% Ambient temperature:
Tamb=17;

% Temperature criterion for each thermocouple tree:
% Excess temperature drops to (1/e) of delta Tmax.
t_crit(1)=max(avg_temp(:,1))*(1/exp(1))+((exp(1)-1)/exp(1))*Tamb;
t_crit(2)=max(avg_temp(:,2))*(1/exp(1))+((exp(1)-1)/exp(1))*Tamb;
t_crit(3)=max(avg_temp(:,3))*(1/exp(1))+((exp(1)-1)/exp(1))*Tamb;
t_crit(4)=max(avg_temp(:,4))*(1/exp(1))+((exp(1)-1)/exp(1))*Tamb;
t_crit(5)=max(avg_temp(:,5))*(1/exp(1))+((exp(1)-1)/exp(1))*Tamb;
t_crit(6)=max(avg_temp(:,6))*(1/exp(1))+((exp(1)-1)/exp(1))*Tamb;

% Determination of ceiling jet thickness at each radial position.
% Start values:
CJT=[0.02 0.02 0.02 0.02 0.02 0.02];
go_on=true;
% Second thermocouple in each tree is placed to catch the entire
% ceiling jet. These are therefore treated separately.
for i=1:3
    if avg_temp(2,i)>=t_crit(i)
        if strcmp(TC_arrangement,'green')
            CJT(i)=CJT(i)+0.06;
        elseif strcmp(TC_arrangement,'red')
            CJT(i)=CJT(i)+0.03;
        elseif strcmp(TC_arrangement,'blue')
            CJT(i)=CJT(i)+0.11;
        end
    else
        go_on=false;
    end
end
if avg_temp(2,4)>=t_crit(4)
    if strcmp(TC_arrangement,'green')
        CJT(4)=CJT(4)+0.08;
    elseif strcmp(TC_arrangement,'red')
        CJT(4)=CJT(4)+0.04;
    elseif strcmp(TC_arrangement,'blue')
        CJT(4)=CJT(4)+0.13;
    end
else
```

```
    go_on=false;
end
if avg_temp(2,5)>=t_crit(5)
    if strcmp(TC_arrangement,'green')
        CJT(5)=CJT(5)+0.08;
    elseif strcmp(TC_arrangement,'red')
        CJT(5)=CJT(5)+0.05;
    elseif strcmp(TC_arrangement,'blue')
        CJT(5)=CJT(5)+0.13;
    end
else
    go_on=false;
end
if avg_temp(2,6)>=t_crit(6)
    if strcmp(TC_arrangement,'green')
        CJT(6)=CJT(6)+0.09;
    elseif strcmp(TC_arrangement,'red')
        CJT(6)=CJT(6)+0.05;
    elseif strcmp(TC_arrangement,'blue')
        CJT(6)=CJT(6)+0.13;
    end
else
    go_on=false;
end
% Further, for all temperatures higher than the temperature
% criterion, 2.5 cm is added to the ceiling jet thickness.
% Moves through each column (termocouple tree) and stores the
% thicknesses in vector CJT.
if go_on==true
    for i=1:size(avg_temp,2)
        for j=3:size(avg_temp,1)
            if avg_temp(j,i)>=t_crit(i)
                CJT(i)=CJT(i)+0.025;
            else
                break
            end
        end
    end
end
```

Appendix D

MATLAB code for plotting temperature results

```matlab
function plot_temp(exp_temp,FLACS_temp,FDS_temp,alpert,...
    TC_arrangement,titlefig)
% plot_temp(exp_temp,FLACS_temp,FDS_temp,alpert,...
%           TC_arrangement,titlefig)
%
% Takes as input matrices of dimension 10x6 with results from
% experiments (exp_temp) and simulations (FLACS_temp and FDS_temp),
% as well as a 1x6 vector of Alpert's temperature correlations,
% thermocouple (TC) arrangement ('green','red' or 'blue') and the
% desired title of the plot. The function then plots maximum
% temperatures vs. radial distance, and temperature vs. distance
% below ceiling for all TC-trees. A pdf-file with name titlefig.pdf
% is produced, containing the plot.

% Radial distances, r:
r=[0.4 0.65 0.9 1.15 1.4 1.65];

% Distances below ceiling, z:
if strcmp(TC_arrangement,'green')
    z=[0.02 0.02 0.02 0.02 0.02 0.02; 0.08 0.08 0.08 0.1 0.1 ...
        0.11; 0.105 0.105 0.105 0.125 0.125 0.135; 0.13 0.13 ...
        0.13 0.15 0.15 0.16; 0.155 0.155 0.155 0.175 0.175 ...
        0.185; 0 0.18 0.18 0.2 0.2 0.21; 0 0 0.205 0.225 0.225...
        0.235; 0 0 0 0.25 0.25 0.26; 0 0 0 0 0.275 0.285; ...
        0 0 0 0 0 0.31];
elseif strcmp(TC_arrangement,'blue')
    z=[0.02 0.02 0.02 0.02 0.02 0.02; 0.13 0.13 0.13 0.15 ...
        0.15 0.15; 0.155 0.155 0.155 0.175 0.175 0.175; 0.18 ...
        0.18 0.18 0.2 0.2 0.2; 0.205 0.205 0.205 0.225 0.225 ...
        0.225; 0 0.23 0.23 0.25 0.25 0.25; 0 0 0.255 0.275 ...
        0.275 0.275; 0 0 0 0.3 0.3 0.3; 0 0 0 0 0.325 0.325; ...
        0 0 0 0 0 0.35];
elseif strcmp(TC_arrangement,'red')
     z=[0.02 0.02 0.02 0.02 0.02 0.02; 0.05 0.05 0.05 0.06 ...
         0.07 0.07; 0.075 0.075 0.075 0.085 0.095 0.095; 0.1 ...
         0.1 0.1 0.11 0.12 0.12; 0.125 0.125 0.125 0.135 0.145 ...
         0.145; 0 0.15 0.15 0.16 0.17 0.17; 0 0 0.175 0.185 ...
         0.195 0.195; 0 0 0 0.21 0.22 0.22; 0 0 0 0 0.245 0.245;...
         0 0 0 0 0 0.27];
end

% Experimental temperatures, radial and TC-tree:
T_r_exp=exp_temp(1,:);
T1_z_exp=exp_temp(:,1);
T2_z_exp=exp_temp(:,2);
T3_z_exp=exp_temp(:,3);
T4_z_exp=exp_temp(:,4);
T5_z_exp=exp_temp(:,5);
```

```
T6_z_exp=exp_temp(:,6);

% FLACS temperatures, radial and TC-trees:
T_r_FLACS=FLACS_temp(1,:);
T1_z_FLACS=FLACS_temp(:,1);
T2_z_FLACS=FLACS_temp(:,2);
T3_z_FLACS=FLACS_temp(:,3);
T4_z_FLACS=FLACS_temp(:,4);
T5_z_FLACS=FLACS_temp(:,5);
T6_z_FLACS=FLACS_temp(:,6);

% FDS temperatures, radial and TC-trees:
T_r_FDS=FDS_temp(1,:);
T1_z_FDS=FDS_temp(:,1);
T2_z_FDS=FDS_temp(:,2);
T3_z_FDS=FDS_temp(:,3);
T4_z_FDS=FDS_temp(:,4);
T5_z_FDS=FDS_temp(:,5);
T6_z_FDS=FDS_temp(:,6);

% Finding the maximum temperature, for optimal limits to the
% temperature axis of the plots:
max_temp=[T_r_exp(1,1) T_r_FLACS(1,1) T_r_FDS(1,1)];
lim=max(max_temp);

% Defining the figure:
fig=figure(’units’,’normalized’,’position’,[.1 .1 .4 .8]);

% Plotting maximum temperature at all radial positions:
T_r_plot = subplot(4,2,1:2);
plot(r,T_r_exp,’-sk’,’MarkerFaceColor’,’k’);
hold on
plot(r,alpert,’-.*k’);
hold on
plot(r,T_r_FLACS,’--ok’);
hold on
plot(r,T_r_FDS,’:^k’);
title(titlefig,’FontSize’,16, ’Units’, ’normalized’,...
    ’Position’,[0.67 1.15])
xlabel(’r, m’,’FontSize’,10);
ylabel(’T, \circC’,’FontSize’,10);
legend(’Experimental’,’Alpert’,’FLACS’,’FDS’,...
    ’Location’,’EastOutside’);
axis([0.4,1.65,0,lim+5]);
grid on;
set(T_r_plot,’XTick’,[0.4:0.25:1.65],’YTick’,[0:25:lim])

% Plotting T at different z’s for all TC-trees:
T1_z_plot = subplot(4,2,3);
plot(T1_z_exp(1:5),z(1:5,1),’-sk’,’MarkerFaceColor’,’k’);
hold on
plot(T1_z_FLACS(1:5),z(1:5,1),’--ok’);
hold on
plot(T1_z_FDS(1:5),z(1:5,1),’:^k’);
ylabel(’z, m’,’FontSize’,10);
xlabel(’T, \circC’,’FontSize’,10);
title(’TC1’);
axis([0,lim+5,0,max(z(1:5,1))+0.02]);
set(T1_z_plot,’YDir’,’Reverse’);
grid on;
set(T1_z_plot,’XTick’,[0:25:lim],’YTick’,[0:0.05:max(z(1:5,1))])

T2_z_plot = subplot(4,2,4);
plot(T2_z_exp(1:6),z(1:6,2),’-sk’,’MarkerFaceColor’,’k’);
hold on
plot(T2_z_FLACS(1:6),z(1:6,2),’--ok’);
hold on
plot(T2_z_FDS(1:6),z(1:6,2),’:^k’);
ylabel(’z, m’,’FontSize’,10);
xlabel(’T, \circC’,’FontSize’,10);
```

```
title(’TC2’);
axis([0,lim+5,0,max(z(1:6,2))+0.02]);
set(T2_z_plot,’YDir’,’Reverse’);
grid on;
set(T2_z_plot,’XTick’,[0:25:lim],’YTick’,[0:0.05:max(z(1:6,2))])

T3_z_plot = subplot(4,2,5);
plot(T3_z_exp(1:7),z(1:7,3),’-sk’,’MarkerFaceColor’,’k’);
hold on
plot(T3_z_FLACS(1:7),z(1:7,3),’--ok’);
hold on
plot(T3_z_FDS(1:7),z(1:7,3),’:^k’);
ylabel(’z, m’,’FontSize’,10);
xlabel(’T, \circC’,’FontSize’,10);
title(’TC3’);
axis([0,lim+5,0,max(z(1:7,3))+0.02]);
set(T3_z_plot,’YDir’,’Reverse’);
grid on;
set(T3_z_plot,’XTick’,[0:25:lim],’YTick’,[0:0.05:max(z(1:7,3))])

T4_z_plot = subplot(4,2,6);
plot(T4_z_exp(1:8),z(1:8,4),’-sk’,’MarkerFaceColor’,’k’);
hold on
plot(T4_z_FLACS(1:8),z(1:8,4),’--ok’);
hold on
plot(T4_z_FDS(1:8),z(1:8,4),’:^k’);
ylabel(’z, m’,’FontSize’,10);
xlabel(’T, \circC’,’FontSize’,10);
title(’TC4’);
axis([0,lim+5,0,max(z(1:8,4))+0.02]);
set(T4_z_plot,’YDir’,’Reverse’);
grid on;
set(T4_z_plot,’XTick’,[0:25:lim],’YTick’,[0:0.05:max(z(1:8,4))])

T5_z_plot = subplot(4,2,7);
plot(T5_z_exp(1:9),z(1:9,5),’-sk’,’MarkerFaceColor’,’k’);
hold on
plot(T5_z_FLACS(1:9),z(1:9,5),’--ok’);
hold on
plot(T5_z_FDS(1:9),z(1:9,5),’:^k’);
ylabel(’z, m’,’FontSize’,10);
xlabel(’T, \circC’,’FontSize’,10);
title(’TC5’);
axis([0,lim+5,0,max(z(1:9,5))+0.02]);
set(T5_z_plot,’YDir’,’Reverse’);
grid on;
set(T5_z_plot,’XTick’,[0:25:lim],’YTick’,[0:0.05:max(z(1:9,5))])

T6_z_plot = subplot(4,2,8);
plot(T6_z_exp(1:10),z(1:10,6),’-sk’,’MarkerFaceColor’,’k’);
hold on
plot(T6_z_FLACS(1:10),z(1:10,6),’--ok’);
hold on
plot(T6_z_FDS(1:10),z(1:10,6),’:^k’);
ylabel(’z, m’,’FontSize’,10);
xlabel(’T, \circC’,’FontSize’,10);
title(’TC6’);
axis([0,lim+5,0,max(z(1:10,6))+0.02]);
set(T6_z_plot,’YDir’,’Reverse’);
grid on;
set(T6_z_plot,’XTick’,[0:25:lim],’YTick’,[0:0.05:max(z(1:10,6))])

% Producing pdf-file:
set(fig,’Units’,’Inches’);
pos = get(fig,’Position’);
set(fig,’PaperPositionMode’,’Auto’,’PaperUnits’,’Inches’,...
    ’PaperSize’,[pos(3), pos(4)]);
print(fig,titlefig,’-dpdf’,’-r0’);
```

Appendix E

Temperature plots

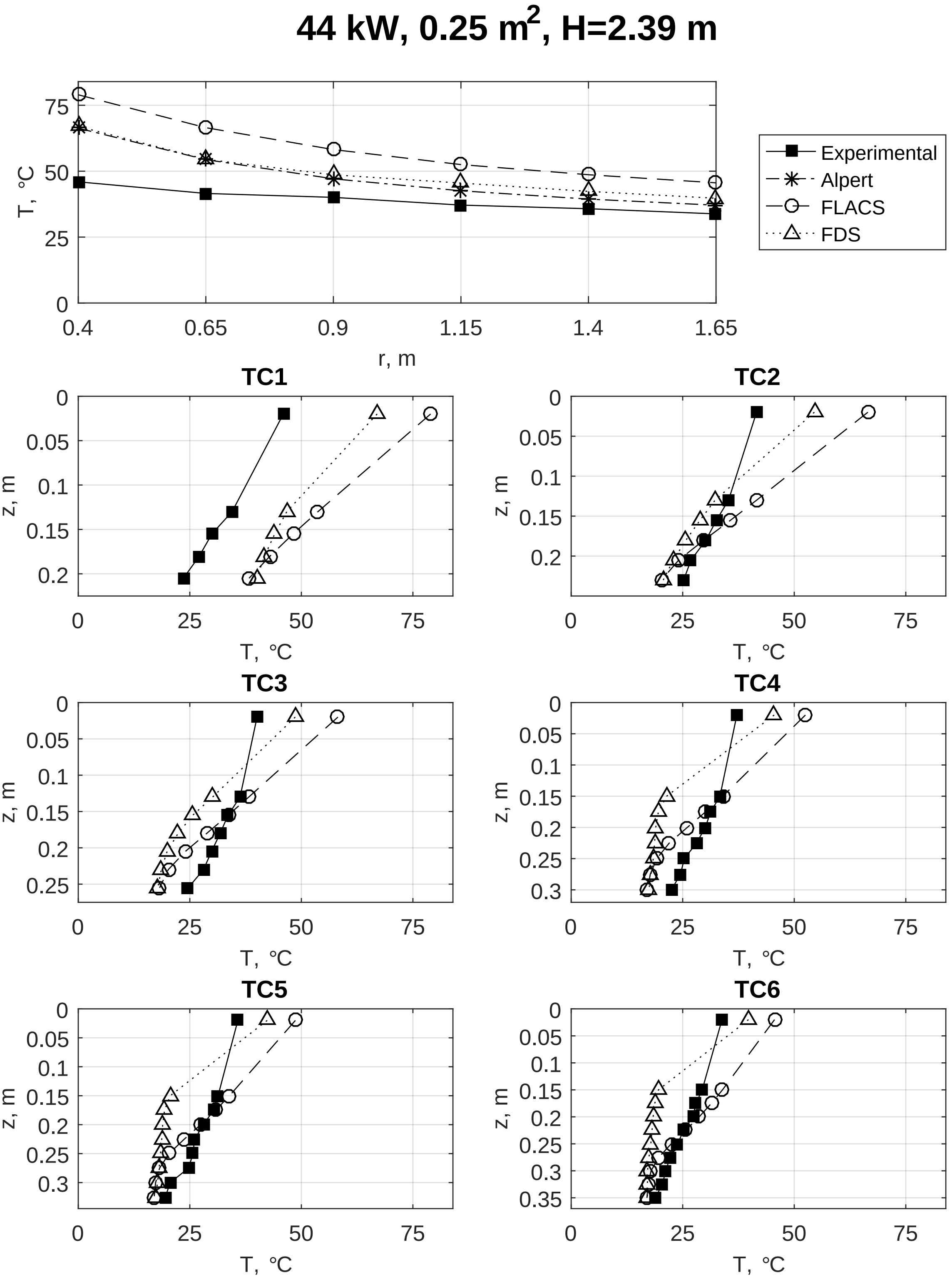

Figure E.1: Temperature results for case 000000, with $\dot{Q}$=44 kW, H=2.39 m and burner area 0.25 m^2.

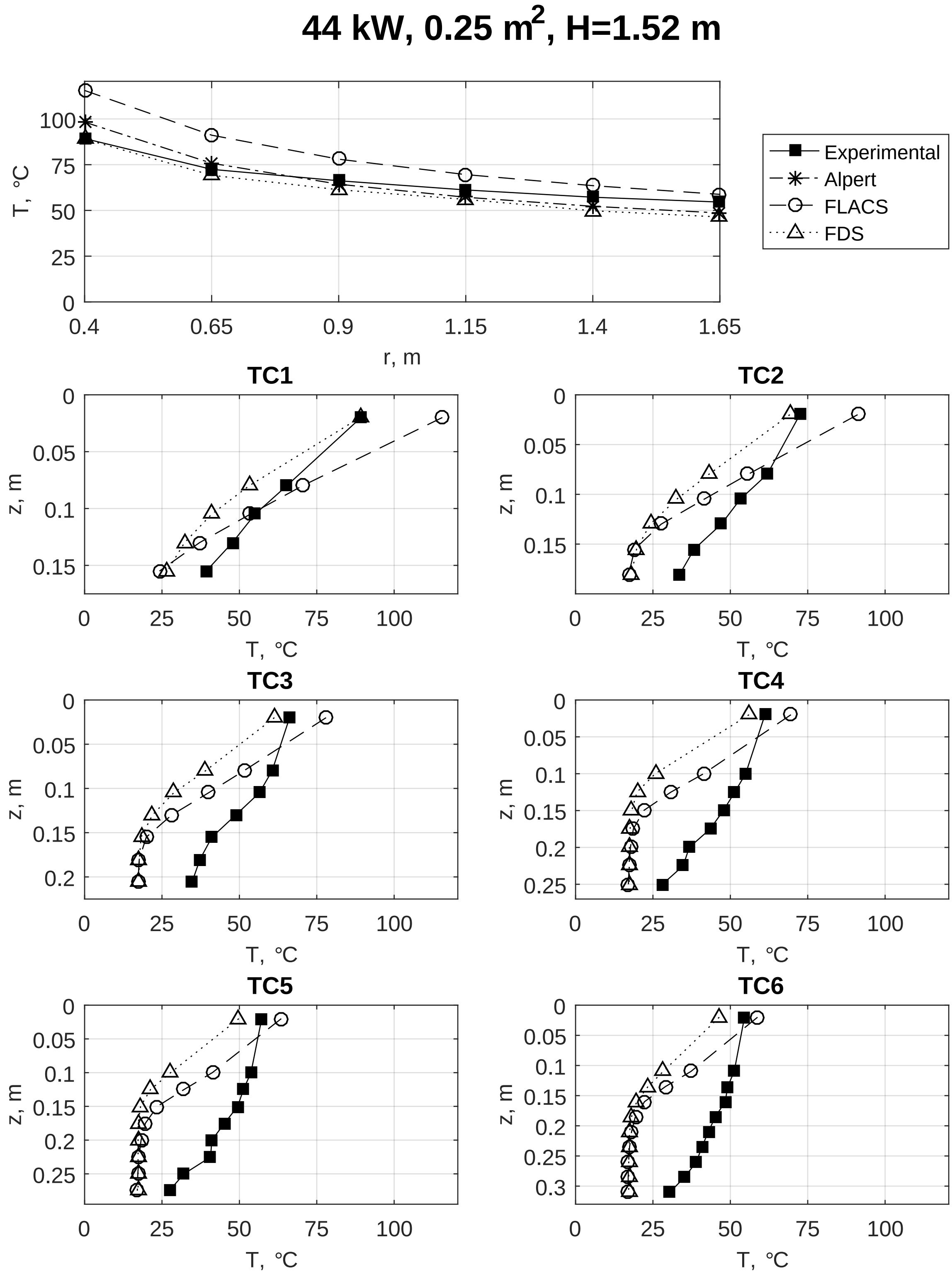

Figure E.2: Temperature results for case 000004, with $\dot{Q}$=44 kW, H=1.52 m and burner area 0.25 m^2.

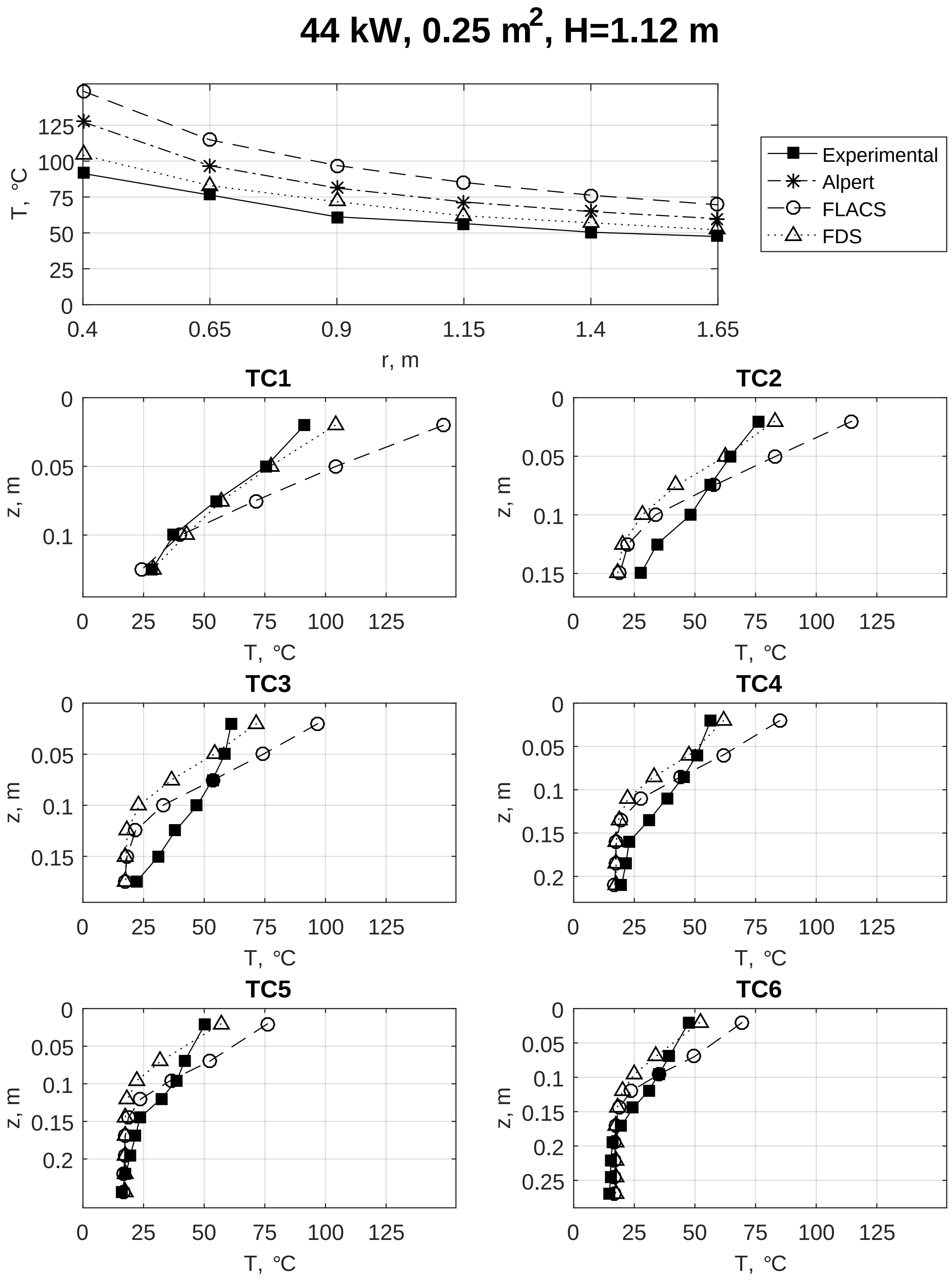

Figure E.3: Temperature results for case 000005, with $\dot{Q}$=44 kW, H=1.12 m and burner area 0.25 m^2.

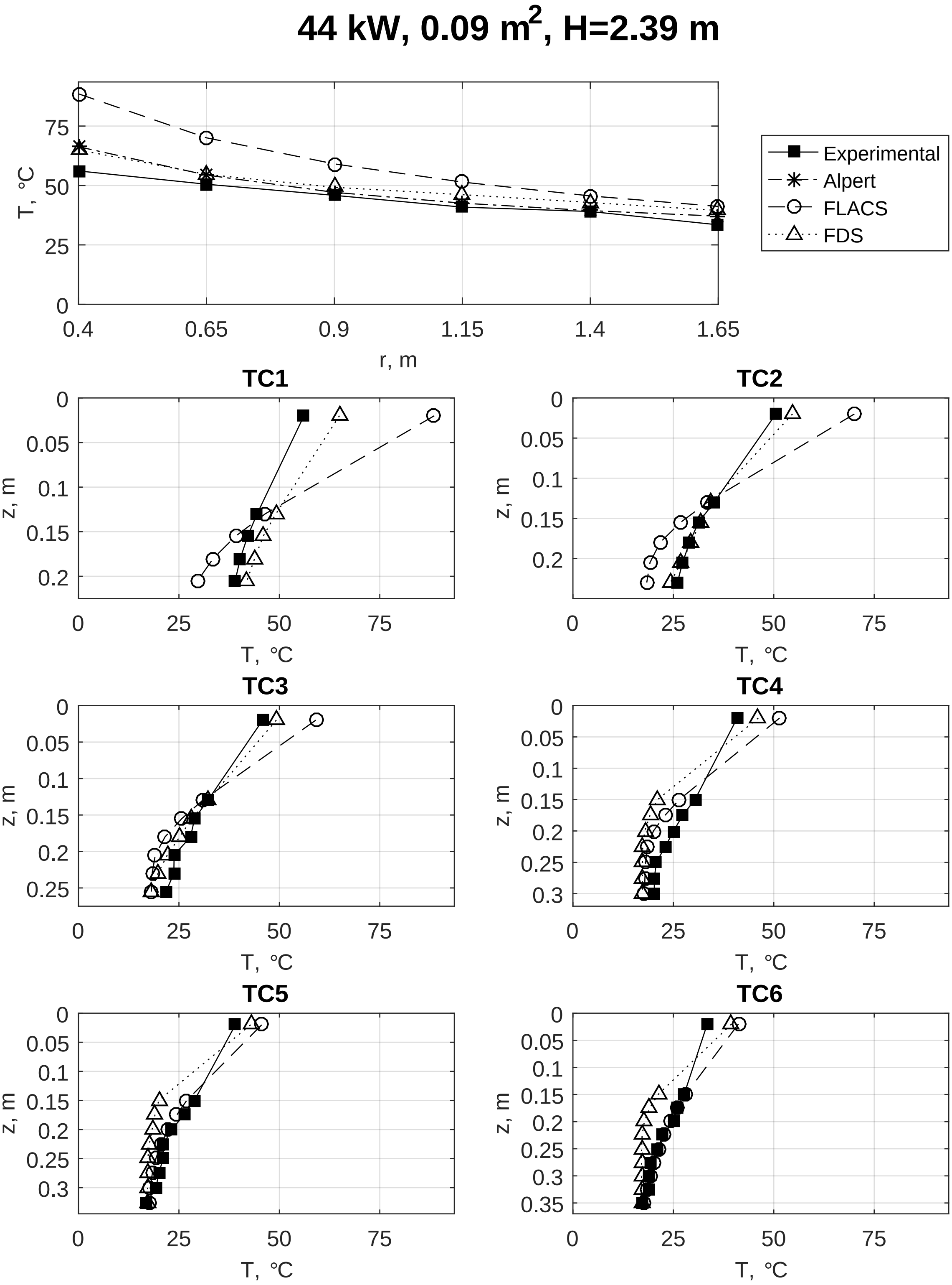

Figure E.4: Temperature results for case 000010, with $\dot{Q}$=44 kW, H=2.39 m and burner area 0.09 m^2.

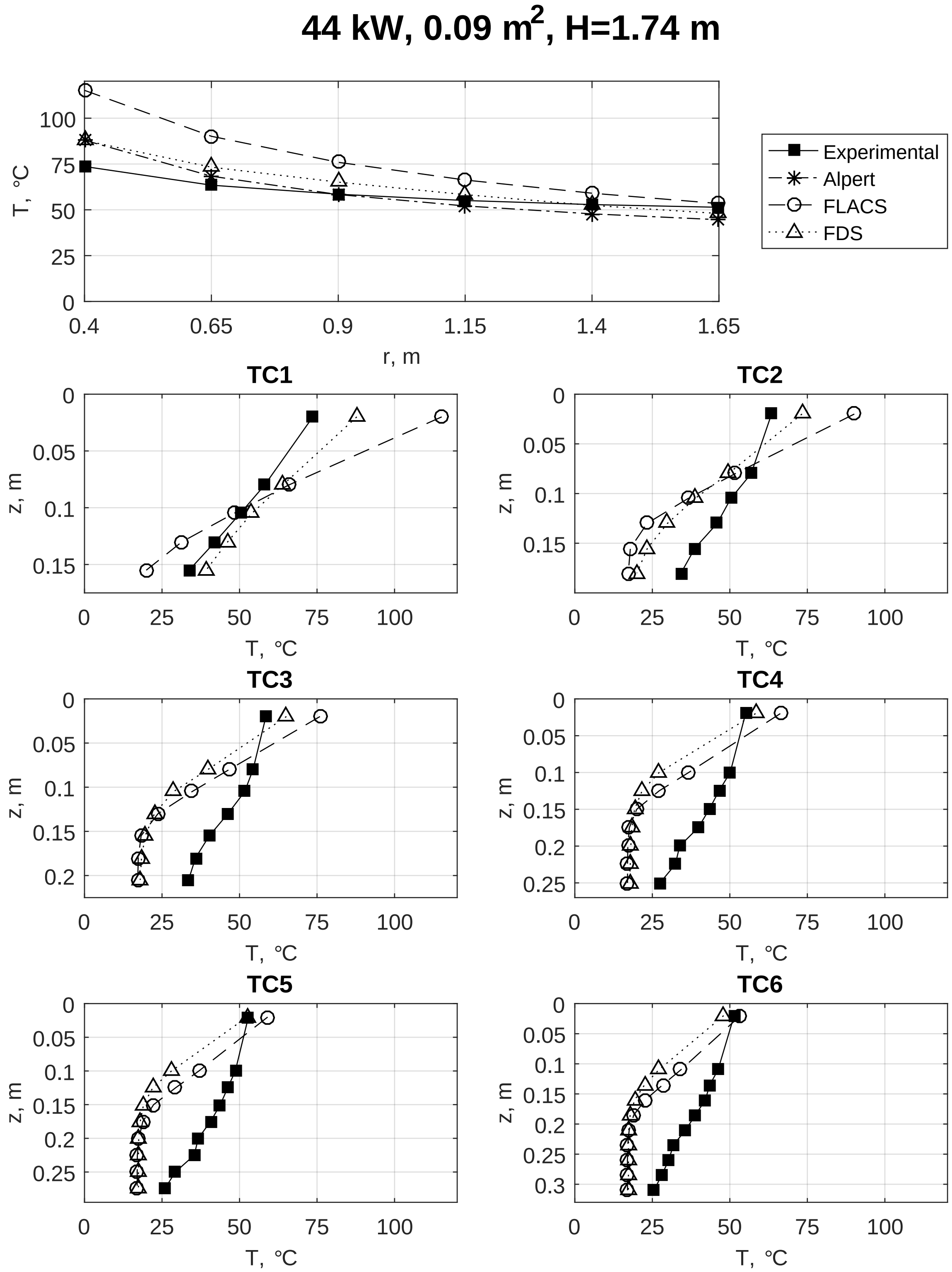

Figure E.5: Temperature results for case 000013, with $\dot{Q}$=44 kW, H=1.74 m and burner area 0.09 m^2.

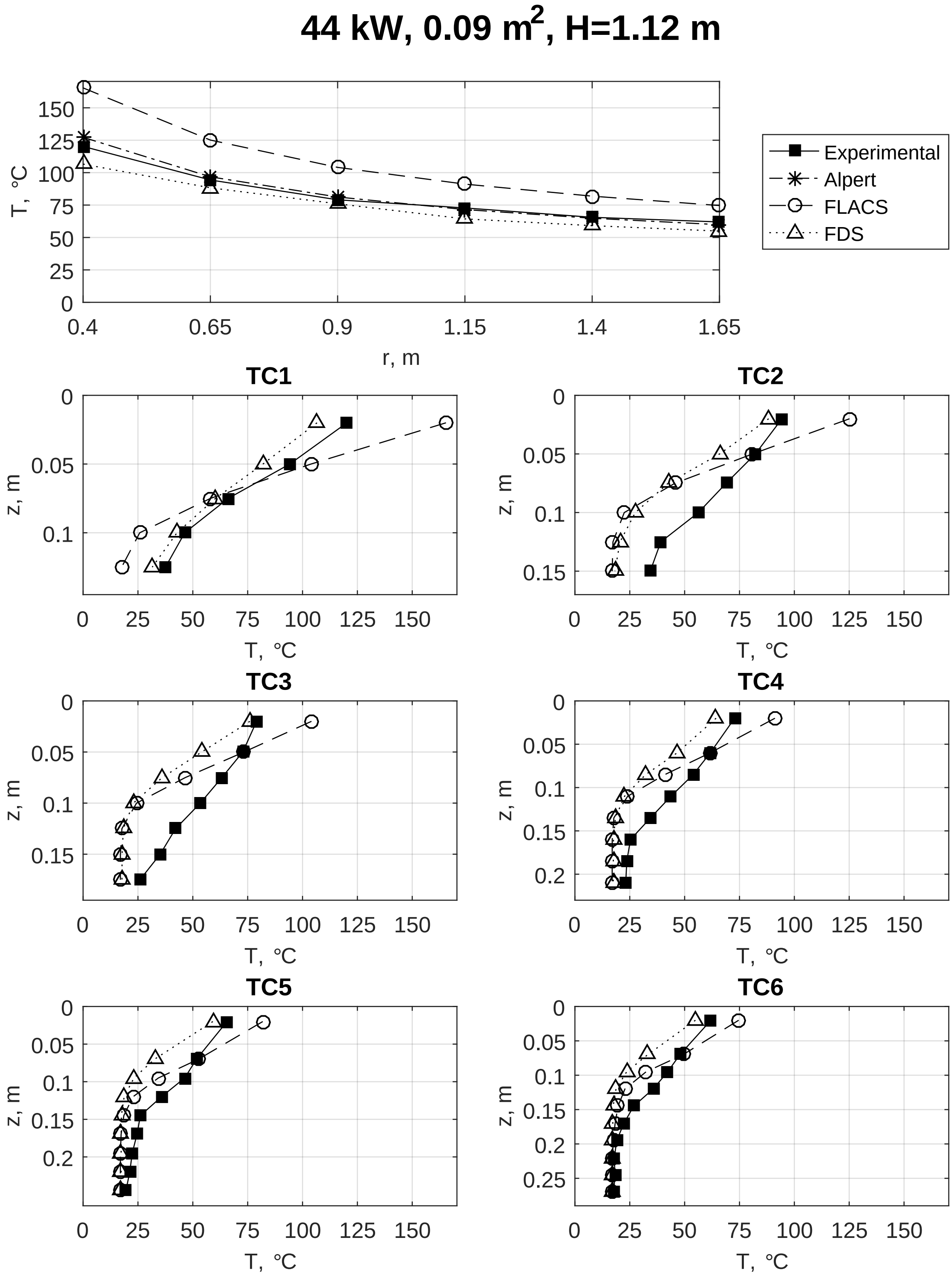

Figure E.6: Temperature results for case 000015, with $\dot{Q}$=44 kW, H=1.12 m and burner area 0.09 m^2.

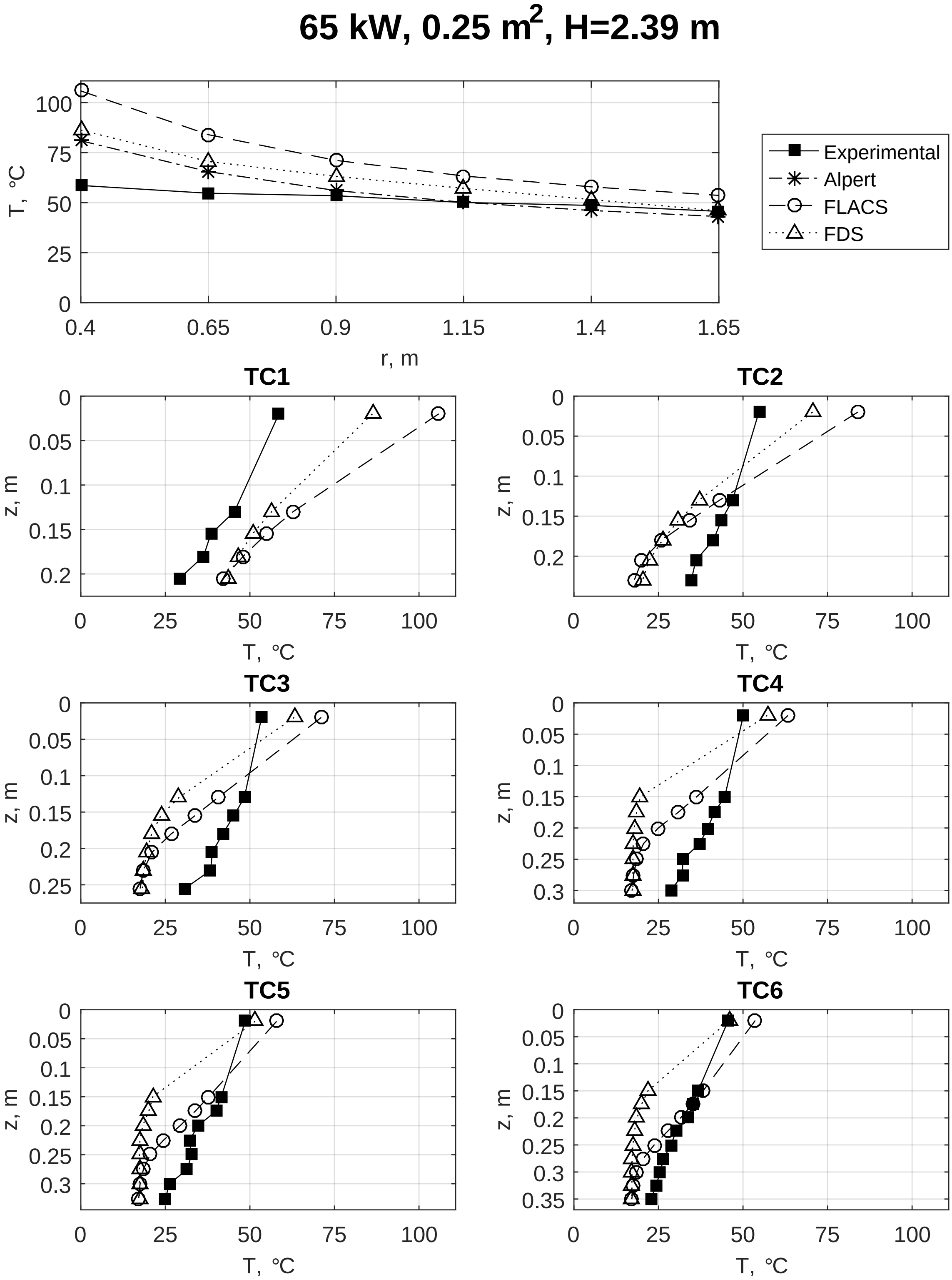

Figure E.7: Temperature results for case 100000, with $\dot{Q}$=65 kW, H=2.39 m and burner area 0.25 m^2.

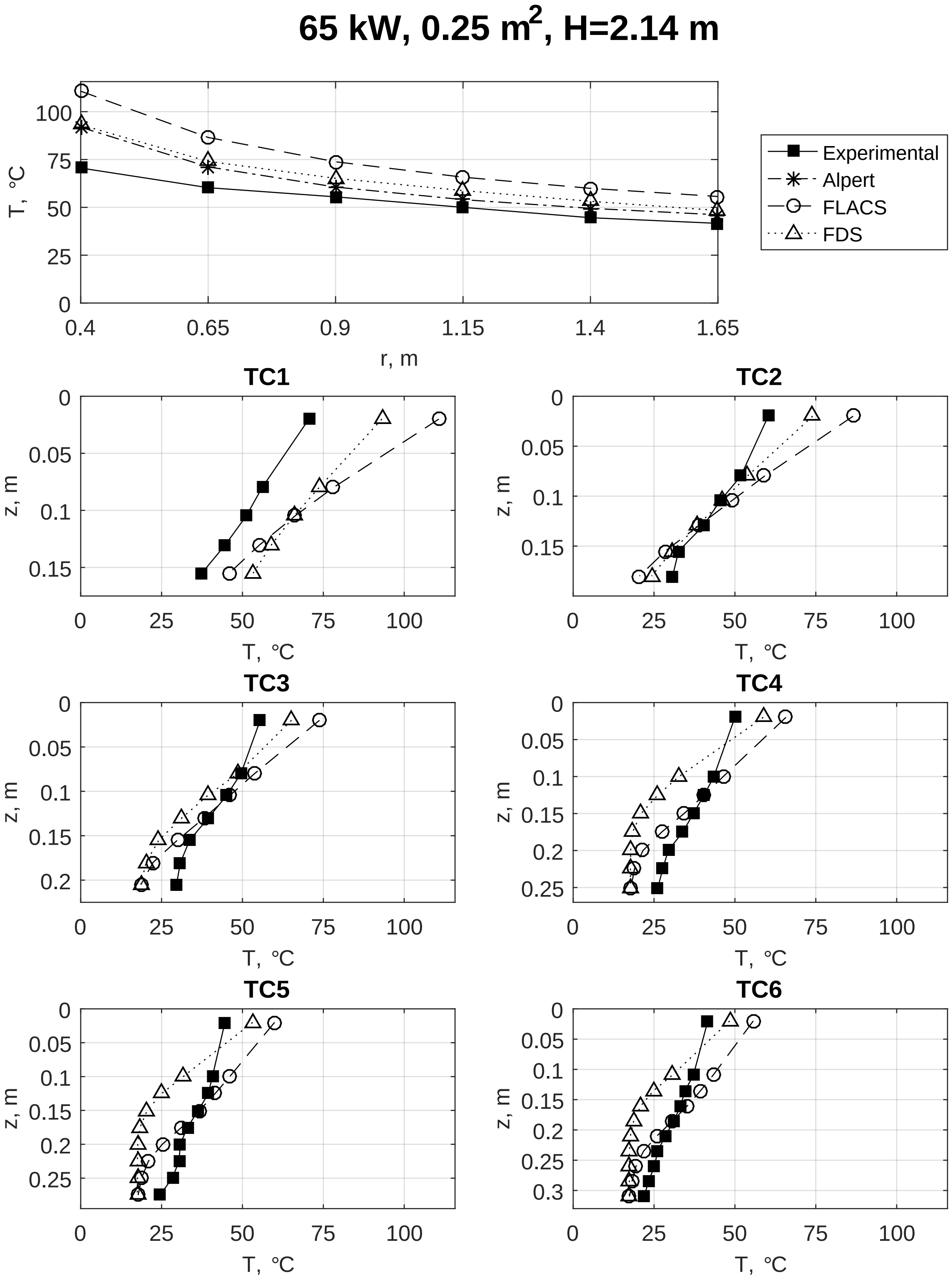

Figure E.8: Temperature results for case 100001, with $\dot{Q}$=65 kW, H=2.14 m and burner area 0.25 m^2.

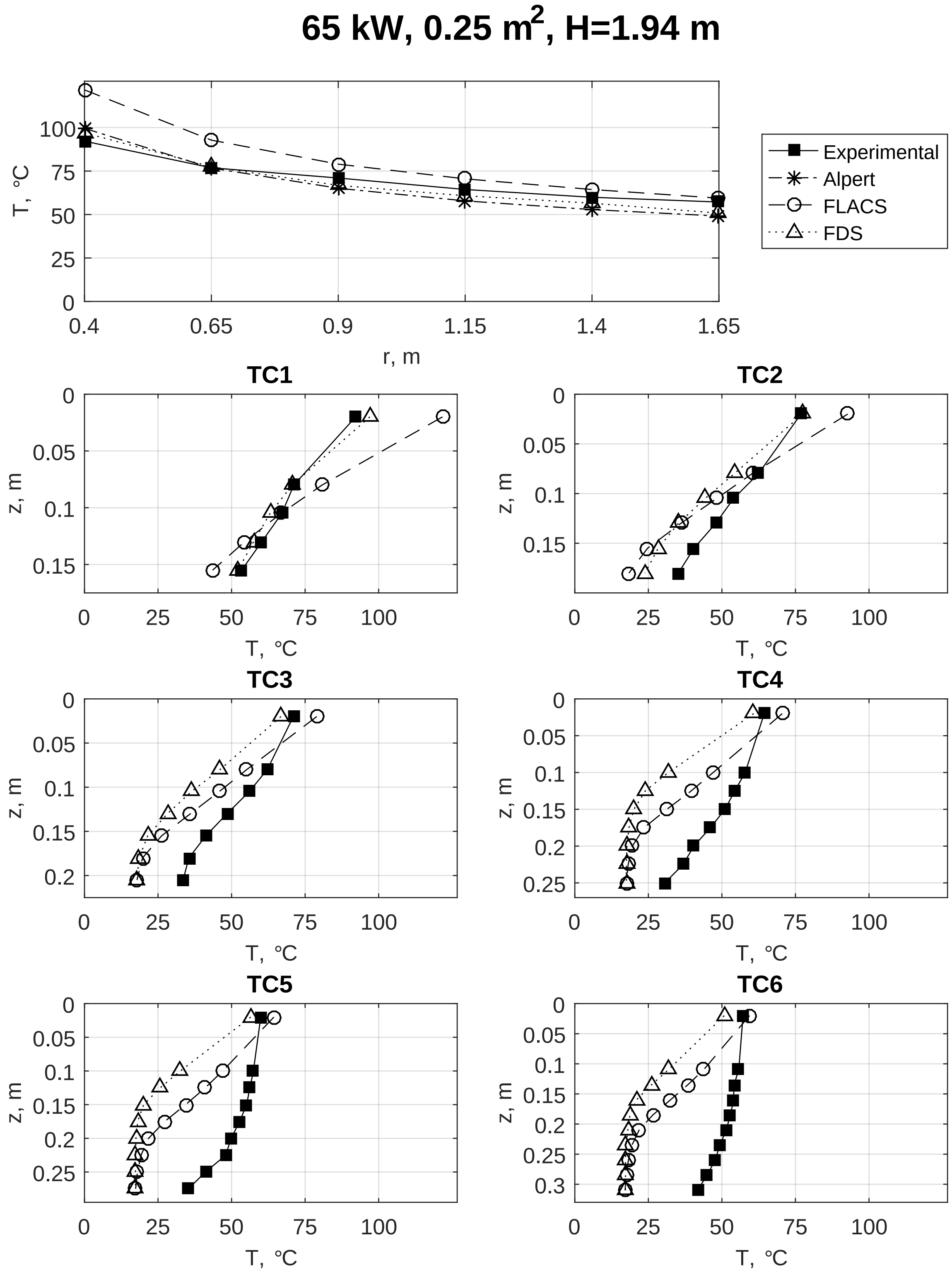

Figure E.9: Temperature results for case 100002, with $\dot{Q}$=65 kW, H=1.94 m and burner area 0.25 m^2.

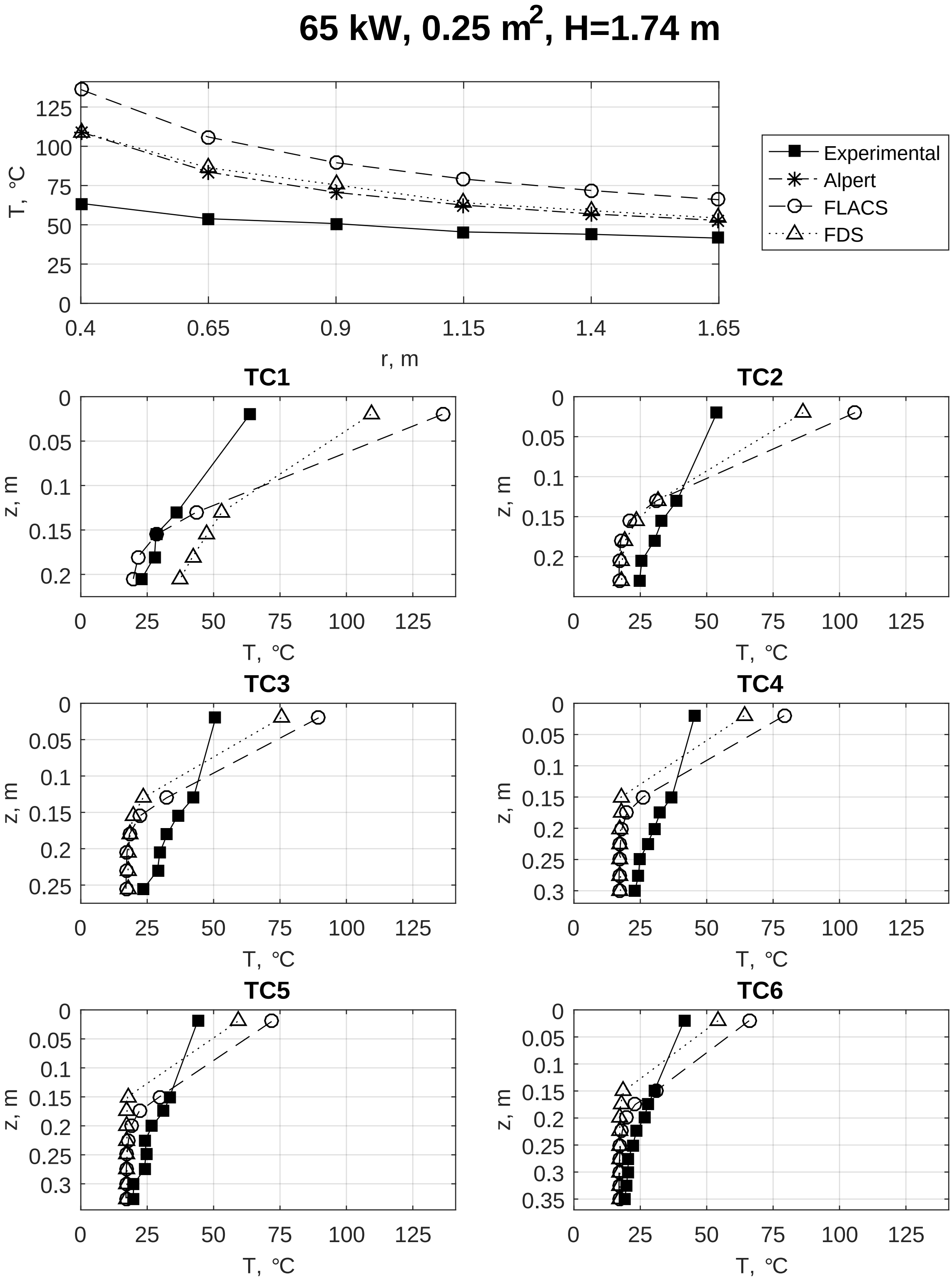

Figure E.10: Temperature results for case 100003, with $\dot{Q}$=65 kW, H=1.74 m and burner area 0.25 m^2.

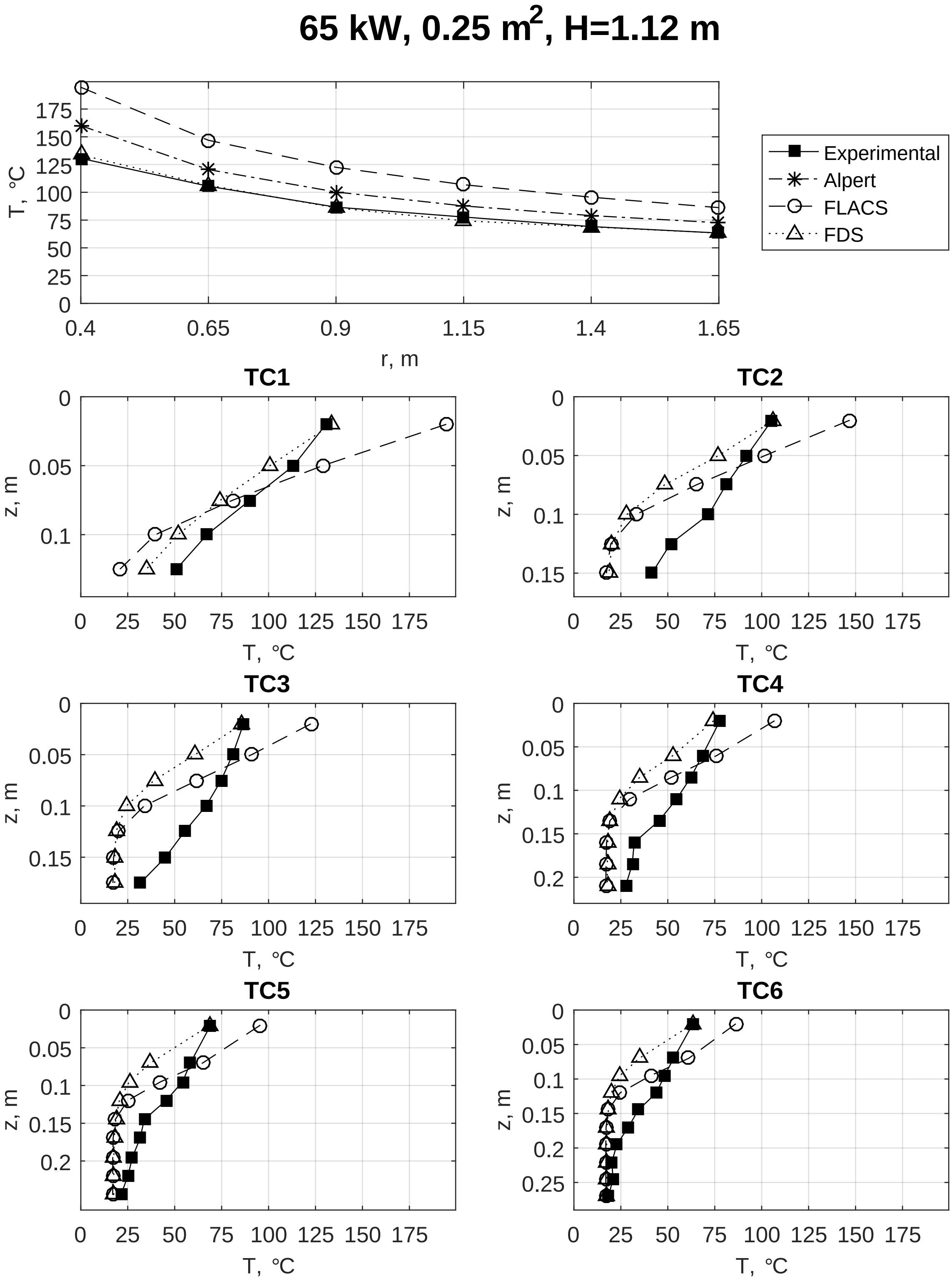

Figure E.11: Temperature results for case 100005, with $\dot{Q}$=65 kW, H=1.12 m and burner area 0.25 m^2.

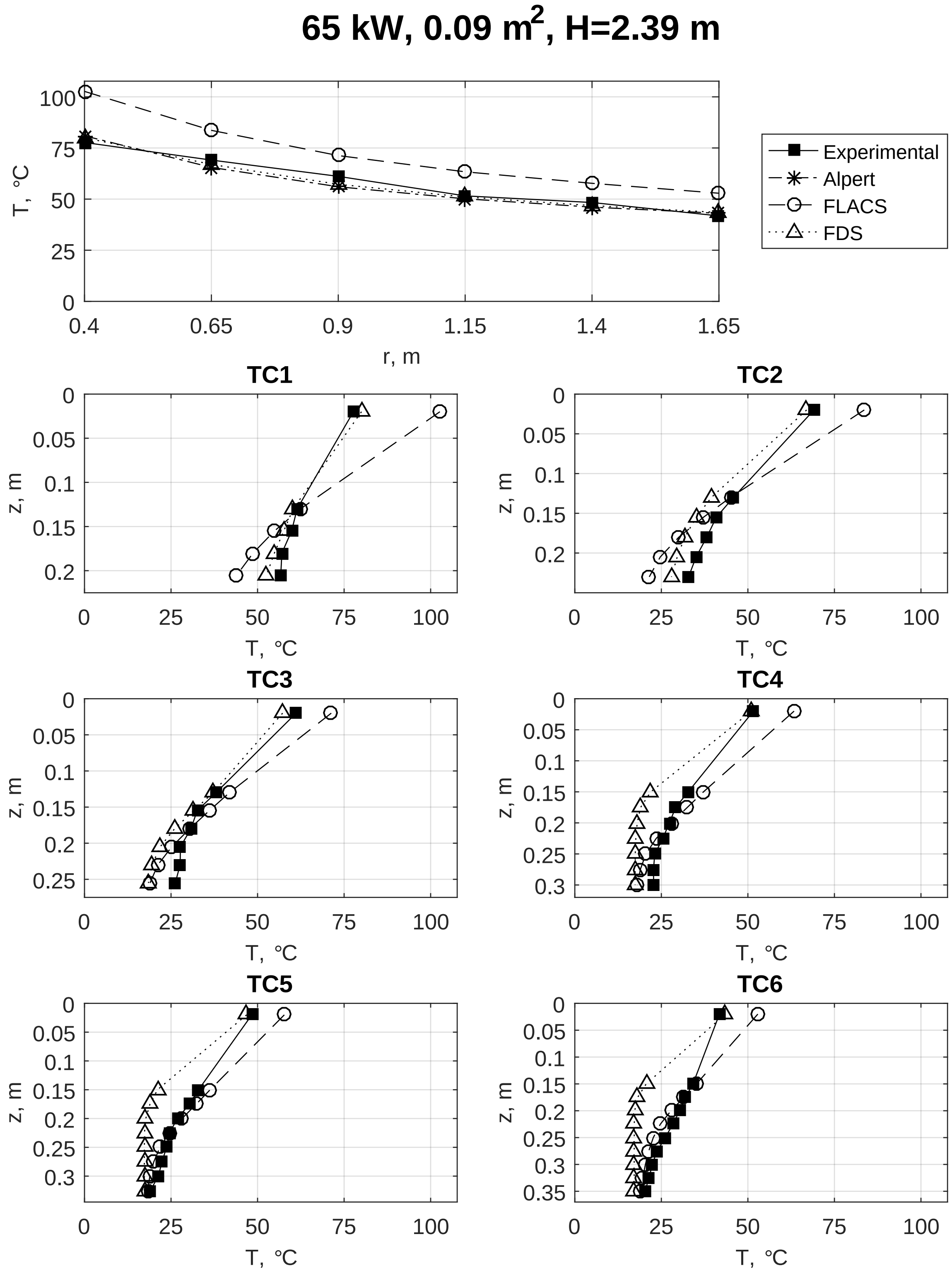

Figure E.12: Temperature results for case 100010, with $\dot{Q}$=65 kW, H=2.39 m and burner area 0.09 m^2.

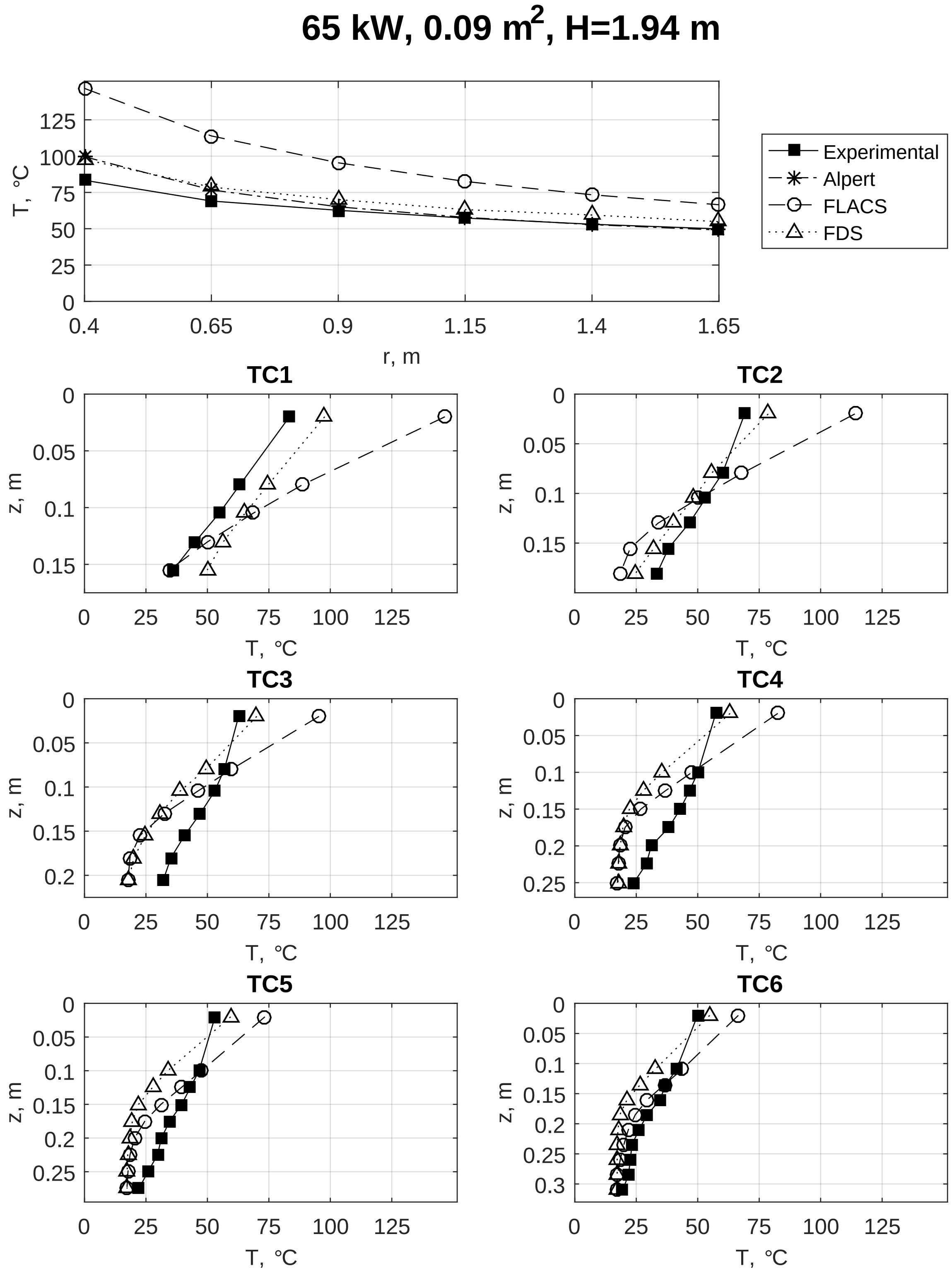

Figure E.13: Temperature results for case 100012, with $\dot{Q}$=65 kW, H=1.94 m and burner area 0.09 m^2.

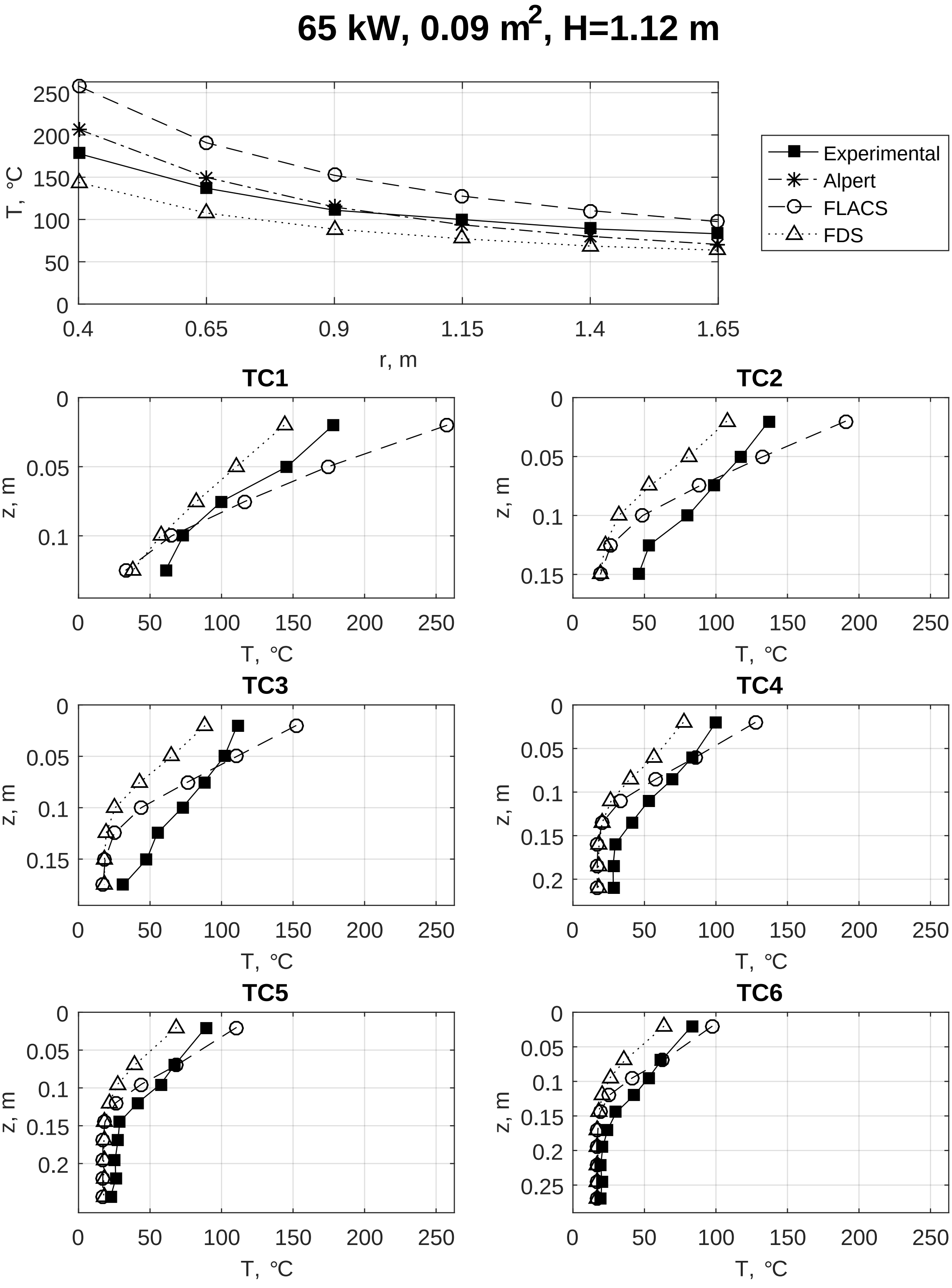

Figure E.14: Temperature results for case 100015, with $\dot{Q}$=65 kW, H=1.12 m and burner area 0.09 m^2.

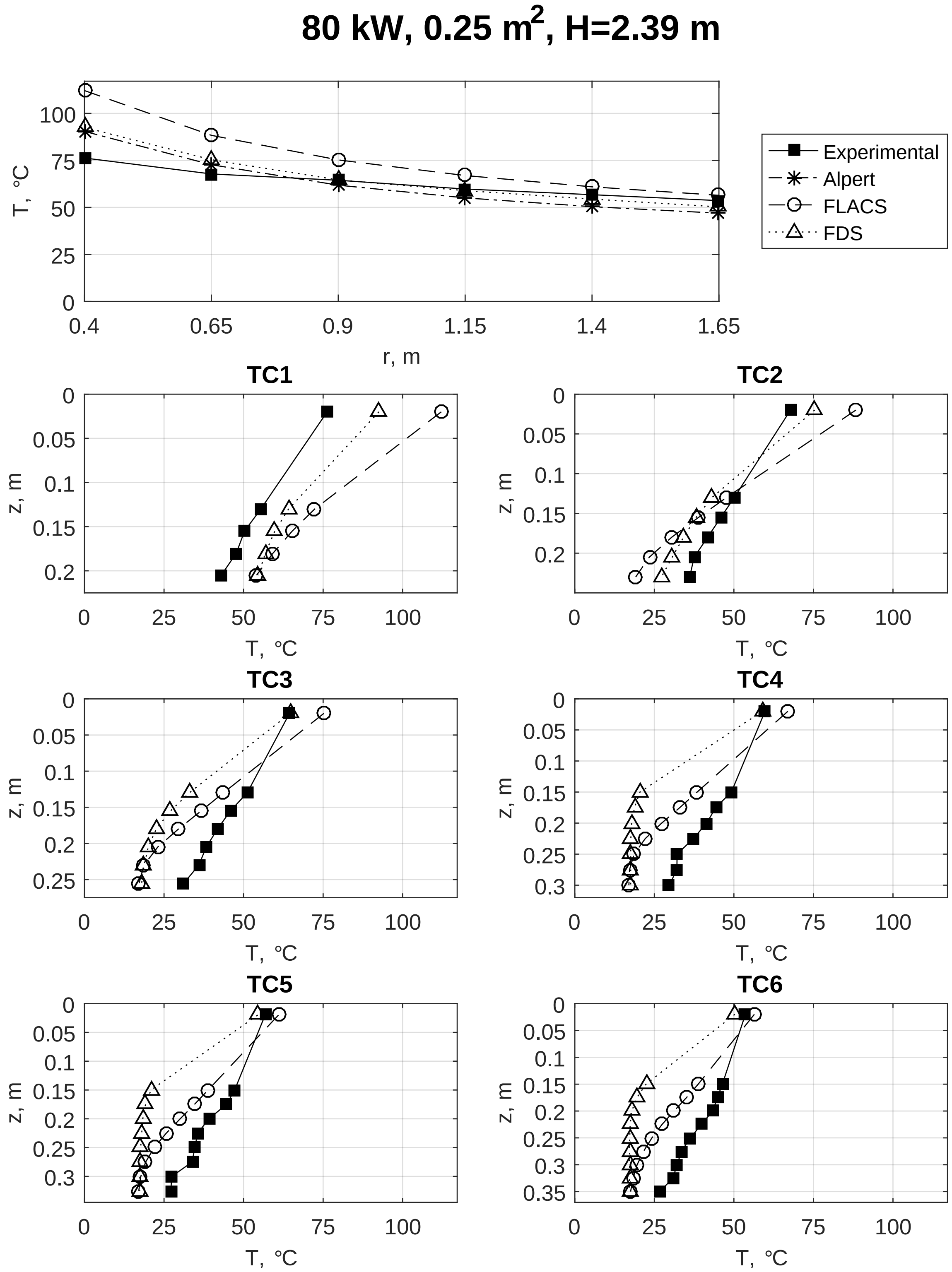

Figure E.15: Temperature results for case 200000, with $\dot{Q}$=80 kW, H=2.39 m and burner area 0.25 m^2.

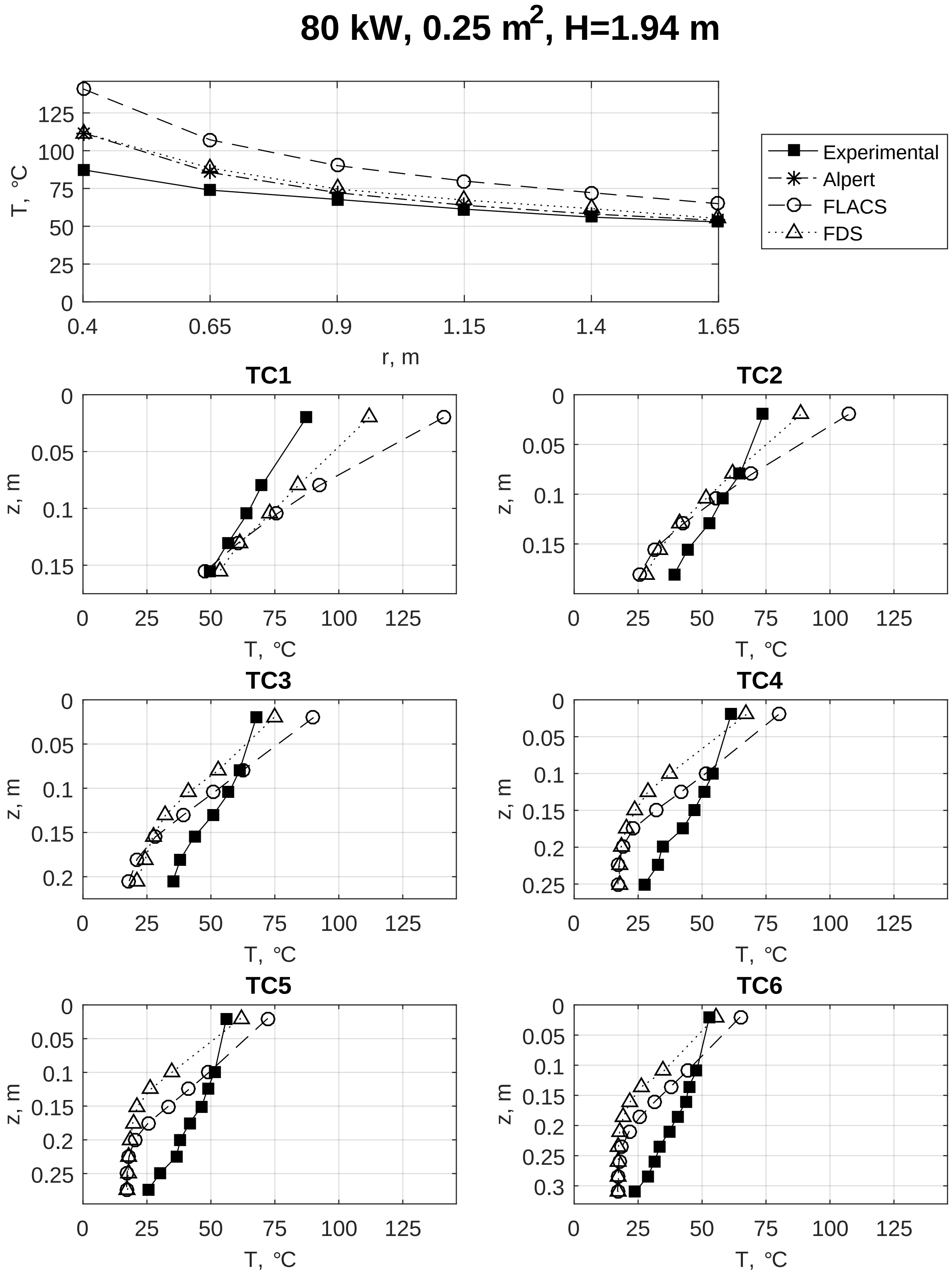

Figure E.16: Temperature results for case 200002, with $\dot{Q}$=80 kW, H=1.94 m and burner area 0.25 m^2.

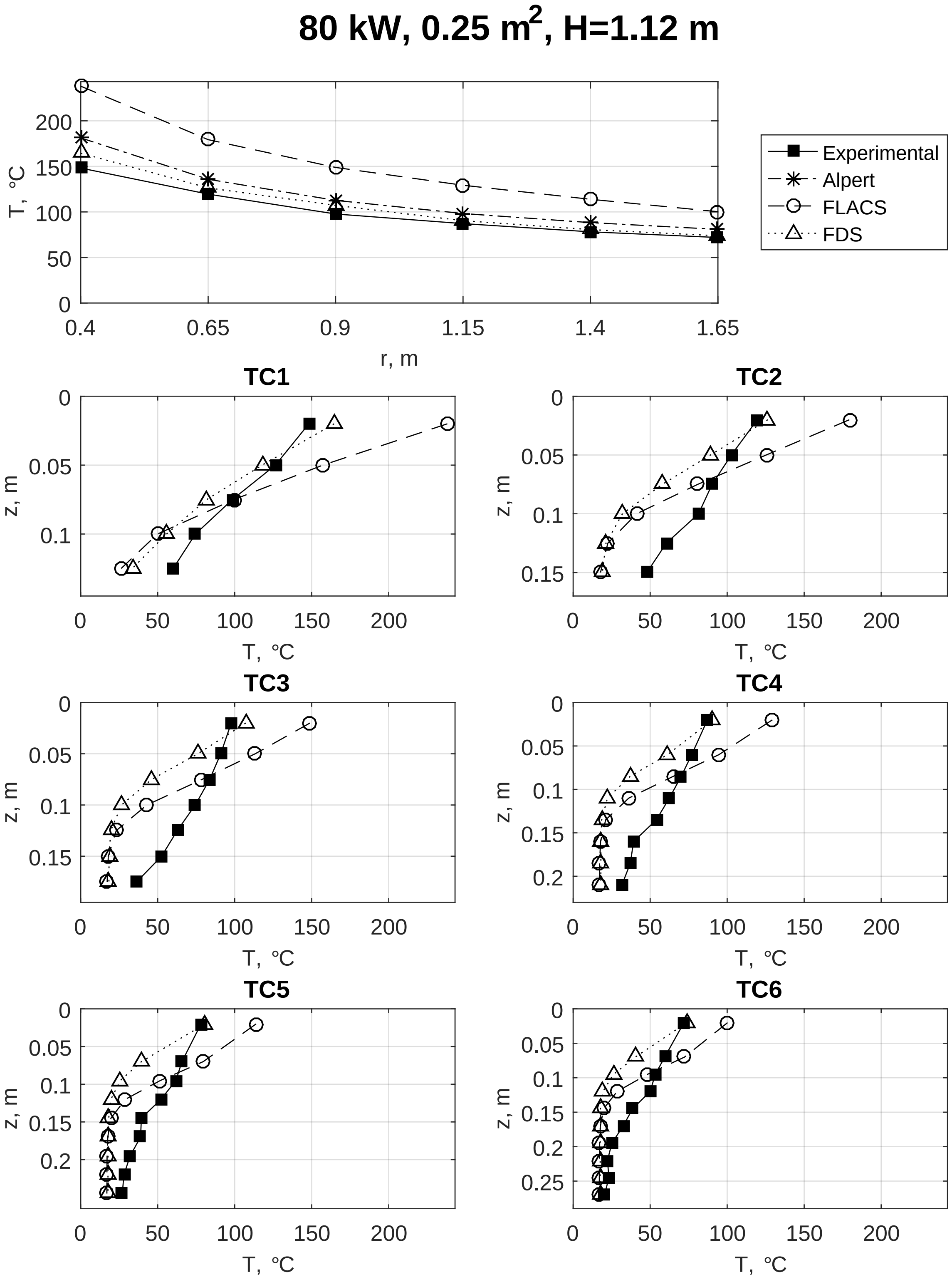

Figure E.17: Temperature results for case 200005, with $\dot{Q}$=80 kW, H=1.12 m and burner area 0.25 m^2.

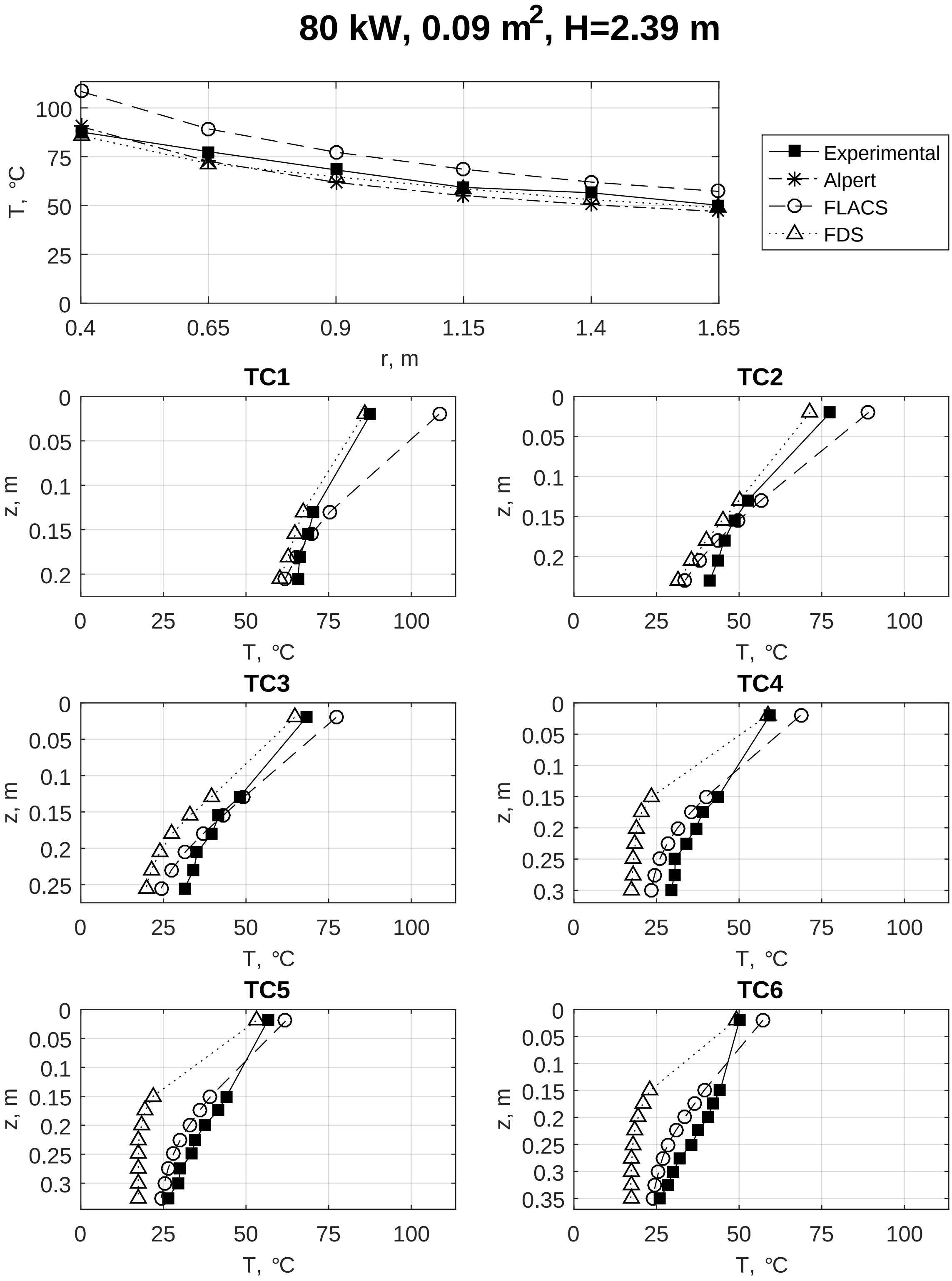

Figure E.18: Temperature results for case 200010, with $\dot{Q}$=80 kW, H=2.39 m and burner area 0.09 m^2.

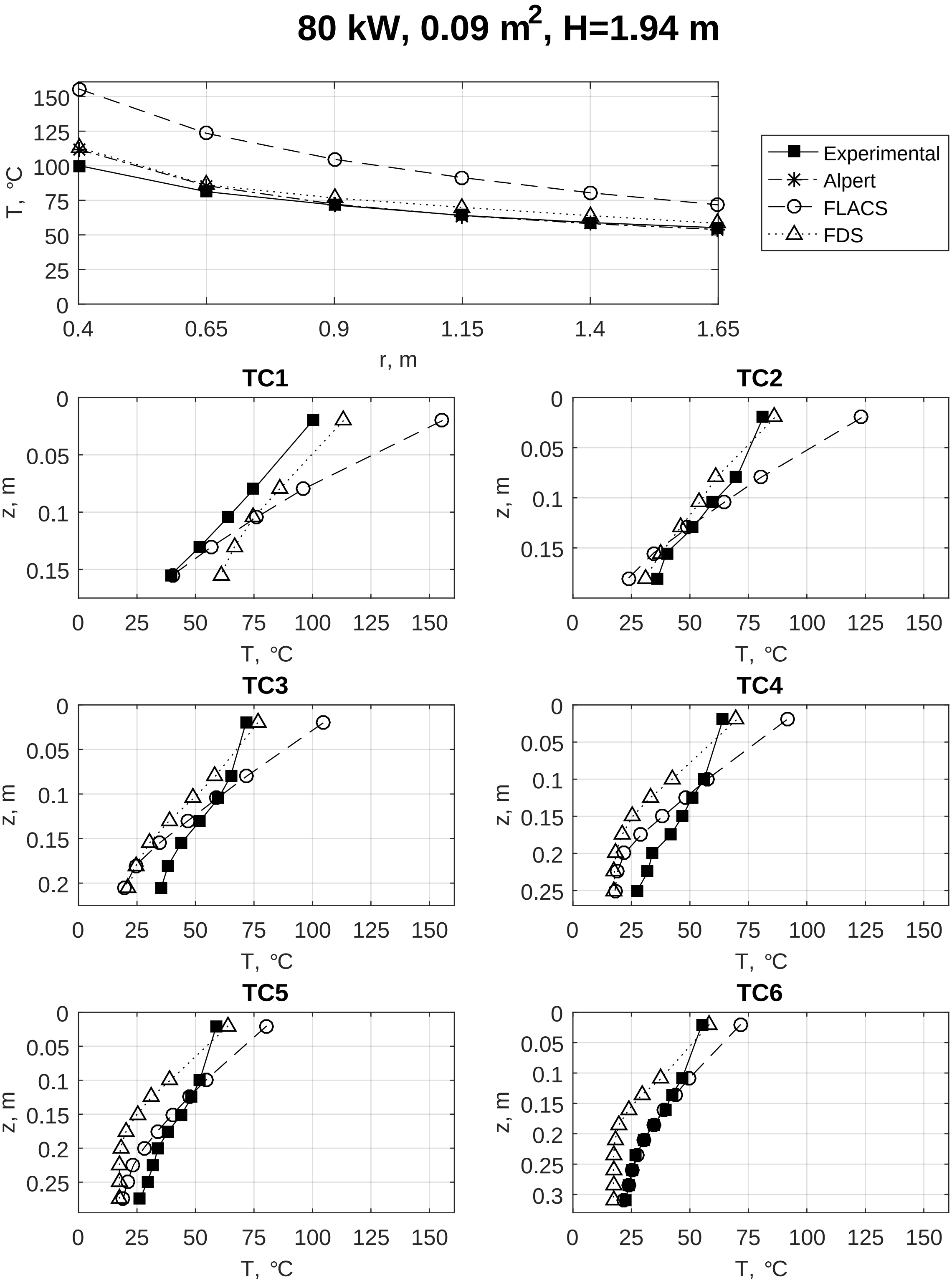

Figure E.19: Temperature results for case 200012, with $\dot{Q}$=80 kW, H=1.94 m and burner area 0.09 m^2.

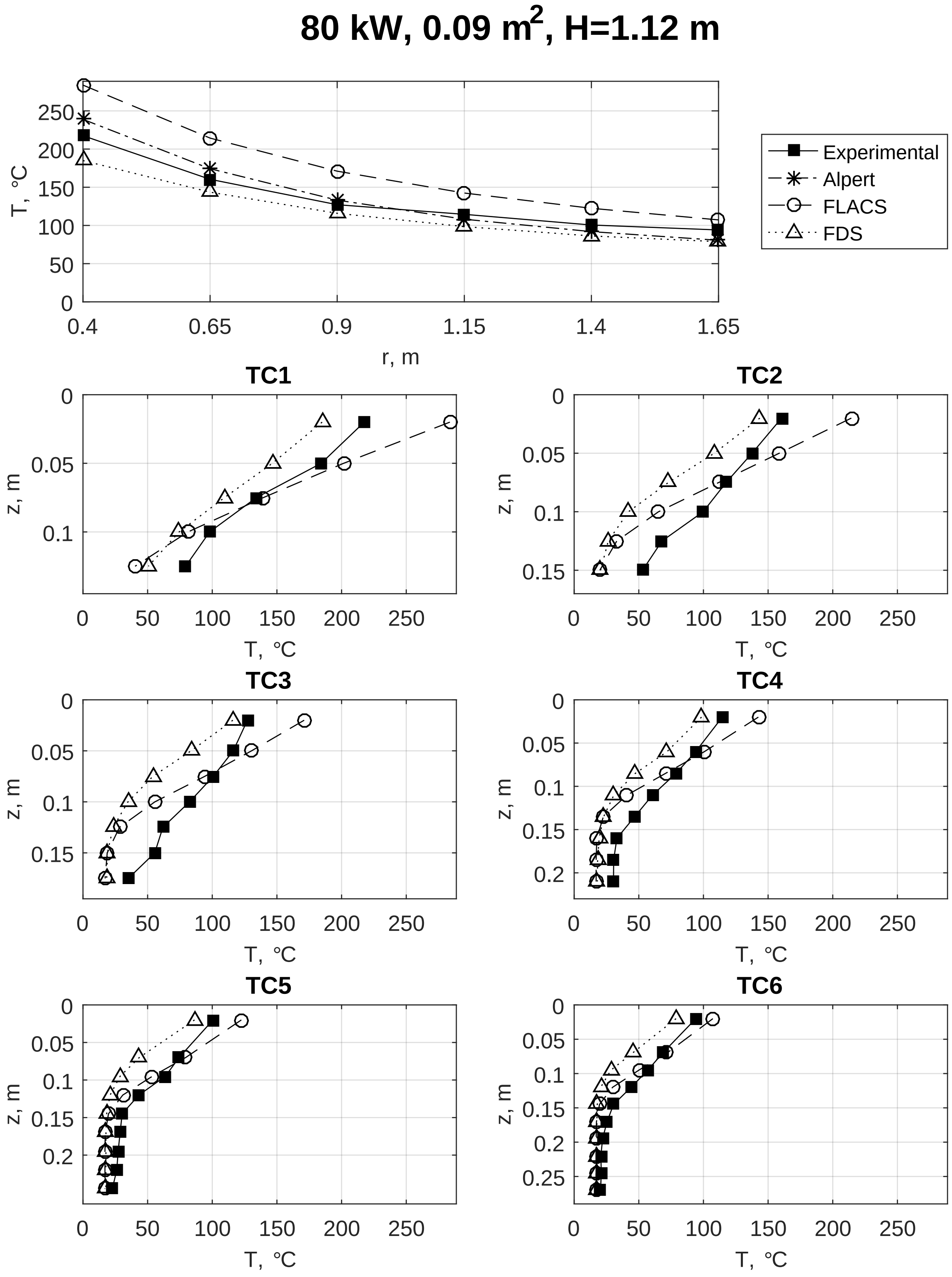

Figure E.20: Temperature results for case 200015, with $\dot{Q}$=80 kW, H=1.12 m and burner area 0.09 m^2.

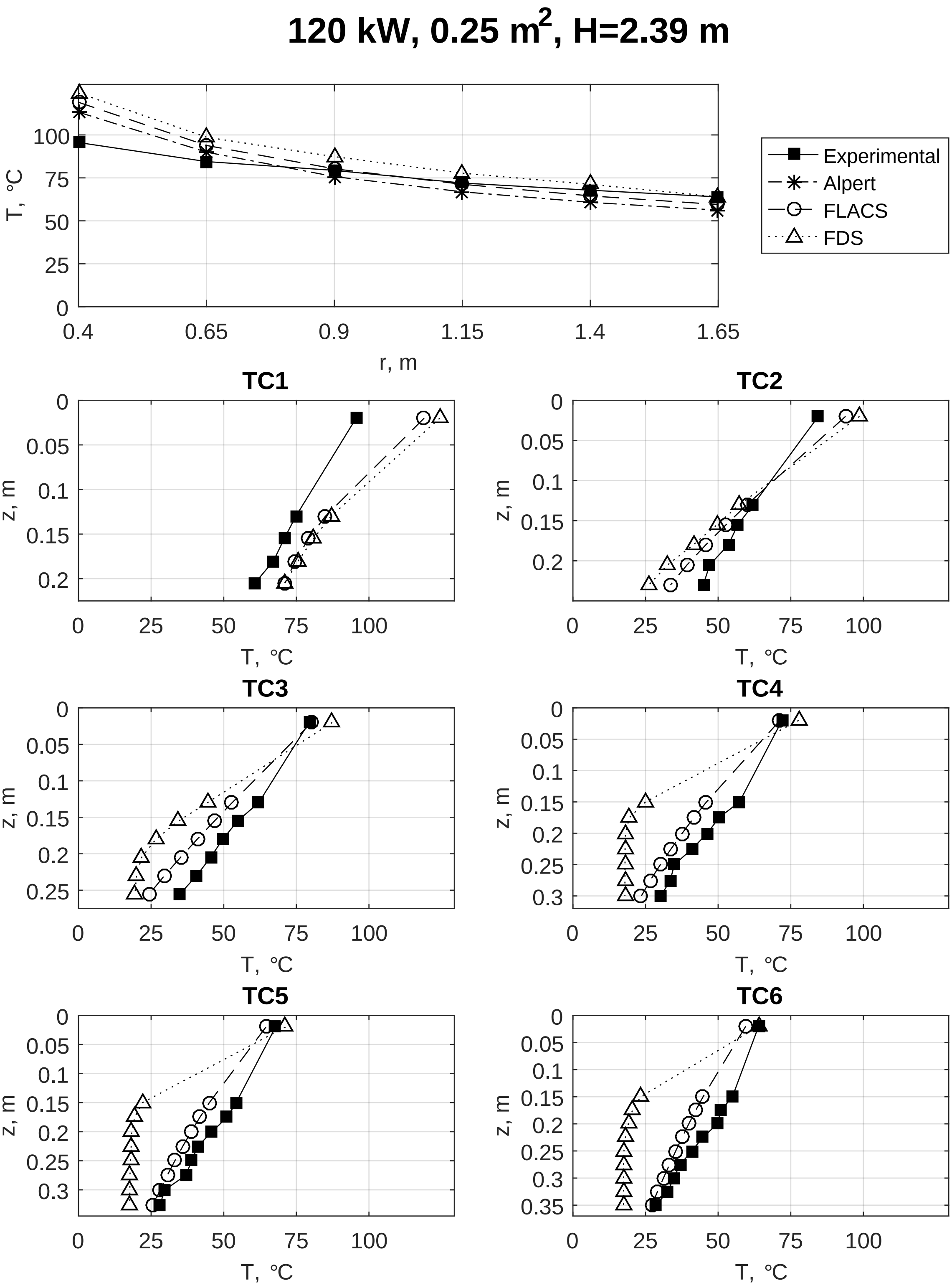

Figure E.21: Temperature results for case 300000, with $\dot{Q}$=120 kW, H=2.39 m and burner area 0.25 m^2.

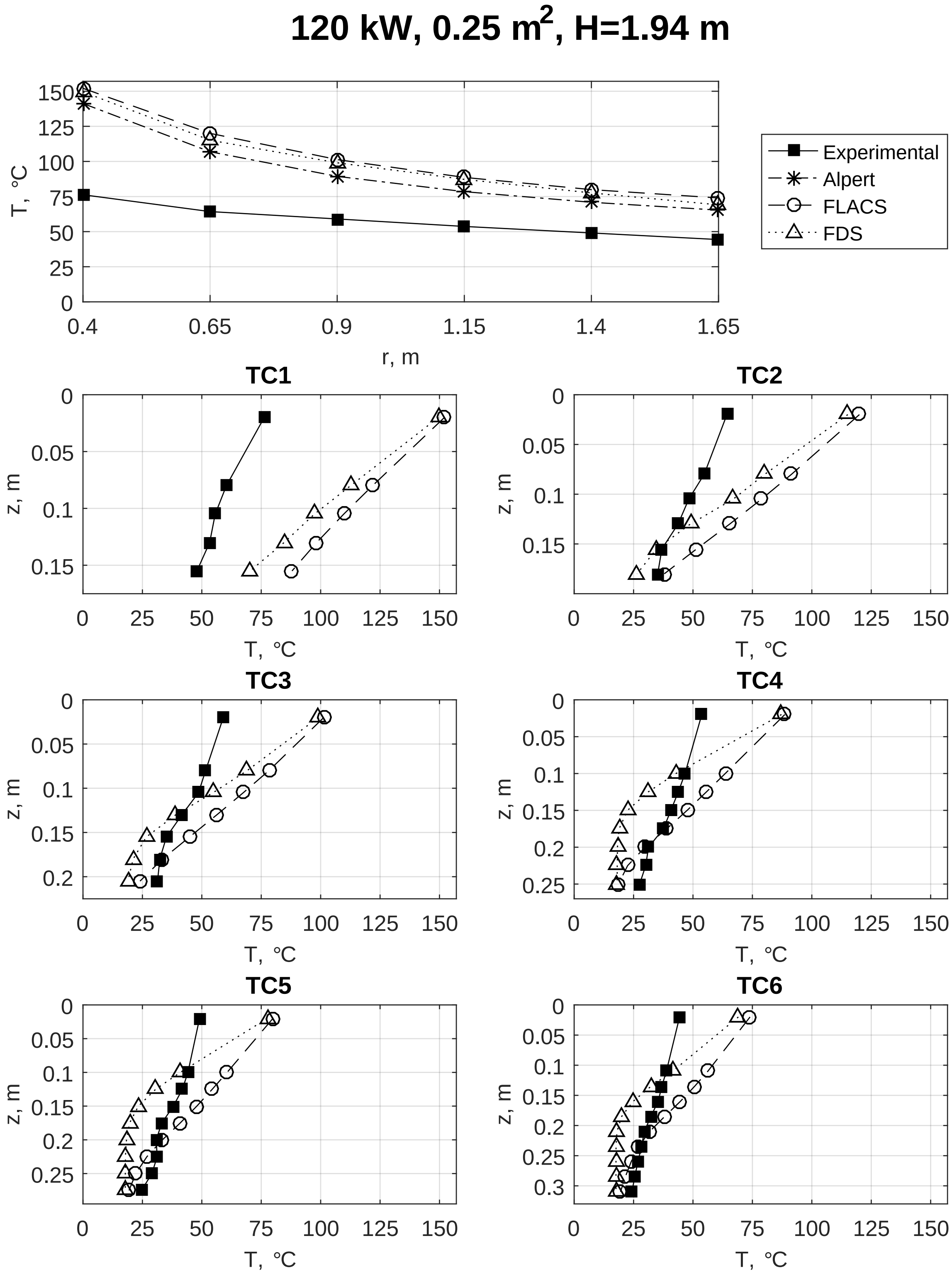

Figure E.22: Temperature results for case 300002, with $\dot{Q}$=120 kW, H=1.94 m and burner area 0.25 m^2.

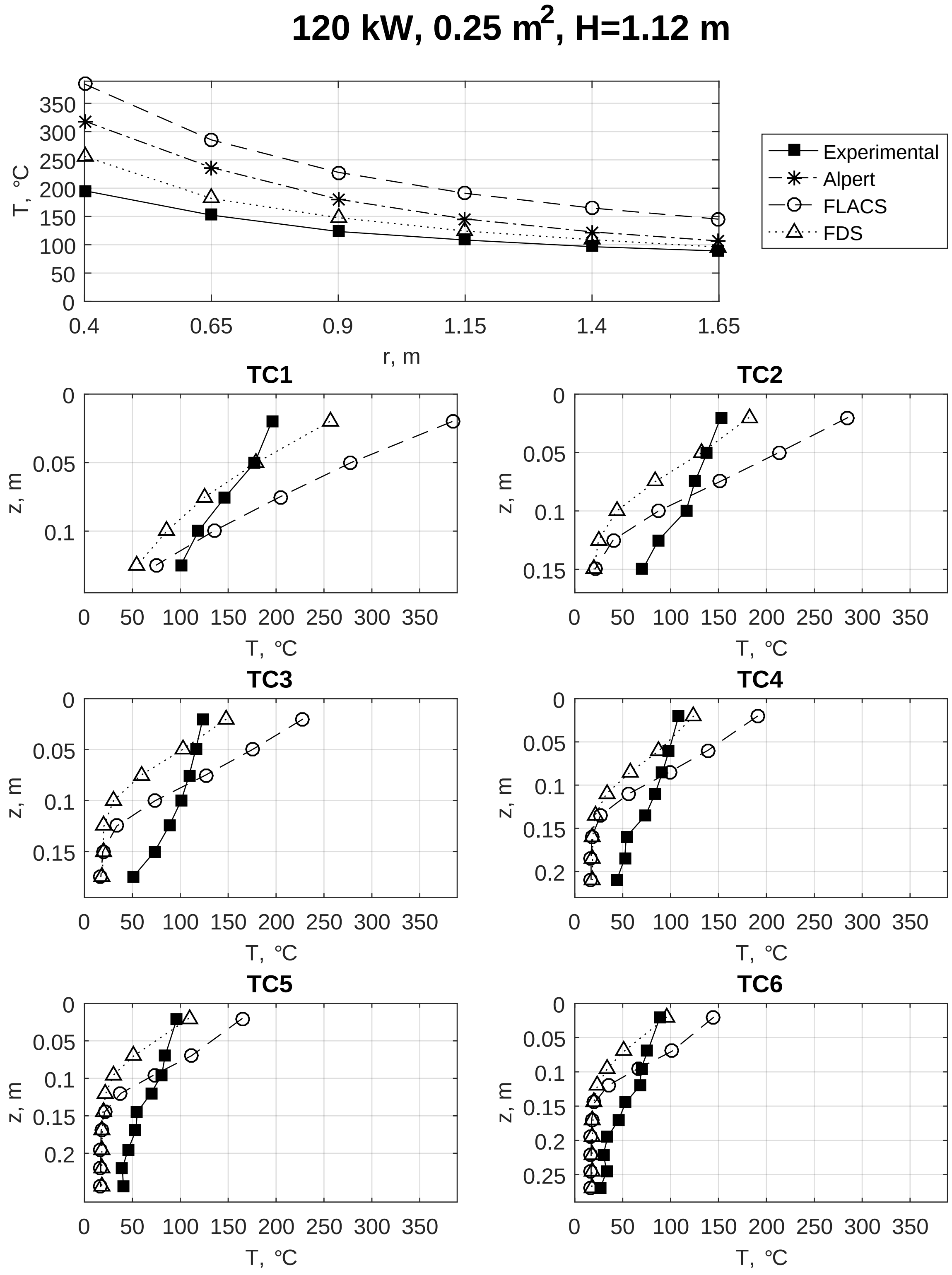

Figure E.23: Temperature results for case 300005, with $\dot{Q}$=120 kW, H=1.12 m and burner area 0.25 m^2.

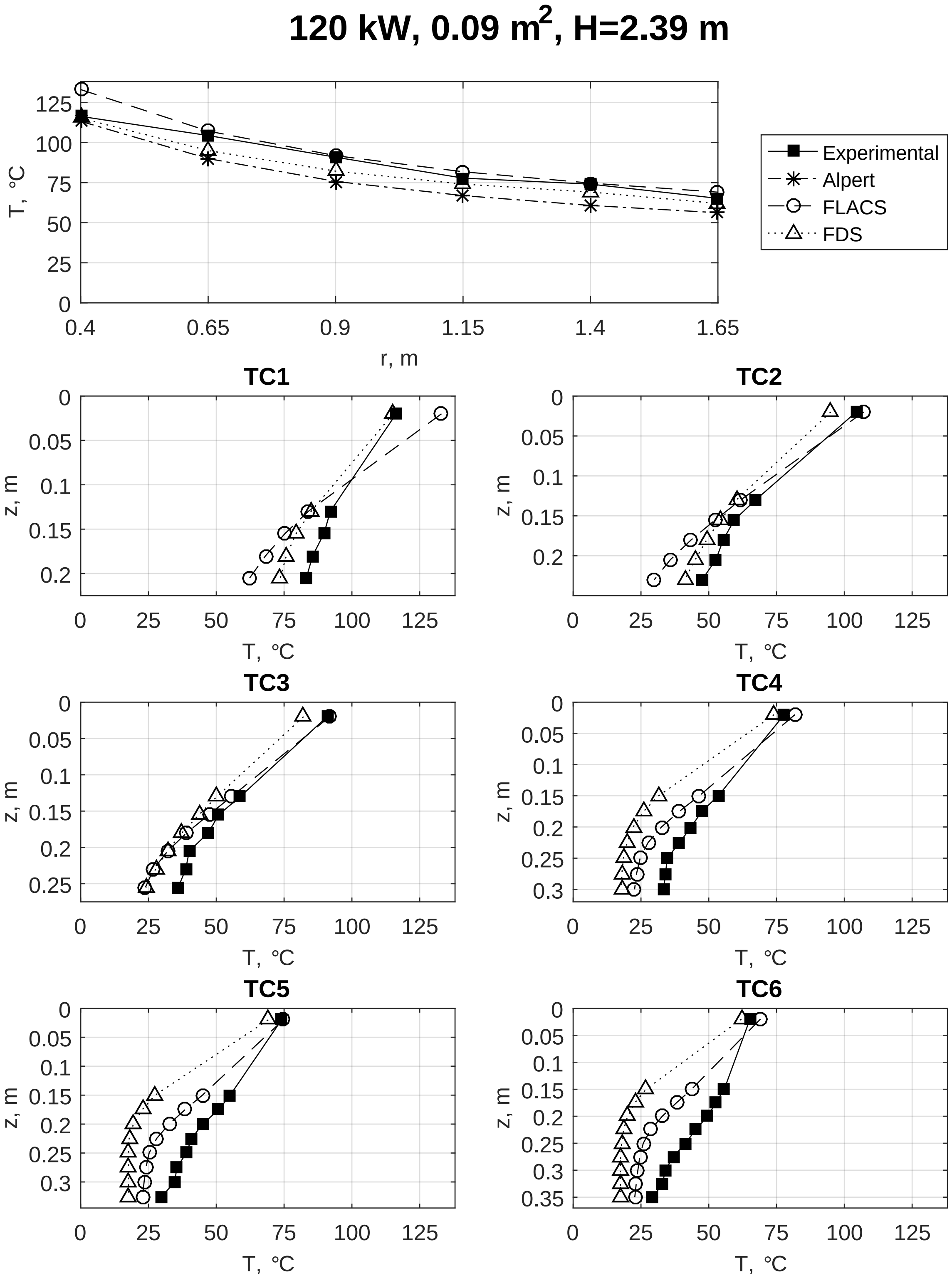

Figure E.24: Temperature results for case 300010, with $\dot{Q}$=120 kW, H=2.39 m and burner area 0.09 m^2.

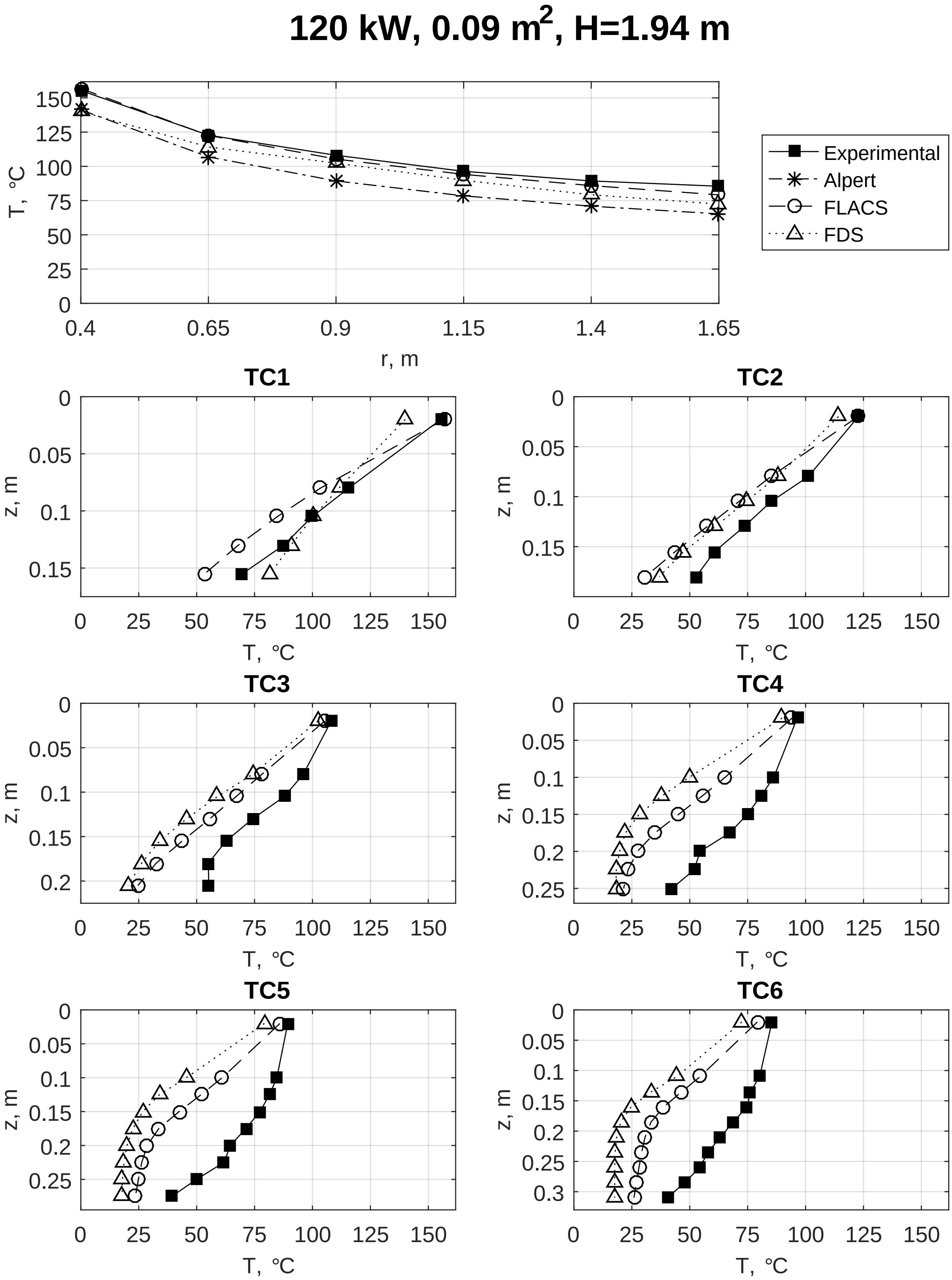

Figure E.25: Temperature results for case 300012, with $\dot{Q}$=120 kW, H=1.94 m and burner area 0.09 m^2.

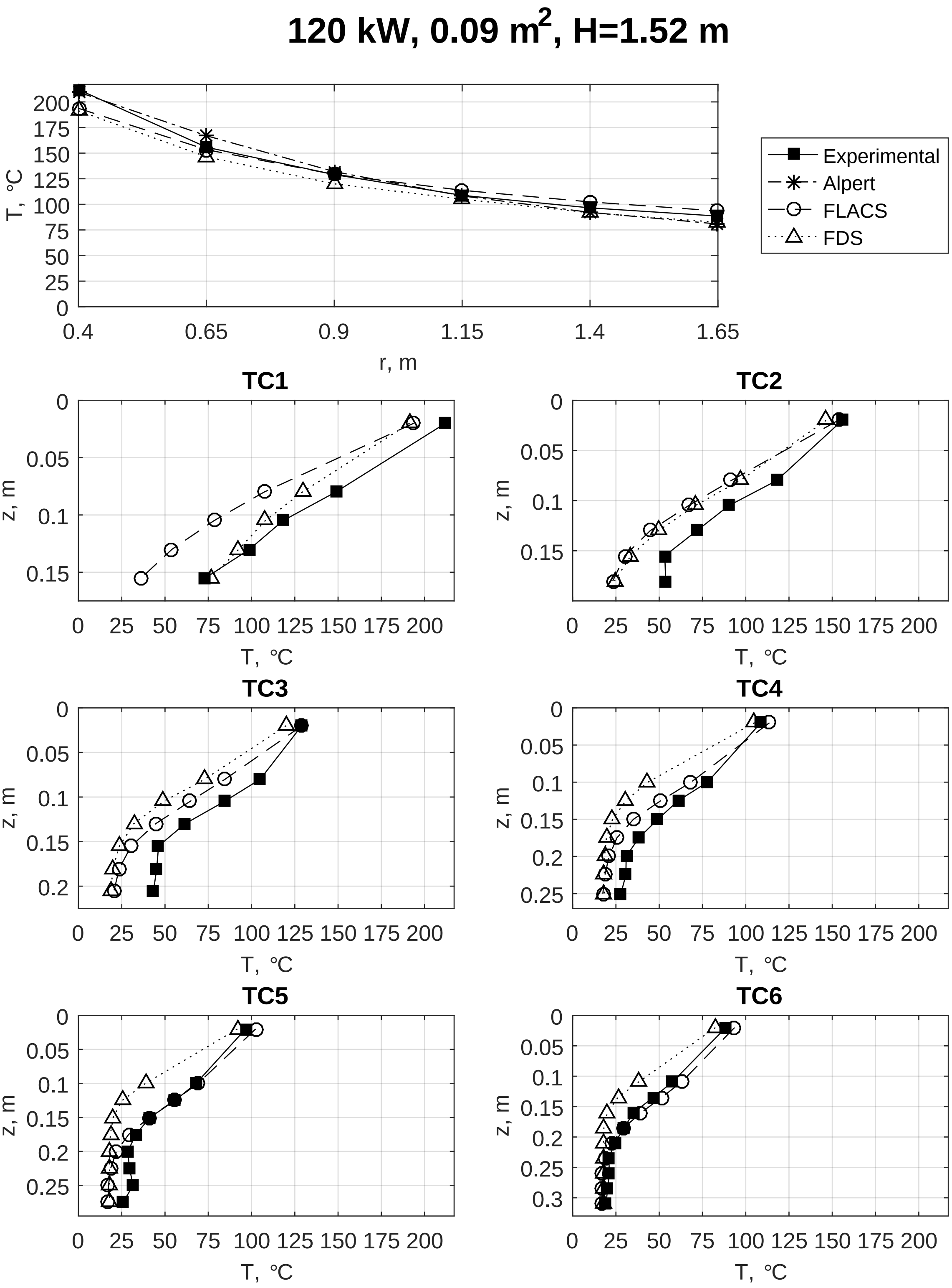

Figure E.26: Temperature results for case 300014, with $\dot{Q}$=120 kW, H=1.52 m and burner area 0.09 m^2.

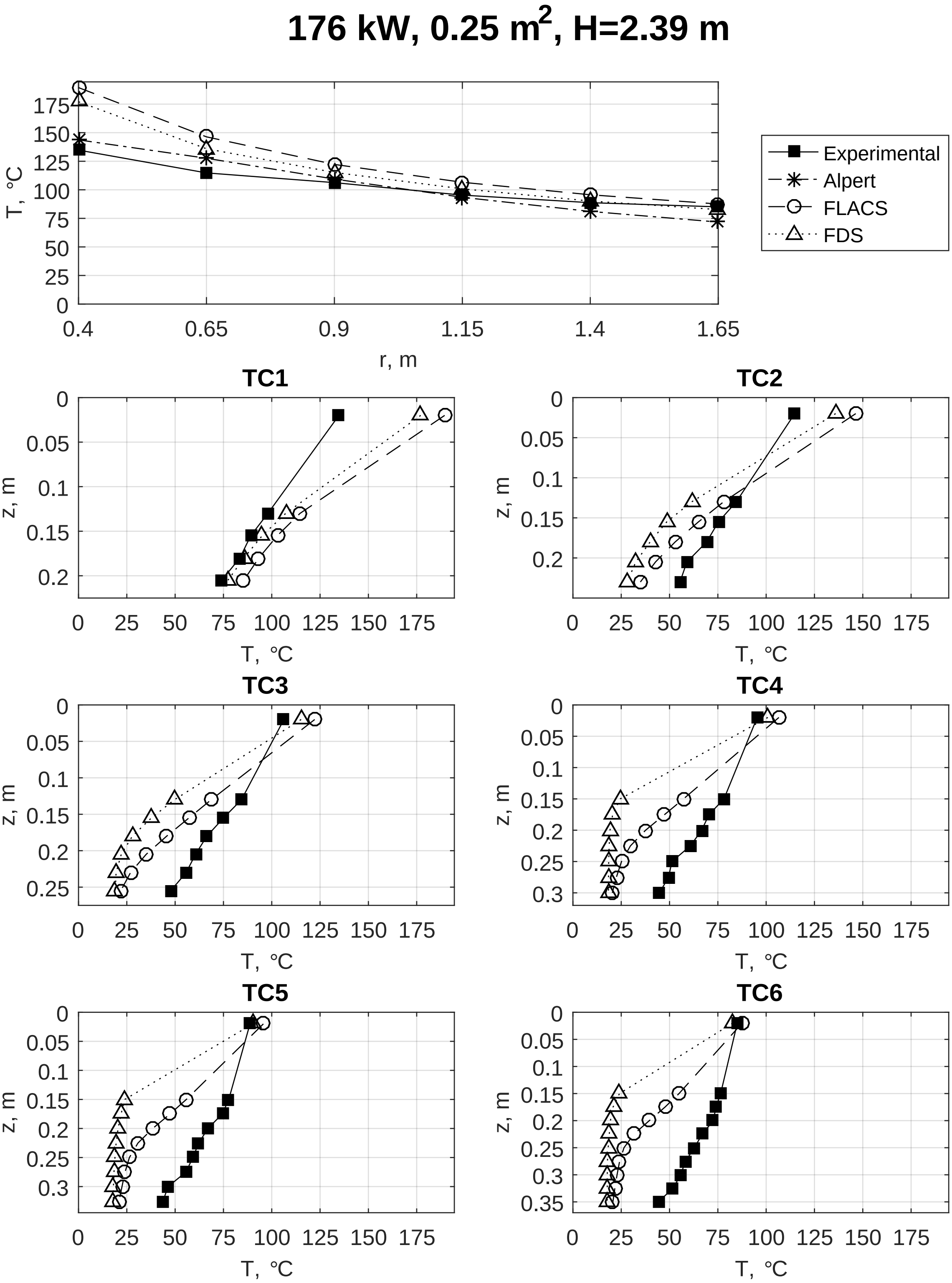

Figure E.27: Temperature results for case 400000, with $\dot{Q}$=176 kW, H=2.39 m and burner area 0.25 m^2.

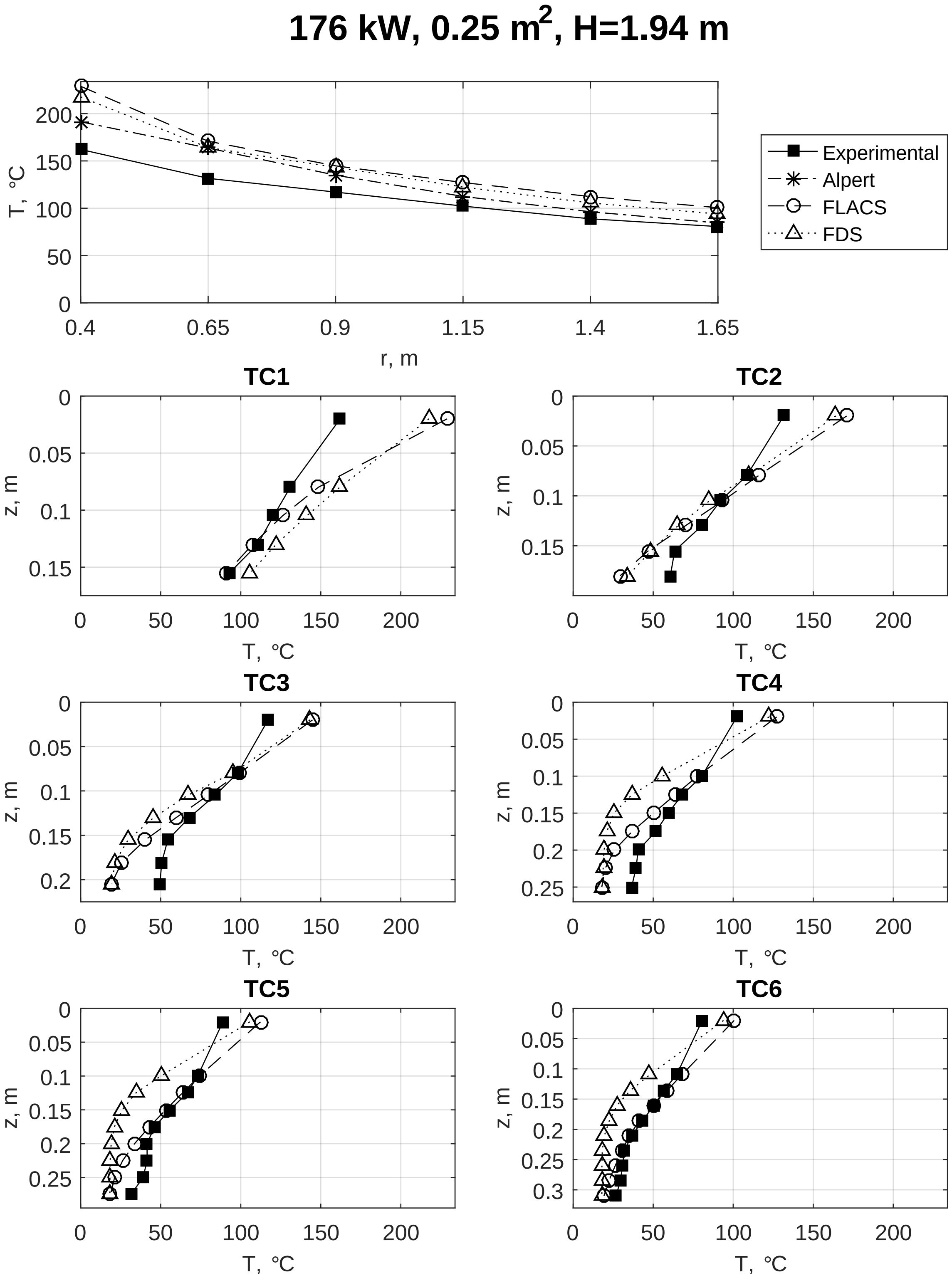

Figure E.28: Temperature results for case 400002, with $\dot{Q}$=176 kW, H=1.94 m and burner area 0.25 m^2.

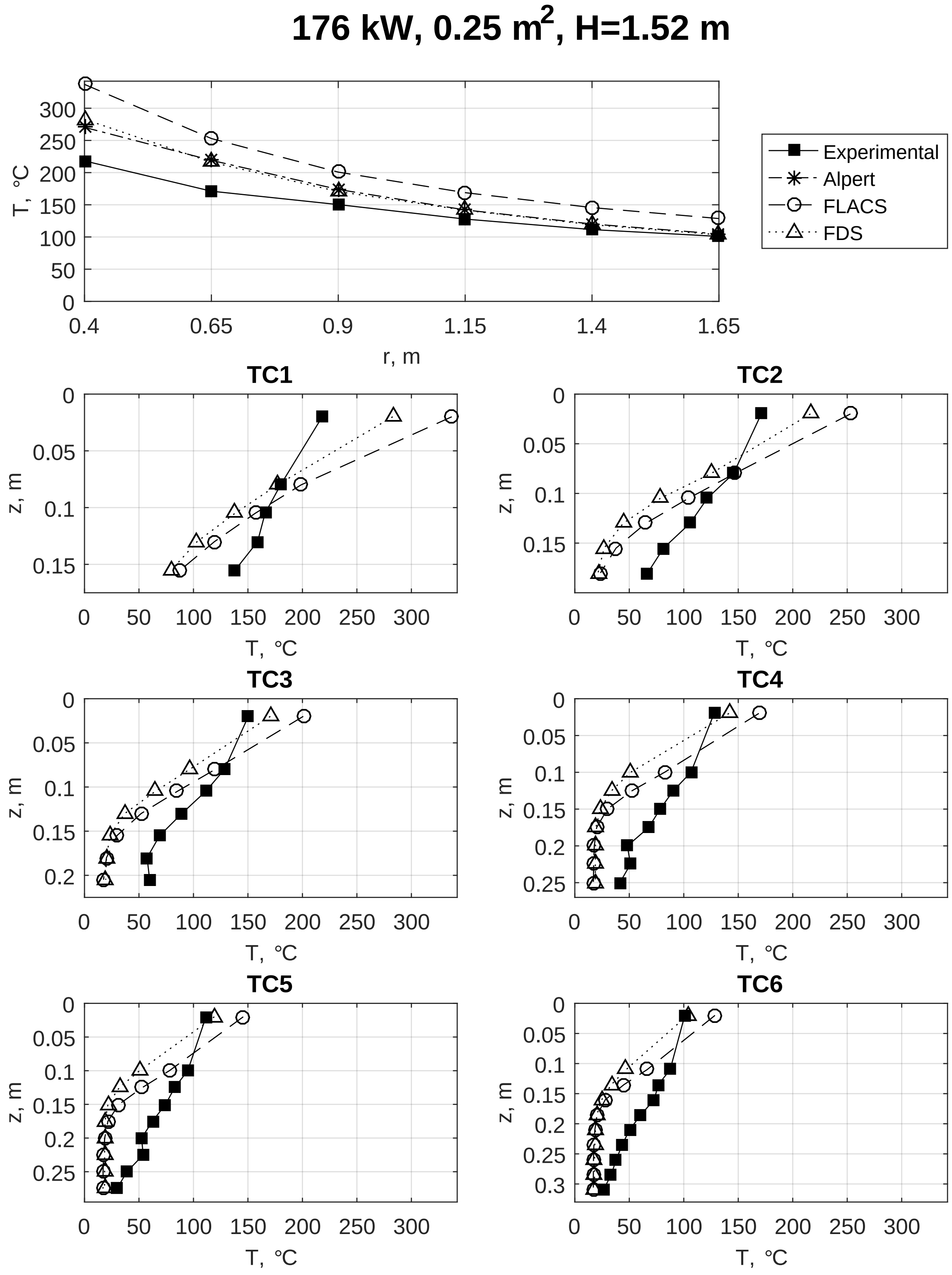

Figure E.29: Temperature results for case 400004, with $\dot{Q}$=176 kW, H=1.52 m and burner area 0.25 m^2.

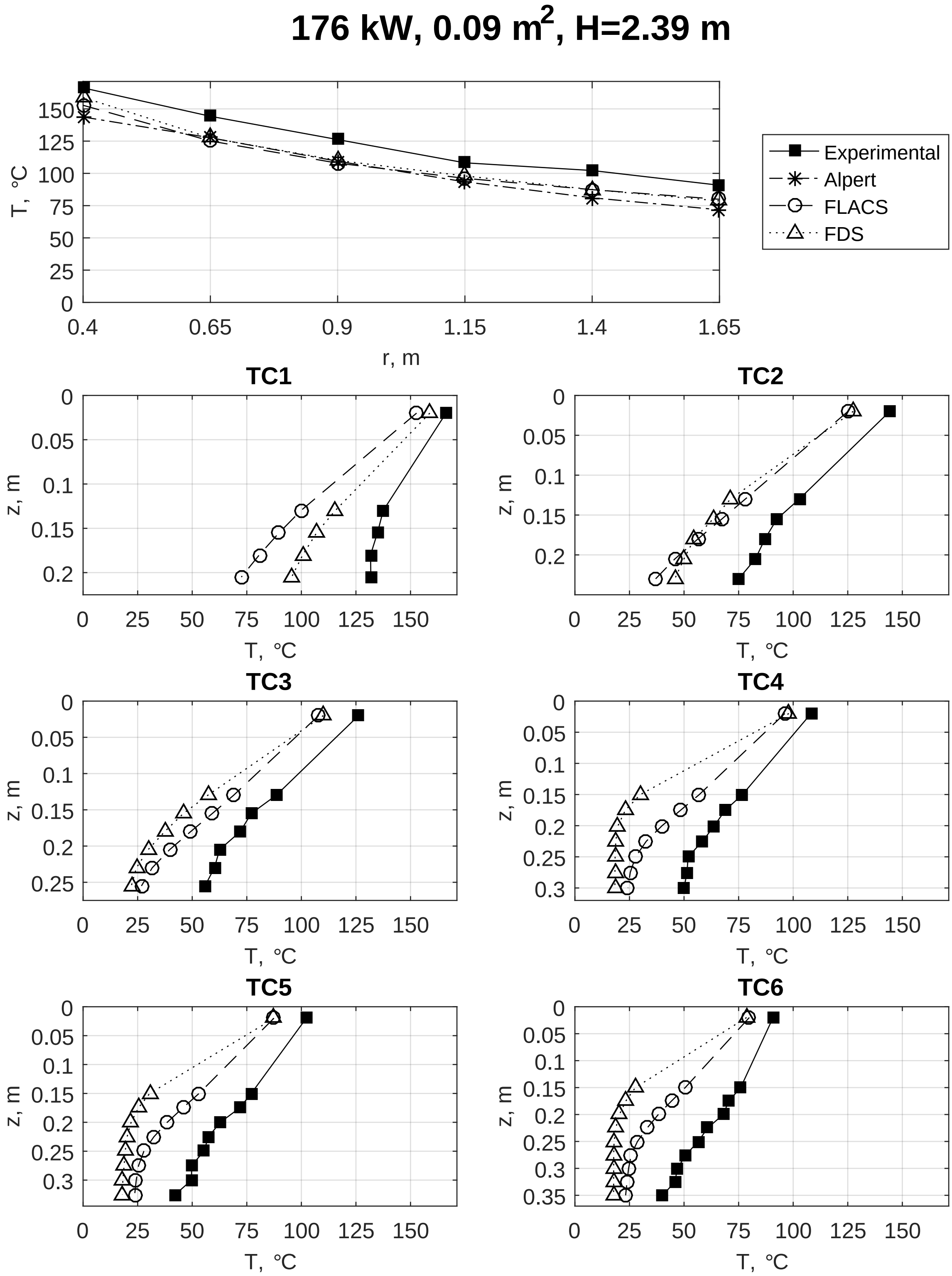

Figure E.30: Temperature results for case 400010, with $\dot{Q}$=176 kW, H=2.39 m and burner area 0.09 m^2.

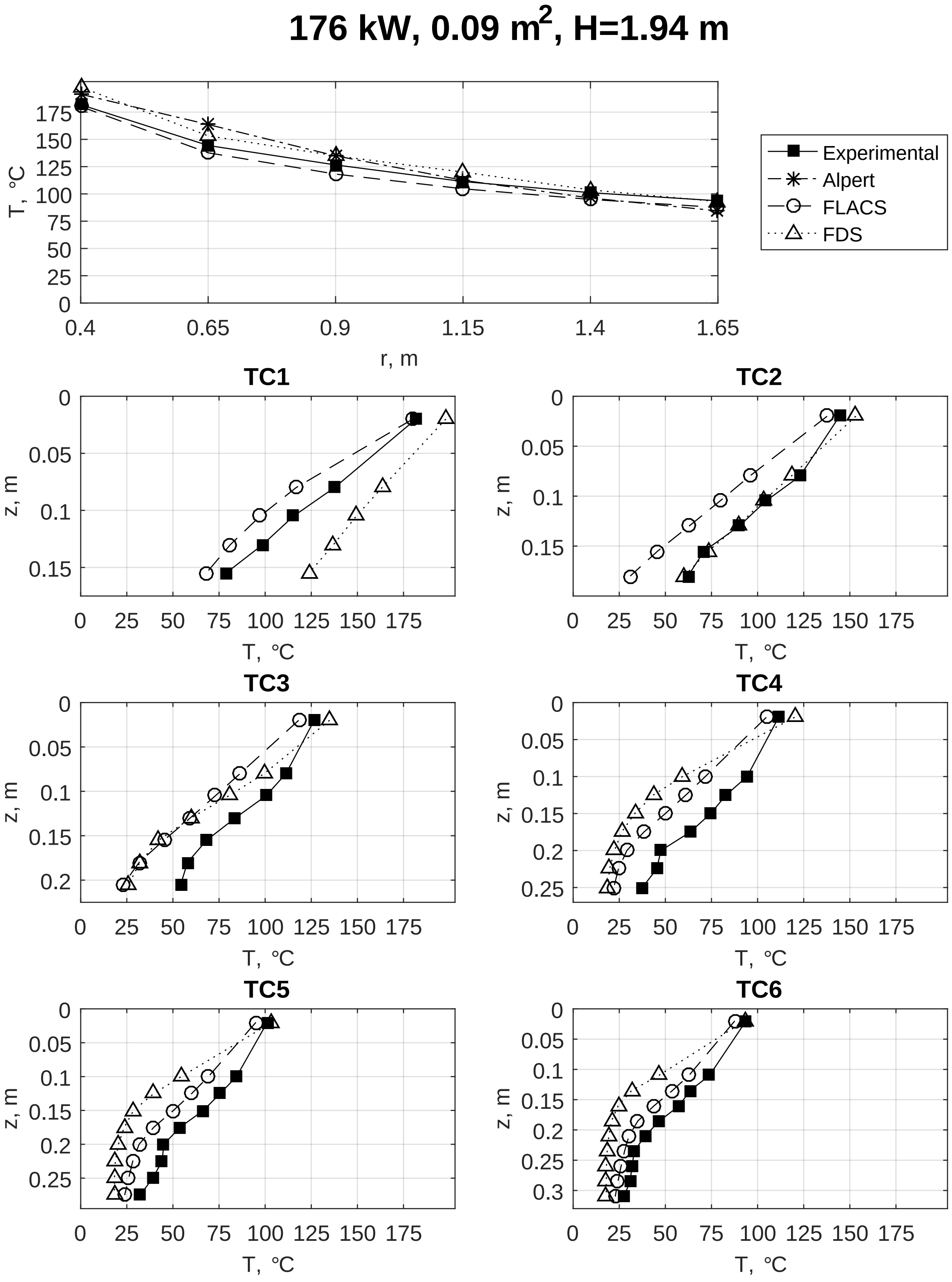

Figure E.31: Temperature results for case 400012, with $\dot{Q}$=176 kW, H=1.94 m and burner area 0.09 m^2.

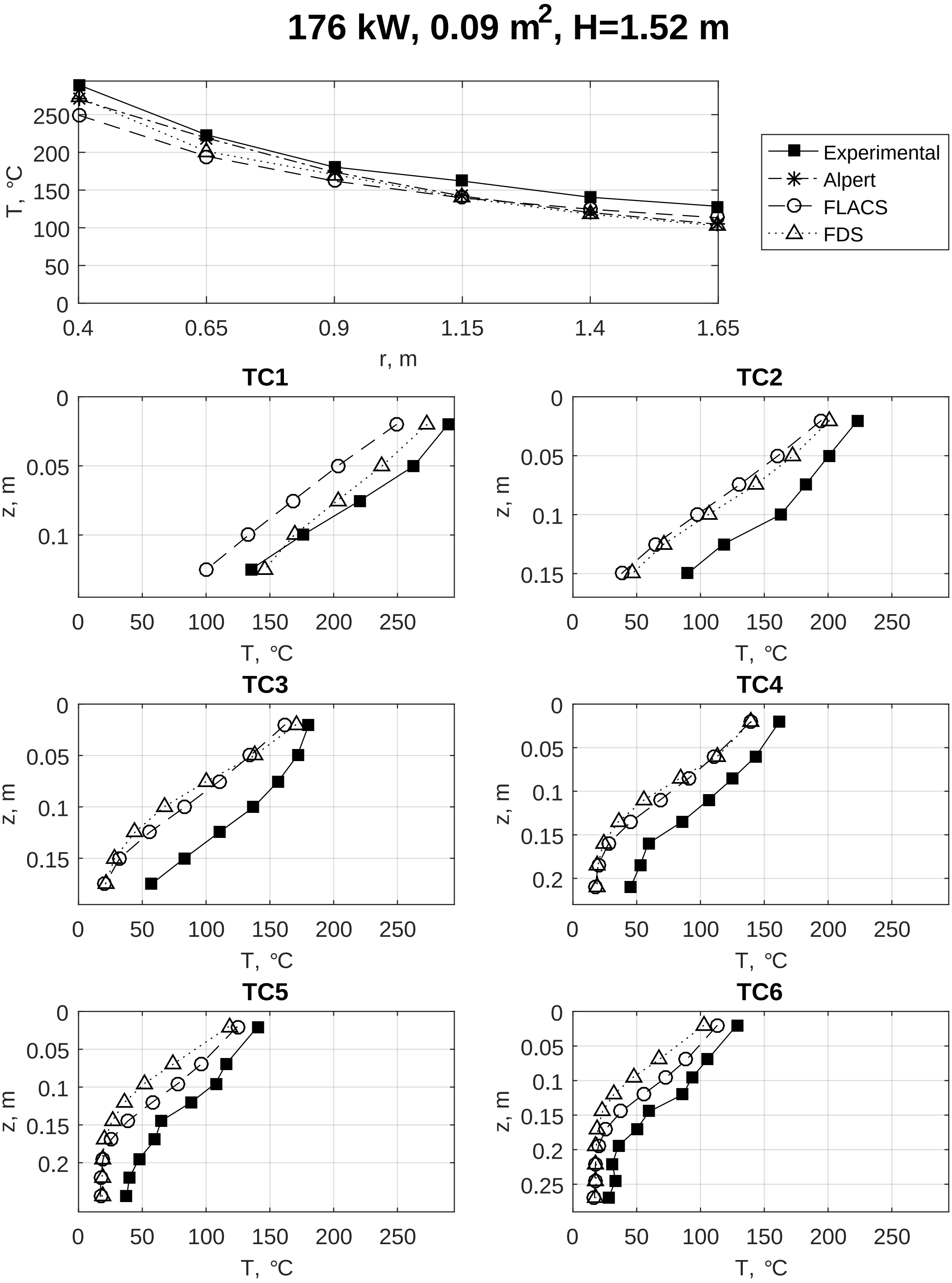

Figure E.32: Temperature results for case 400014, with $\dot{Q}$=176 kW, H=1.52 m and burner area 0.09 m^2.

Appendix F

Ceiling jet thickness plots

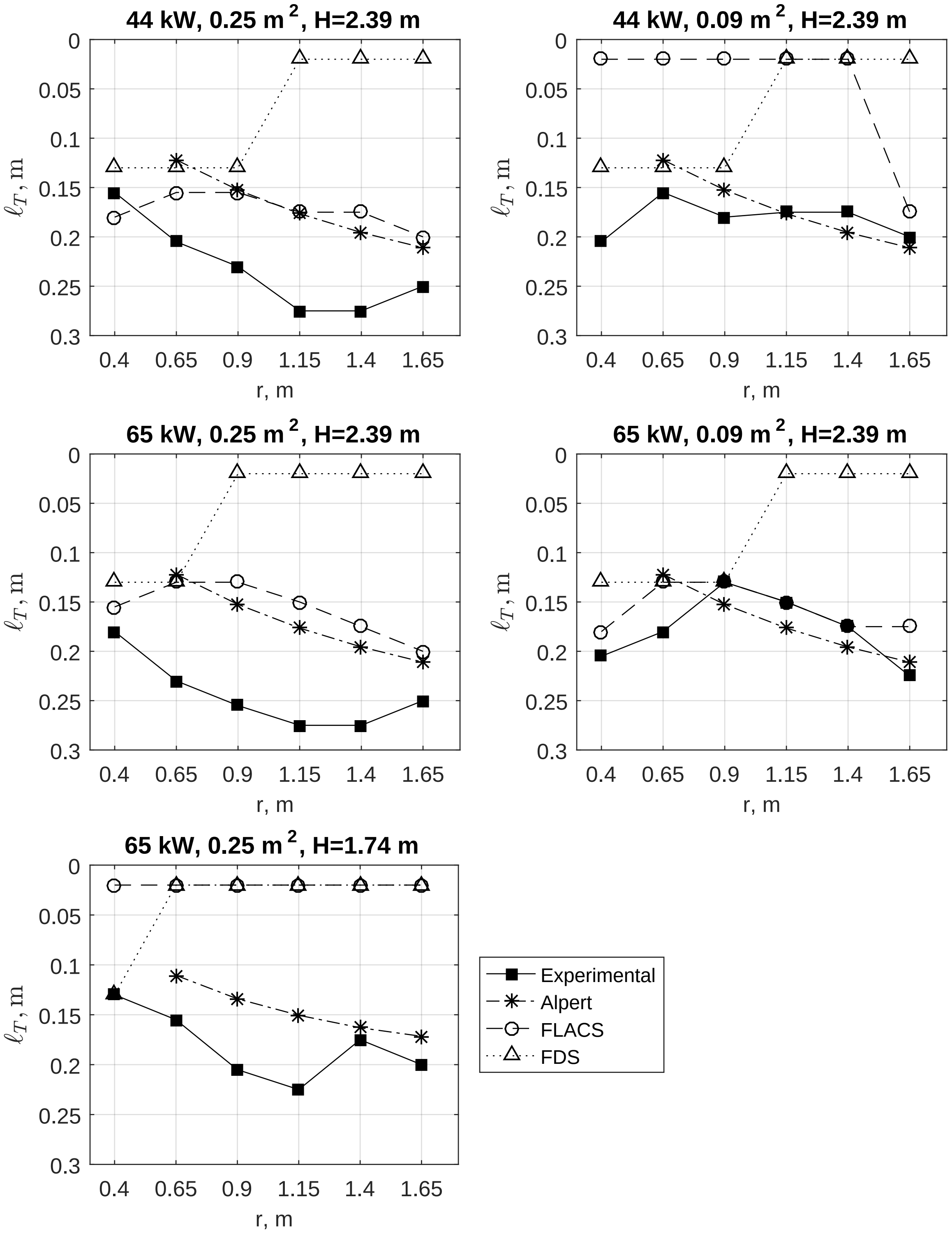

Figure F.1: Resulting ceiling jet thicknesses from experiments, simulations and correlations, versus radial distance away from fire source for cases 000000, 000010, 100000, 100010 and 100003 (see description in subplot title).

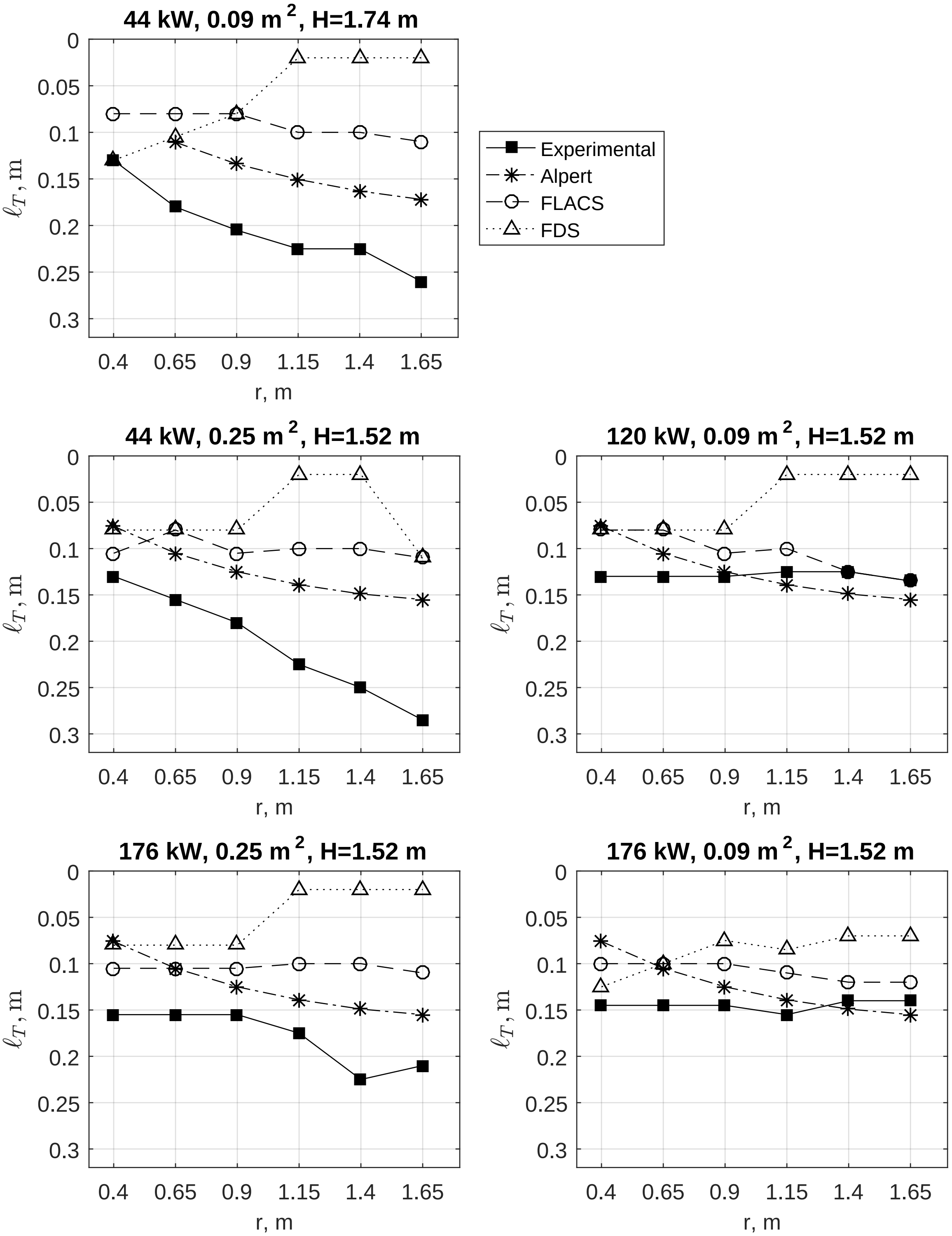

Figure F.2: Resulting ceiling jet thicknesses from experiments, simulations and correlations, versus radial distance away from fire source for cases 000013, 000004, 300014, 400004 and 400014 (see description in subplot title).

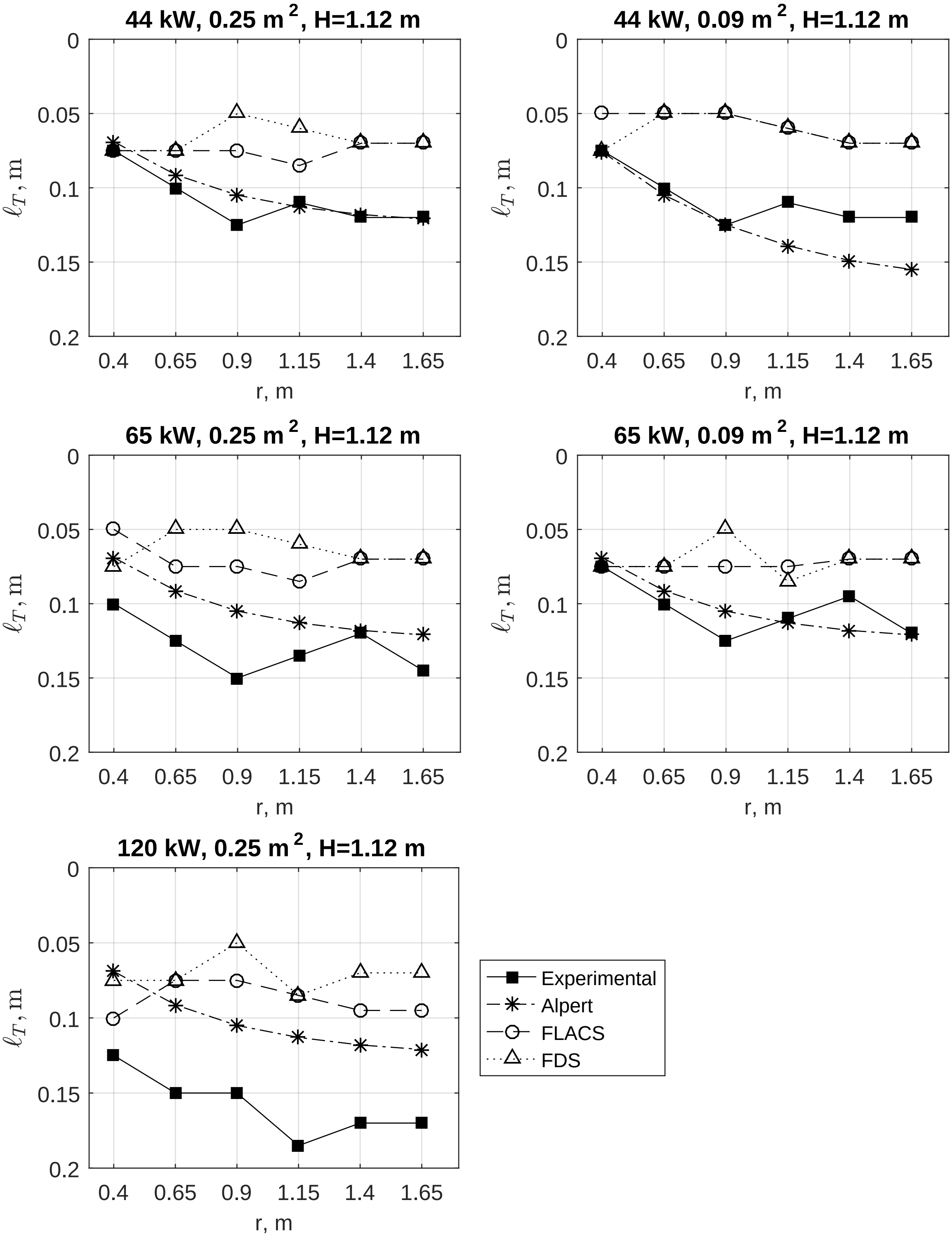

Figure F.3: Resulting ceiling jet thicknesses from experiments, simulations and correlations, versus radial distance away from fire source for cases 000005, 000015, 100005, 100015 and 300005 (see description in subplot title).

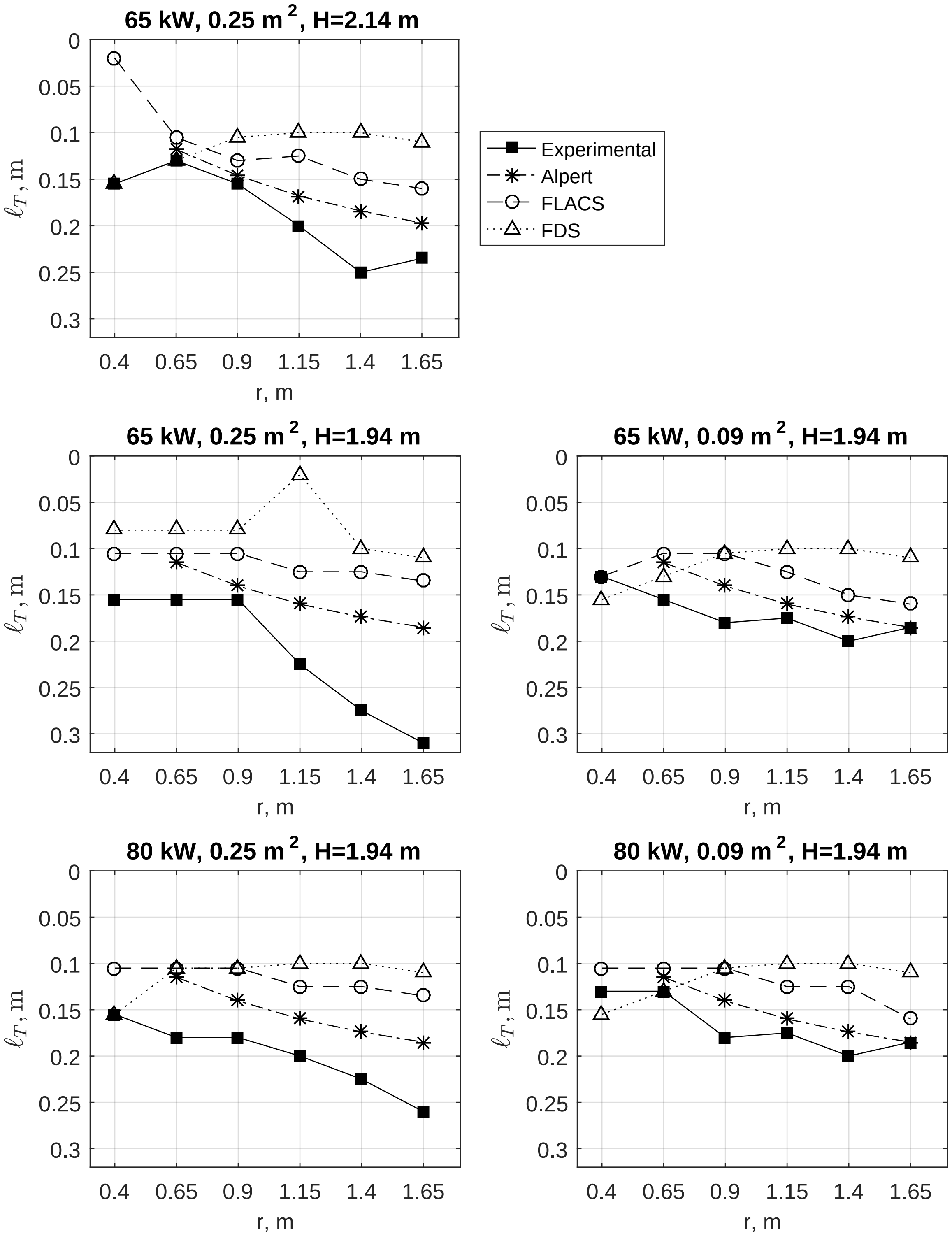

Figure F.4: Resulting ceiling jet thicknesses from experiments, simulations and correlations, versus radial distance away from fire source for cases 100001, 100002, 100012, 200002 and 200012 (see description in subplot title).

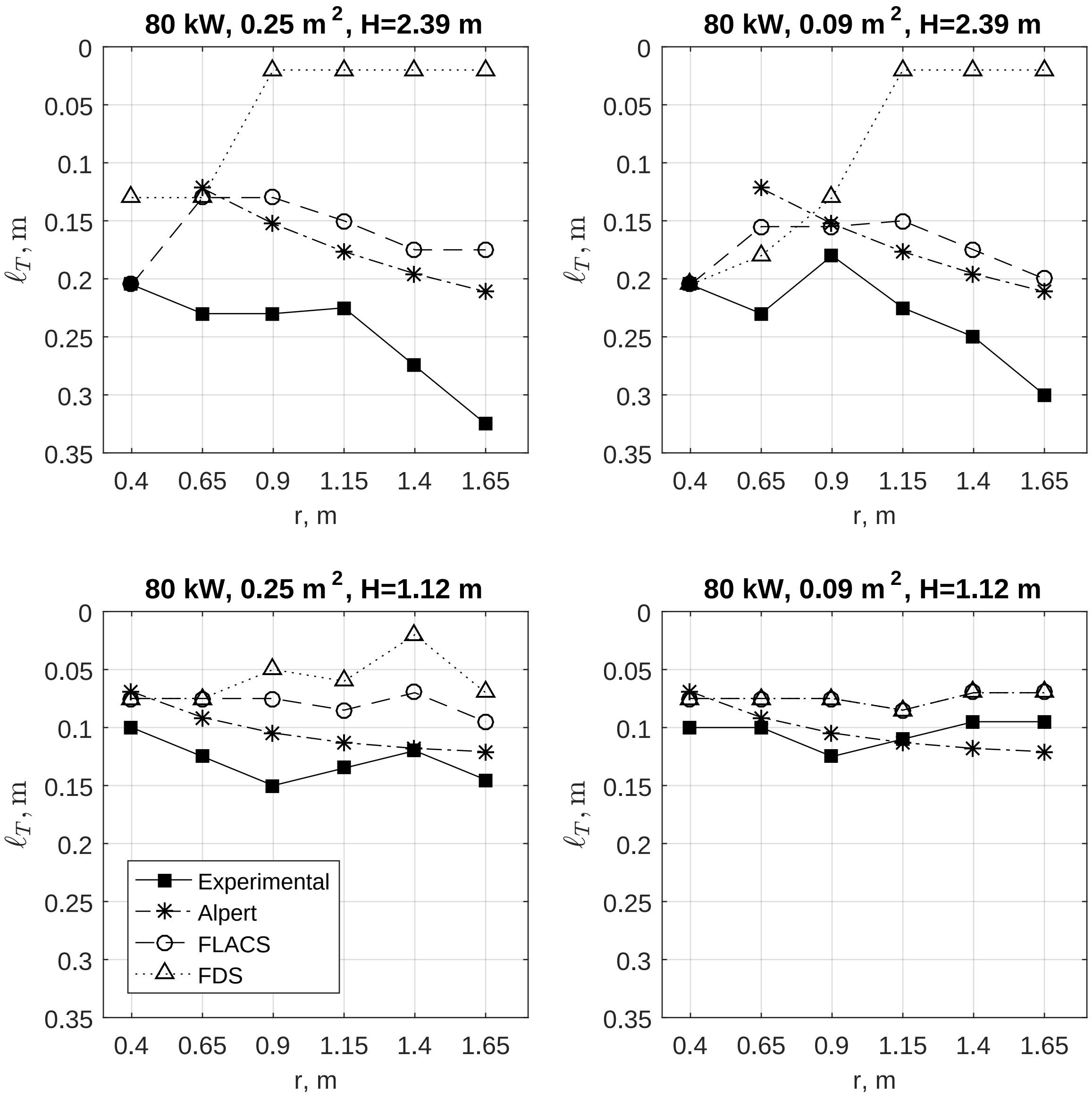

Figure F.5: Resulting ceiling jet thicknesses from experiments, simulations and correlations, versus radial distance away from fire source for cases 200000, 200010, 200005 and 200015 (see description in subplot title).

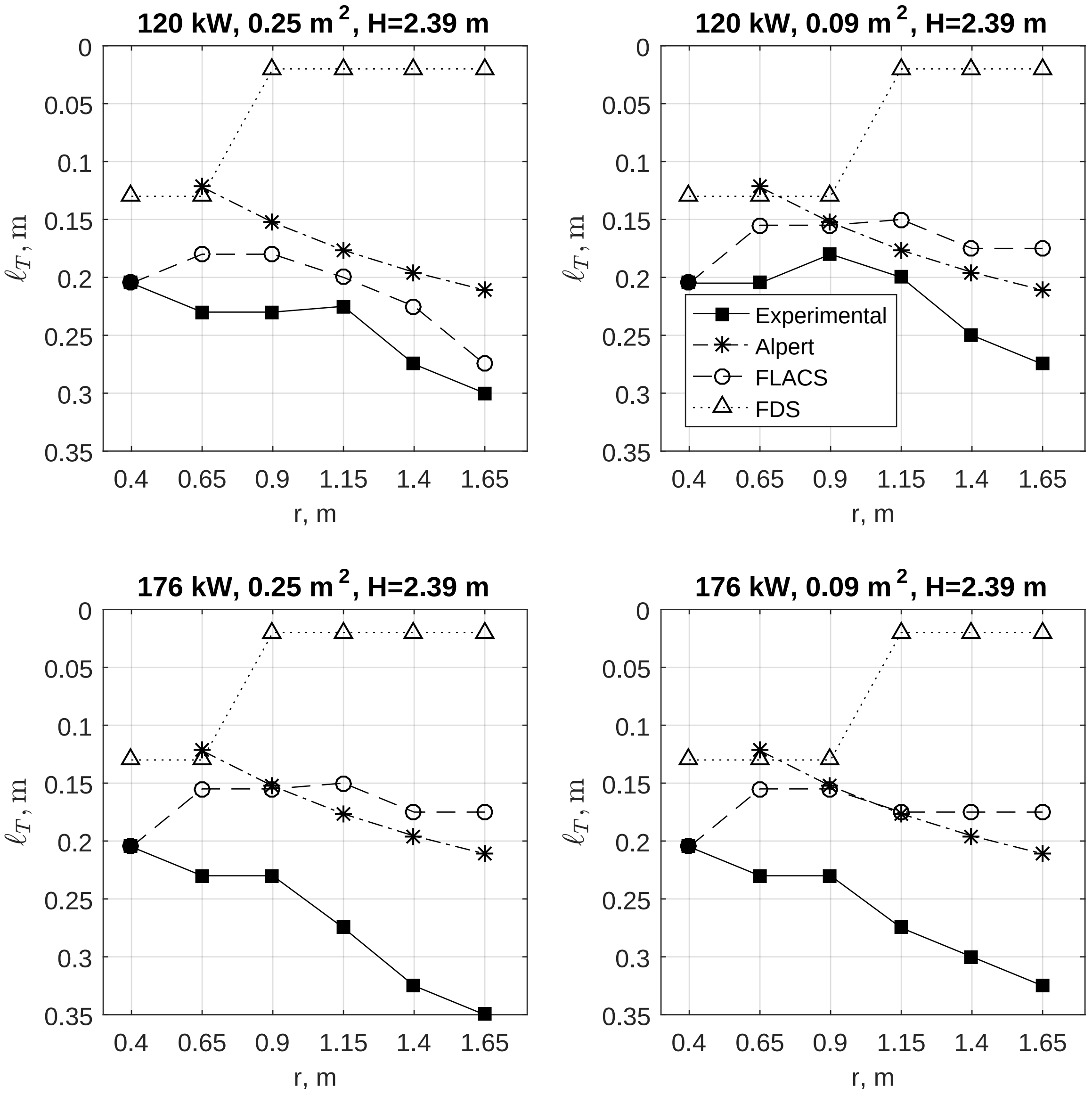

Figure F.6: Resulting ceiling jet thicknesses from experiments, simulations and correlations, versus radial distance away from fire source for cases 300000, 300010, 400000 and 400010 (see description in subplot title).

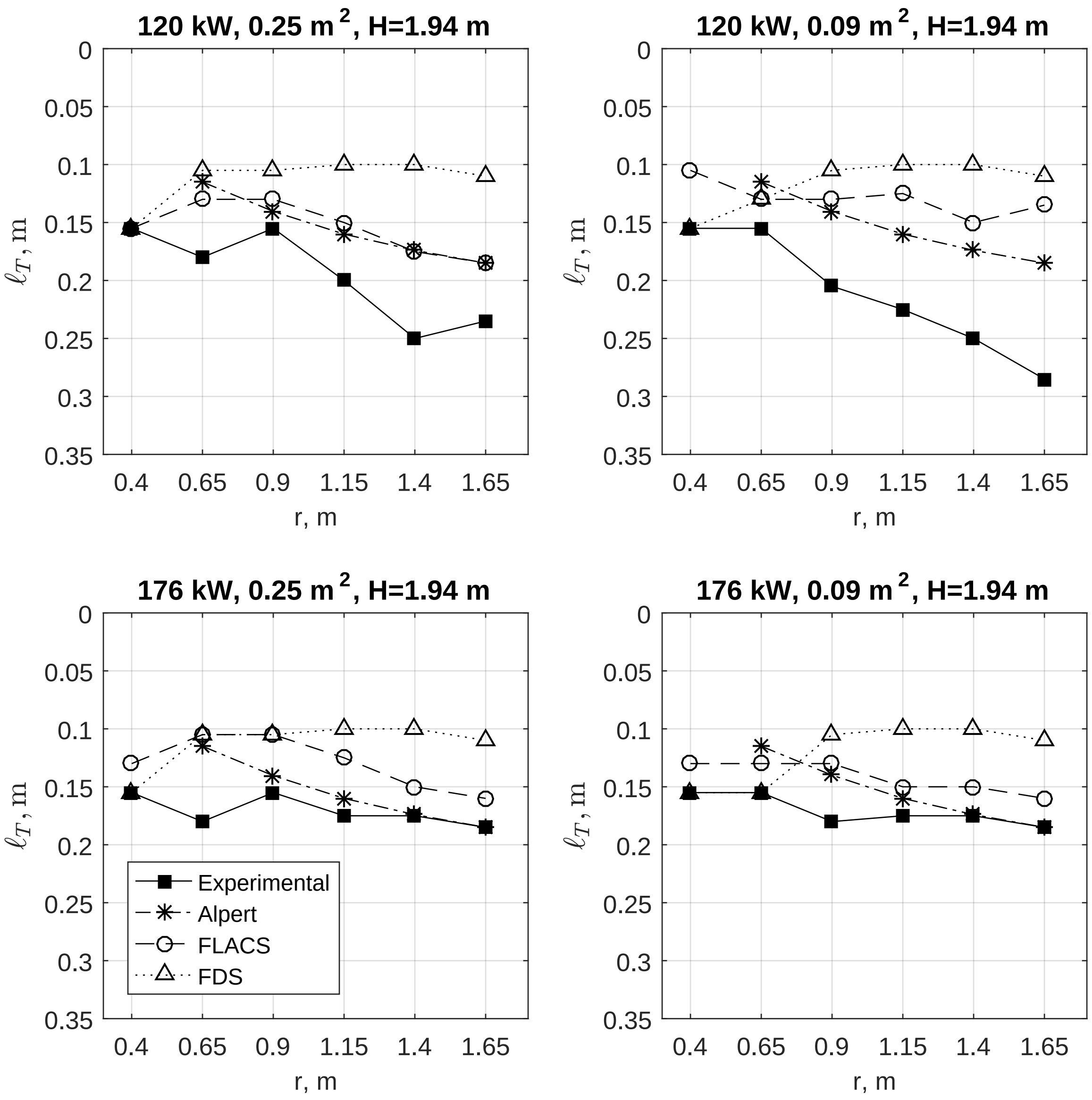

Figure F.7: Resulting ceiling jet thicknesses from experiments, simulations and correlations, versus radial distance away from fire source for cases 300002, 300012, 400002 and 400012 (see description in subplot title).